Electrochemical and Spectroelectrochemical Studies of Dyes used in Dye-sensitized Solar Cells

Fattori, Alberto

Award date:
2010

Awarding institution:
University of Bath

Electrochemical and Spectroelectrochemical Studies of Dyes used in Dye-sensitized Solar Cells

Alberto Fattori

A thesis submitted for the degree of Doctor of Philosophy

University of Bath
Department of Chemistry

Bath March 2010

Abstract

Electrochemical and spectroelectrochemical techniques were employed to investigate the redox characteristics of dyes for dye sensitized solar cells (DSCs) adsorbed at the surface of fluorine-doped tin oxide (FTO) and FTO TiO_2 electrodes. In this work are studied Ru-based dyes such as *cis*-bis(isothiocyanato)-bis(2,2'-bipyridyl-4,4'dicarboxylato)-ruthenium(II) (N719) and (*cis*-RuLL'$(SCN)_2$ with L=4,4'-dicarboxylic acid-2,2'-bipyridine and L'=4,4'-dinonyl-2,2'-bipyridine) known as Z907, and indoline organic dyes coded as D102, D131, D149, and D205.

The adsorption, diffusion and stability of adsorbed dyes were studied using cyclic voltammetry in acetonitrile and 0.1 M NBu_4PF_6. The adsorption technique at FTO electrodes was optimized in order to be reproducible so that electrochemical studies as a function of dye coverage were carried out. Langmuirian binding constants were approximately estimated for all dyes adsorbed at FTO electrodes.

Rate constants for the chemical degradation of the oxidized dye were also obtained. Is shown that degradation of the dyes mainly occurs at the surface of FTO and only insignificant degradation is evident once the dyes are adsorbed on TiO_2. The degradation of dye adsorbed on FTO is shown to affect charge transport from the nonporous TiO_2 via electron hopping.

Spectroelectrochemical studies of indoline dyes adsorbed on FTO/TiO_2 electrodes revealed a red shift of absorption peaks after oxidation and the presence of a strong charge transfer band in the near IR that suggest delocalization of holes in the dye layer. This is consistent with observation that the diffusion coefficient for hole conduction in the adsorbed dye layer is several orders of magnitude higher for the organic dyes compared to the Ru-based dyes.

DSCs fabricated using indoline dyes showed good performance. Incident photon-to-current conversion efficiency (IPCE) spectra and I-V characteristics are presented.

Acknowledgements

My first thanks goes to my supervisor Professor Laurie Peter, for is guidance, support and suggestions during my PhD.

I would like to thank all the past members of LMP group for their help when I started and in particular Wendy, Oanh, Anura and Killian.

Thank you to Halina, Jon, Ibrahim, Claire, James, Hongxia and Diego who I shared the up and down of the PhD life. Not just colleagues but friends that I could have always count on.

A special thanks goes to Dr Frank Marken, for his guidance, enthusiasm, patience and motivation that help me throughout the last two years of my PhD. Also, another special thanks goes to Professor Francesco Paolucci and Dr Massimo Marcaccio without whom I would never have started this adventure.

I would like also to thank for technical support Dr Mark Russell who helped me with IT problems, Mr Paul Frith who made my spectroelectrochemical cell that gave me the results that I was aiming for, and Mr Luca Bonaventura one of my oldest friends who helped me with the drawing of the cell.

Thanks to the guys that I met in the Chemistry Department who became more than very good friends, Stuart, Mike Andy and Nathan (team Vistec!), also thank you to Lorena and Domenico for their encouragement and motivation.

My deepest thanks go to my parents, Franco and Maria Cristina, always available always encouraging and always listening to me! Thank you!

Declaration of work done in conjunction with others

All of the work described in this thesis was carried out by the author apart from the following exceptions:

The compound $RuL(bipy)_2^{2+}$ with L=4,4'-dicarboxylic acid-2,2'-bipyridine used in Chapter 5 were synthesized by Keri McCall at the University of Edinburgh.

The dye sensitized cells presented in Chapter 7 were made by Dr Hongxia Wang.

Contributing work and publications

The work presented in this thesis has produced two peer reviewed publications. A further manuscript based on the penultimate chapter is in preparation.

The following paper from Chapter 4:

Cis-bis(isothiocyanato)-bis(2,20-bipyridyl-4,40dicarboxylato)-Ru(II) (N719) dark-reactivity when bound to fluorine-doped tin oxide (FTO) or titanium dioxide (TiO2) surfaces, Alberto Fattori, Laurence M. Peter, Stephen R. Belding, Richard G. Compton, Frank Marken, Journal of Electroanalytical Chemistry 640, **2010** 61–67.

The following paper from Chapter 5:

Adsorption and Redox Chemistry of cis-RuLL'(SCN)$_2$ with L=4,4'-Dicarboxylic acid-2,2'-bipyridine and L'=4,4'-Dinonyl-2,2'-bipyridine (Z907) at FTO and TiO_2 Electrode Surfaces, Alberto Fattori, Laurence M. Peter, Keri L. McCall, Neil Robertson, and Frank Marken Journal of Solid State Electrochemistry **2010** (accepted for publication).

Table of Contents

Chapter 1: Introduction

1.1 The need for renewable sources of energies

At present, human world energy use is made up mainly of fossil fuels (gas, coal and oil), hydroelectricity, nuclear power and tiny fractions from biomass and other solar energy sources. Fossil fuels are causing environment pollution and becoming gradually exhausted. Nuclear energy obtained from nuclear fission raises safetly and security issues, and is limited due to deficiency of heavy elements. Hence, seeking a renewable energy source has become important. Solar energy is one of the best alternative candidates. The first scientist who established that current and voltage could be generated by light studying the interaction between light and matter was Edmond Becquerel who discovered the photovoltaic effect in 1839[1] while experimenting with an electrolytic cell made up of two metal electrodes placed in conducting solution. He observed that current increased when the electrolytic cell was exposed to light. At that time there was not any relevant interest in finding new sources of energy that could be environmentally friendly. In the next decades with the increase of the world population and environmental problems, a better interest and sensitivity rose about this issue and especially about exploiting different energetic sources.

The modern era of solar cells started in the 1950's. In 1954 Chapin, Fuller and Pearson at Bell labs reported the first pn-junction photovoltaic device. This began the revolution in the application of photovoltaic devices as a power source.[2]

1.2 What is a solar cell

The photovoltaic effect is the main physical principle behind a class of devices known as solar cells. A photovoltaic (PV) cell converts any source of light into electrical power (current and voltage). Study on solar cells has been intensified after the Second World War when scientists became more sensitive towards the need for sustainable energies. Three generations of PV cells have so far been attempted. The most commonly available PV cell has been the first generation cell, which is essentially a silicon homojunction device. They are available in 3 different types such as single crystal, polycrystalline and amorphous, all of them exploiting the charge transfer characteristic of p-n semiconductor junctions.[3-4]

A p-n junction is a region formed by bringing a p-type and an n-type semiconductor into close contact. When p-type and n-type materials are placed in contact with each other, the junction behaves very differently than either type of material alone. Specifically, current will flow readily in one direction (forward biased) but not in the other (reverse biased). This diode behaviour arises from the nature of the charge transport process in the two types of materials.

The second generation of PC cells generally consist of two different semiconductors to form a p-n junction, known as hetero-junction devices. The third generation of PV cells is a different kind of solar cells which do not have a p-n junction and include dye sensitized solar cells (DSCs), organic polymer SC and quantum dot solar cells.

A simple conventional PV junction solar cell structure is shown in figure 1.1. Sunlight is incident on the solar cell through the transparent front contact. A metallic grid forms the electrical contacts of the cell and allows light to fall on the semiconductor between the grid lines where it can be absorbed and converted into electrical energy. An antireflective layer between the grid lines increases the amount of light transmitted to the semiconductor. This is achieved by diffusion or implantation of specific impurities (dopants) or via a deposition process. The back electrical contact is a metallic substrate made to complete the cell. The photons with energy greater than the semiconductor energy band gap generate electron-hole pairs

that will contribute to the energy conversion process. Therefore the solar spectrum has to be taken as an important consideration in the designing of efficient solar cells.

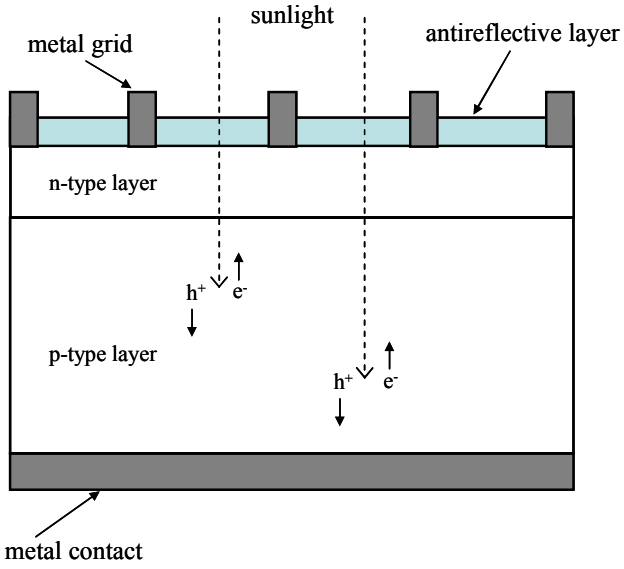

Figure 1.1 Schematic solar cell. Creation of electron–hole pairs, e− and h^+, respectively.[5]

1.3 Dye sensitized solar cells (DSCs)

The concept of dye sensitization was first applied in 1873 when Vogel in Berlin associated dyes with silver halide grains.[6] This technique has been improved during the decades with the study of spectrally selective dyes for colour photography.[7] In the 1960's Gerischer and Tributsch investigated the properties of a system with a dye adsorbed on a semiconductor substrate.[8] Years later (1991) Grätzel used this concept to invent the so-called dye sensitized solar cells (DSCs) using as a semiconductor titanium dioxide and ruthenium based bisbipyridyl dyes.[9] DSCs were developed from the motivation to find low cost photovoltaic devices with acceptable conversion efficiency. To date, an efficiency of 11% has been obtained. [10]

The device is based on an optically transparent mesoporous film of titanium dioxide, with 3 to 10μm thickness and consisting of nanocrystalline particles with diameter in the range 20-30 nm coated on a conductive glass. The dye is adsorbed on the semiconductor substrate.[9] The sensitizer harvests light in the visible range and injects electrons in the semiconductor conduction band. The oxidized dye is then

regenerated by electron donation from the electrolyte, which usually contains the iodide/triiodide redox couple. (See chapter 2 for more detailed explanation of principle of operation of a DSC)

In summary the main constituents of a DSC are:

- two sheets of FTO (fluorine-doped tin oxide coated) transparent glass. One is the cathode the other is the anode. The cathode is coated with a thin layer of Pt.
- an n-type semiconductor (titanium dioxide colloid)
- a dye, usually polypyridine ruthenium (II) complex or organic dye
- an electrolyte containing the triiodide/iodide redox couple in an organic solvent (usually acetonitrile)

This work has been focused on the study of the stability of ruthenium-based and organic dyes used in DSCs.

1.3.1 Dye requirements for DSCs

Not every dye can be a sensitizer; this depends on its physical and chemical properties which need to satisfy certain requirements in order to maximize electron injection when adsorbed on the semiconductor. The important dye properties for a DSC are summarized here.

1) Absorption spectra

In a DSC the fraction of light which is adsorbed in a layer of TiO_2 depends on the concentration and on the extinction coefficient of dye adsorbed in the semiconductor. Therefore the dye should have a high extinction coefficient and an absorption spectrum in the region between 400-900 nm in order to maximize the light harvesting.[11]

2) Attachment groups

The attachment group of the dye is needed to form a monomolecular layer upon exposing the oxide film to a dye solution. This molecular dispersion ensures a high probability that, once a photon is absorbed, the excited state of the dye molecule will relax by electron injection into the semiconductor conduction band. A common anchoring groups is carboxylate which can form an ester bond with TiO_2 surface and allow facile electronic communication. Other anchoring groups are phosphonate or hydroxomate.[12-14]

3) Energy levels

The energy levels of the dye excited state should be well matched to the conduction band of the oxide to minimize energetic losses during electron injection.[12] This means that the LUMO (lowest unoccupied molecular orbital) of the dye should be sufficiently high in energy in order to inject electrons into the semiconductor, and the HOMO (highest occupied molecular orbital), should be low enough in order that electrons can be regenerated by the electrolyte.

4) Redox potentials

The redox potentials of a dye are crucial to optimize the correct functioning of the cell. It should be sufficiently positive so that it can be regenerated via electron donation from the redox electrolyte. It is important to characterize the nature of the dye oxidized species because this is related to its stability which is a fundamental requirement for a long-lived DSC.[13]

5) Stability

For practical application the dye should be stable enough to resist about 20 years of exposure to natural light. Figure 1.2 shows the catalytic cycle of the sensitizer S under illumination in a DSC. The stability is negatively influenced by side reactions that involve the excited state S^* or the oxidized state S^+. These reactions compete with the injection of electrons from the excited dye into the conduction band of the semiconductor and with the regeneration of the dye by the electrolyte.[14]

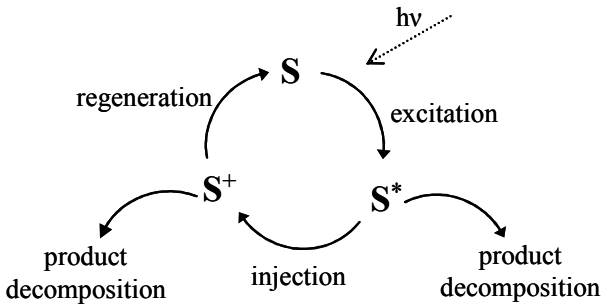

Figure 1.2 Catalytic cycle of a dye in its three states, reduced form (S), excited form (S^*), oxidized from (S^+).

1.3.1.1 Ruthenium-based sensitizers

Ruthenium polypyridine complexes are a class of compounds that have been widely studied in the past three decades due to their chemical stability, redox properties (they have stable oxidized and reduced forms),[15] lifetime and reactivity of the excited state.[16]They also have a good solubility in many solvents, among them organic aprotic solvents, which are mainly used for dye baths in DSCs. Furthermore, photophysical properties such as absorption in the visible range made this class of compounds attractive for fundamental and practical science studies.

A good dye for DSCs should have a broad range of visible light absorption that can render it an attractive sensitizer for homogeneous and heterogeneous redox reactions. Figure 1.3 shows the molecular structure of the first successful dye for DSCs cis-bis(isothiocyanato)bis(2,2'-bipyridyl-4,4'-dicarboxylato)-ruthenium(II) known as N3 synthesized in 1993.[17] The light absorption is attributed to the transition metal-to-ligand charge transfer (MLCT) and the molecular orbitals HOMO and LUMO, are mainly derived from the d-orbital of the ruthenium and π^* orbital of the ligand. The isothiocyanato ligands are the chromophore of the molecule, they shift the HOMO level negatively towards a red shift in its absorbtion spectra.[17]

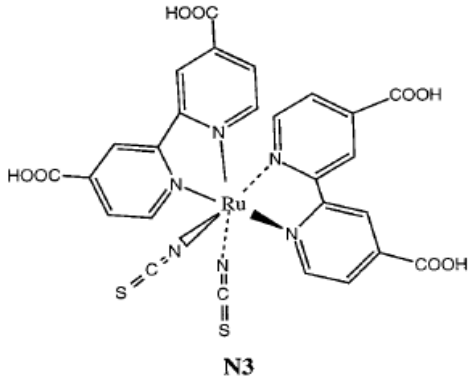

Figure 1.3 Molecular structure of N3 dye *cis*-bis(isothiocyanato)bis(2,2'-bipyridyl-4,4'-dicarboxylato)-ruthenium(II).

N3 has been used as reference dye and its synthesis as a starting point to improve electronic and optical properties of dyes and the overall cell efficiency.[18] There are different routes to modify the dye structure, depending on the aim of the improvement. For example in order to have a dye which absorbs in the red or IR, the chromophore can be substituted with other ligands like acetylacetonate.[19] This gives as a result a red shift and better absorption compared to the thiocyanate ligands of N3 but not an enhancement of the cell efficiency. Other ways to modify the dye structure involve the use of different anchoring groups. Usually carboxylic acid groups are the most employed to anchor to the TiO_2 surface ensuring a strong bond and a good electronic communication. The disadvantage of using this linker is that it is sensitive to traces of water. The presence of water can hydrolyze the link weakening the bond of the dye on TiO_2 and negatively influences the stability of the dye.[18] In a DSC this can happen when a liquid electrolyte is employed for dye regeneration. The dye Z955 has been synthesized to answer these requirements. Instead of carboxylic linkers, Z955 has phosphonic acid linker groups[20] which give a blue shift in the absorption compared to N3. In order to minimize the influence of traces of water on the long-term performance of a DSC, dyes with attached hydrophobic chains have been designed. Among them Z907 dye is one of the most stable towards desorption from TiO_2 surface.[21] The hydrogen of the carboxylic acid linkers in N3 can be replaced by other ligands such as TBA (tetrabutylammonium) group. Changing the protonation of the acid groups has been found a successful improvement to the dye structure since led to the synthesis of N719 which has been so far the most successful

dye for DSCs.[12] Figure 1.4 shows the molecular structure of N719 and Z907. These 2 dyes have been studied in this work via electrochemical experiments at FTO and FTO/TiO_2 substrates (see chapter 5).

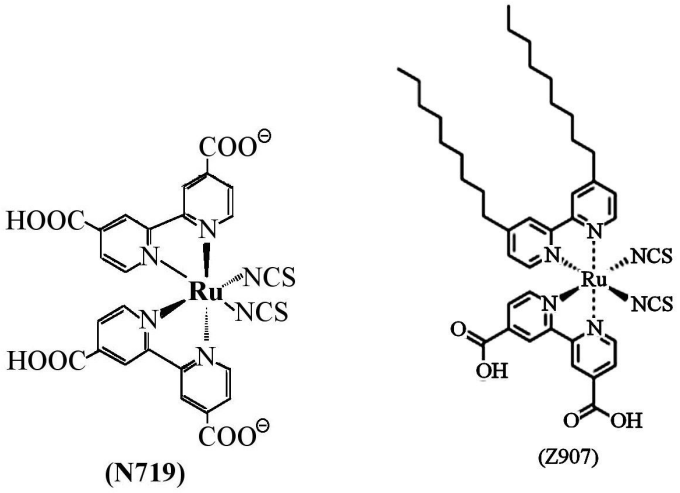

Figure 1.4 Molecular structures of ruthenium based dyes N719 and Z907

1.3.1.2 Organic sensitizers

The idea of developing organic sensitizers originates from the need to find cheaper and easier ways to synthesize dyes compared to those based on the ruthenium. The main advantages of organic dyes can be summarized as follows:[22]

- very high molar extinction coefficients (allow the use of thinner TiO_2 layer)
- simple modelling and facile synthesis
- absorption energies that can be easily tuned
- easy incorporation in solid state electrolyte thin cells
- low cost

In terms of molecular structure, organic dyes can be divided in three major parts; donors, linkers and acceptors.[23] Linkers are usually π-conjugated system that link by bridges electron-donating (D) and electron-accepting (A) groups; so-called D-π-A sensitizers. Light absorption induces charge separation between the donor and the

acceptor moieties of the chromophore where the photoabsorption properties involve intermolecular charge transfer (ICT) between A and D. In many cases the HOMOs of a D-π-A system are delocalized over the π-conjugated system in configurations centring on the donor side, and the LUMOs are mainly delocalized on the acceptor side.[24] One of the most relevant features that researchers would like to improve in the design of a new organic sensitizer is its absorption in the red region of the visible spectra. This can be obtained by expanding the π-conjugation of the linkers and increasing the electron-donating and electron-accepting capability of donors and acceptors. In a DSC using organic dyes there is a factor which is generally thought influences negatively the electron injection from the dyes to the CB of TiO_2. This is π-stacked aggregation of dye molecules on TiO_2 surface. Dye aggregation is usually considered a phenomenon that should be avoided although a controlled aggregation could be considered beneficial.[25] One way to avoid this problem is to incorporate long alkyl chains and aromatic groups into the dye structure to prevent π aggregation. There are many classes of organic sensitizers that have been studied for DSCs but the most promising are coumarin, porphyrins and indoline dyes.[26]

Coumarin is a chemical compound which is found in many plants. It is widely and successfully used in dye lasers. Coumarin (figure 1.5) is used as donor group and its skeleton is usually incorporated in a variety of acceptors and linkers in order to improve its physical and chemical properties as a dye for DSCs. The first coumarine dye named C343 (figure 1.5) was synthesized by Grätzel and demonstrated fast electron injection from the dye to a TiO_2 substrate.[27] Since then Hara studied systematically coumarin dyes improving their light harvesting and reaching DSC efficiency comparable to the ruthenium based dyes.[28]

Another class of sensitizers are porphyrins (figure 1.5) which are compounds present in nature characterized by four modified pyrrole subunits interconnected via methane bridges (=CH-). This assembly gives a macrocycle which is a high π-conjugated system with very intense absorption in the visible region and high extinction coefficient. Due to these characteristics and to the fact that linkers can be easily attached to the macrocycle for TiO_2 sensitization, porphyrins became attractive as sensitizers for DSCs[29] reaching efficiency of about 5%.[30]

To date, the most successful class of organic dyes for DSCs is represented by indoline dyes which have been introduced by Uchida in 2003.[31] The indole moiety acts as electron donor and is connected to a rhodanine group which act as electron acceptor. Furthermore, the introduction of aromatic units in the indoline core enhances the absorbance in the red region of the visible spectra and the absorption coefficient of the dye. Indoline dyes coded as D102, D131, D149 (figure 1.5) and D205[32] have been studied in this work via electrochemical and spectroelectrochemical experiments in order to acquire information on their stability when adsorbed on different substrates such as FTO and FTO/TiO_2 (see chapter 6).

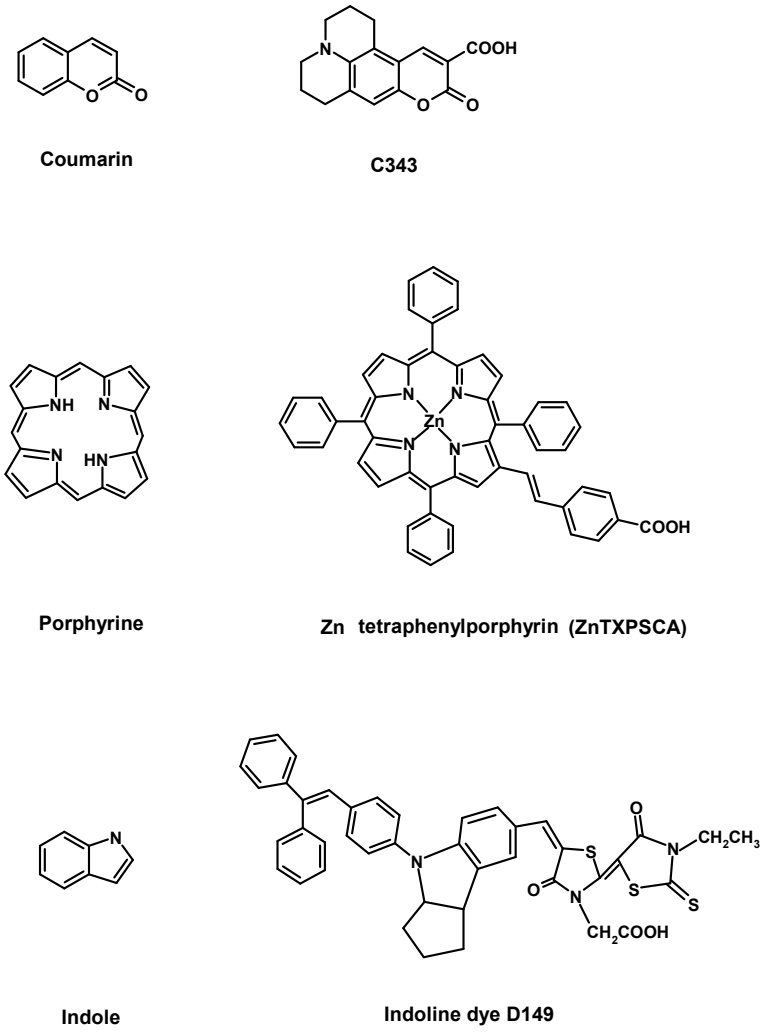

Figure 1.5 Functional groups of coumarine porphyrine and indoline dyes with their relative sensitizers.

References

1. Becquerel, A. E., *Comt. Rend. Acad. Sci* **1839,** *9*, 561.
2. D.M. Chapin, C. S. F., and G.L. Pearson, *J. Appl. Phys* **1954,** *25*, 676.
3. Sze, S. M., *Physics of Semiconductor Devices*. John Wiley and Sons: Singapore, 1981.
4. Green, M. A., *Silicon Solar Cells: Advanced Principles and Practice*. John Wiley and Sons: New York, 1998.
5. A.Luque, S. H., *Handbook of Photovoltaic Science and Engineering* John Wiley & Sons: 2003.
6. Vogel, *Photogr. Sci.Eng.* **1874,** *18*, 35.
7. West, W., *Photogr. Sci. Eng.* **1974,** *18*, 35.
8. Tributsch, H. G. a. H., *Ber. Bunsenges. Phys. Chem* **1968,** *72*, 437.
9. O'regan, B.; Gratzel, M., *Nature* **1991,** *353* (6346), 737-740.
10. Gratzel, M., *Journal of Photochemistry and Photobiology a-Chemistry* **2004,** *164* (1-3), 3-14.
11. Wang, Z. S.; Kawauchi, H.; Kashima, T.; Arakawa, H., *Coordination Chemistry Reviews* **2004,** *248* (13-14), 1381-1389.
12. Gratzel, M., *Inorg. Chem.* **2005,** *44* (20), 6841-6851.
13. Wolfbauer, G.; Bond, A. M.; MacFarlane, D. R., *Inorg. Chem.* **1999,** *38* (17), 3836-3846.
14. Gratzel, M., *Comptes Rendus Chimie* **2006,** *9* (5-6), 578-583.
15. Tokeltak.Ne; Hemingwa.Re; Bard, A. J., *Journal of the American Chemical Society* **1973,** *95* (20), 6582-6589.
16. Juris, A.; Balzani, V.; Barigelletti, F.; Campagna, S.; Belser, P.; Vonzelewsky, A., *Coordination Chemistry Reviews* **1988,** *84*, 85-277.
17. Nazeeruddin, M. K.; Kay, A.; Rodicio, I.; Humphrybaker, R.; Muller, E.; Liska, P.; Vlachopoulos, N.; Gratzel, M., *Journal of the American Chemical Society* **1993,** *115* (14), 6382-6390.
18. Robertson, N., *Angewandte Chemie-International Edition* **2006,** *45* (15), 2338-2345.
19. Takahashi, Y.; Arakawa, H.; Sugihara, H.; Hara, K.; Islam, A.; Katoh, R.; Tachibana, Y.; Yanagida, M., *Inorganica Chimica Acta* **2000,** *310* (2), 169-174.
20. Wang, P.; Klein, C.; Moser, J. E.; Humphry-Baker, R.; Cevey-Ha, N. L.; Charvet, R.; Comte, P.; Zakeeruddin, S. M.; Gratzel, M., *Journal of Physical Chemistry B* **2004,** *108* (45), 17553-17559.
21. Kroon, J. M.; Bakker, N. J.; Smit, H. J. P.; Liska, P.; Thampi, K. R.; Wang, P.; Zakeeruddin, S. M.; Gratzel, M.; Hinsch, A.; Hore, S.; Wurfel, U.; Sastrawan, R.; Durrant, J. R.; Palomares, E.; Pettersson, H.; Gruszecki, T.; Walter, J.; Skupien, K.; Tulloch, G. E., *Progress in Photovoltaics* **2007,** *15* (1), 1-18.
22. Mosurkal, R.; He, J. A.; Yang, K.; Samuelson, L. A.; Kumar, J., *Journal of Photochemistry and Photobiology a-Chemistry* **2004,** *168* (3), 191-196.
23. Park, S. S.; Won, Y. S.; Choi, Y. C.; Kim, J. H., *Energy & Fuels* **2009,** *23* (7), 3732-3736.
24. Oyama, Y.; Harima, Y., *European Journal of Organic Chemistry* **2009,** (18), 2903-2934.
25. Pastore, M.; De Angelis, F., *Acs Nano* **2010,** *4* (1), 556-562.
26. Mishra, A.; Fischer, M. K. R.; Bauerle, P., *Angewandte Chemie-International Edition* **2009,** *48* (14), 2474-2499.

27. Rehm, J. M.; McLendon, G. L.; Nagasawa, Y.; Yoshihara, K.; Moser, J.; Gratzel, M., *Journal of Physical Chemistry* **1996,** *100* (23), 9577-9578.
28. Hara, K.; Tachibana, Y.; Ohga, Y.; Shinpo, A.; Suga, S.; Sayama, K.; Sugihara, H.; Arakawa, H., *Solar Energy Materials and Solar Cells* **2003,** *77* (1), 89-103.
29. Campbell, W. M.; Burrell, A. K.; Officer, D. L.; Jolley, K. W., *Coordination Chemistry Reviews* **2004,** *248* (13-14), 1363-1379.
30. Nazeeruddin, M. K.; Humphry-Baker, R.; Officer, D. L.; Campbell, W. M.; Burrell, A. K.; Gratzel, M., *Langmuir* **2004,** *20* (15), 6514-6517.
31. Horiuchi, T.; Miura, H.; Uchida, S., *Chemical Communications* **2003,** (24), 3036-3037.
32. Horiuchi, T.; Miura, H.; Sumioka, K.; Uchida, S., *Journal of the American Chemical Society* **2004,** *126* (39), 12218-12219.

Chapter 2: Theory

2.1 Dye sensitized solar cells (DSC): principle of operation

The device is based on a layer of porous optically transparent film of titanium dioxide, with an average 10μm thickness and consisting of nanocrystalline particles with diameter in the range of 20-30 nm coated on a conductive glass. For high efficiency cells another layer of TiO_2 is deposited on top of the first one with particle in the range of 400 nm resulting in light scattering effect.[1] On the titanium dioxide is an absorber dye that transfers electrons to the TiO_2 to sensitize the film for light harvesting. Figure 2.1 shows the principle of operation of a DSC. Light is absorbed by a monolayer of dye which is attached to the titanium dioxide by the anchoring groups e.g. carboxylate, phosphonate or hydroxamate. Light excites dye molecules to a D^*(excited state), and the electron is injected into the conduction band of the semiconductor. The positive charge formed in the light-induced charge separation, is transferred from the dye to an electron donor mediator present in the electrolyte. The injected electrons flow through the titanium dioxide and pass through the external circuit, delivering power to the load. They re-enter into the cell via the platinum coated counterelectrode and reduce triiodide ions to iodide ions. The photovoltage generated under illumination corresponds to the difference between the Fermi level of electrons in the titanium dioxide film and the redox potential of the triiodide/iodide couple. Generation of electrical power by the device does not lead to any permanent chemical transformation.

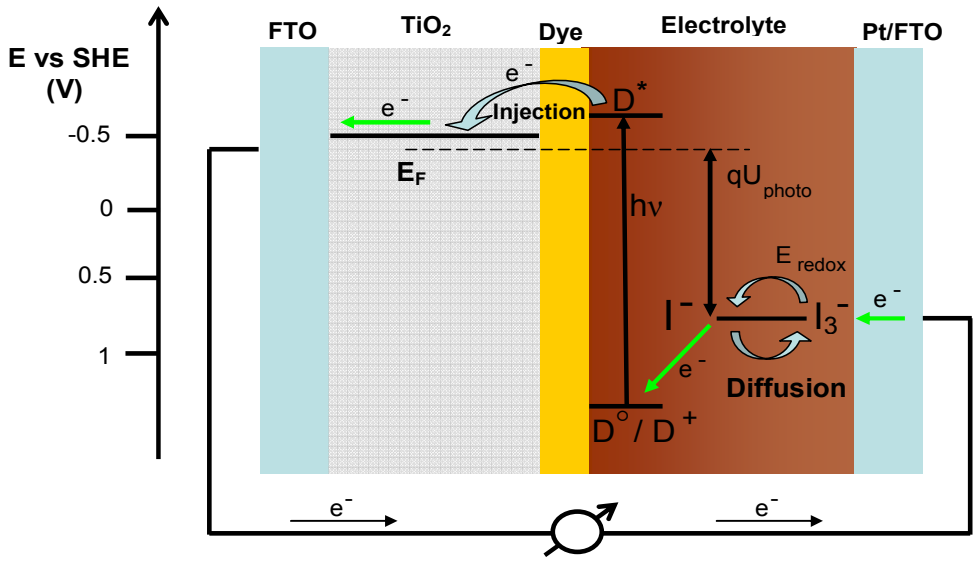

Figure 2.1 Principle of operation and energy level scheme of the dye-sensitized nanocrystalline solar cell. Potentials are referred to the standard hydrogen electrode (SHE), and the energy levels are drawn for the N3 dye and the triiodide/iodide couple.[2]

2.2 Factors controlling the efficiency of DSC

The factors that influence the short circuit photocurrent of a DSC are the light harvesting efficiency η_{LHE}, the net injection efficiency η_{inj}, and the collection efficiency η_{coll}. η_{LHE} is determined by the number of dye molecules on the titanium dioxide film, the absorption of the dye, and the scattering of light by the titanium dioxide film. The net η_{inj} is determined by the intramolecular decay of the excited state of the dye, the electron injection by the photoexcited dye, the regeneration of the dye by iodide ions and the recombination of dye cations with injected electrons. Finally, η_{coll} is determined by the competition between the transport of injected electrons in the titanium dioxide and their back reaction with triiodide ions in the electrolyte. In fact the open circuit voltage of a DSC is determined by the energy difference between the quasi-Fermi level of TiO_2 and the potential of the redox couple in the electrolyte and by the electron lifetime. As electron lifetime decreases, recombination increases resulting in a decrease of the open circuit voltage.

2.3 Photocurrent

The incident photon-to-current efficiency (IPCE) is a measure of the ability of solar cell to convert monochromatic light into current (electrons). The IPCE value of a DSC is the ratio of the observed photocurrent and the incident photon flux, uncorrected for reflective losses. The IPCE can be measured from the substrate side and from the electrolyte side.

2.1 $$IPCE = \frac{j_{photo}}{qI_0}$$

where j_{photo} is the flux of electrons through the external circuit and qI_0 is the flux of incident photons.

The IPCE can also be expressed as:

2.2 $$IPCE = \eta_{LHE} \times \eta_{inj} \times \eta_{coll}$$

where, η_{LHE} depends on the spectral and photophysical properties of dyes, and the term is easily quantified by visible absorption spectroscopy and accounts for the solvent dependent changes in spectral sensitivity of solar cell. η_{LHE} is related to the molecular extinction coefficient, which will be discussed later in the chapter. η_{inj} denotes the fraction of the photons absorbed by the dye that are converted into the electrons in the conduction band of the semiconductor oxide, and η_{coll} is the efficiency of collecting the injected electrons in the external circuit, and is related to electron diffusion length. Figure 2.2 shows the IPCE plot of a DSC made with one of the organic dyes (D102) studied in this work. (See chapter 5)

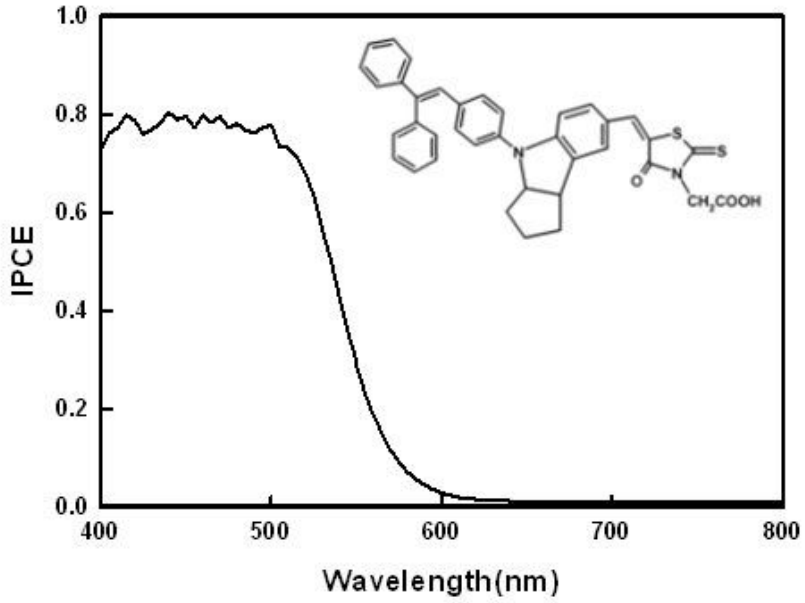

Figure 2.2 IPCE spectrum for DSC sensitized with D102 dye. The inset shows the dye structure.

2.4 Current-voltage characteristic

A current-voltage (I-V) curve shows the possible combinations of current and voltage output of a solar cell. The cell produces its maximum current when there is no resistance in the circuit, i.e., when there is a short circuit between its positive and negative terminals. This maximum current density is known as the short circuit current density and is abbreviated J_{sc}. When the cell is shorted, the voltage in the circuit is zero. The maximum voltage occurs when there is a break in the circuit. This is called the open circuit voltage (V_{oc}). Under this condition the resistance is infinitely high and there is no current, since the circuit is incomplete. The power of the cell, which is its work per unit time expressed in watts, is calculated by the product of current in amps and voltage in volts.

2.3 $$P = IV$$

A parameter that can be calculated and gives a measure of cell quality is the fill factor (*FF*) which is the ratio of the power at the maximum power point, divided by the product V_{oc} and J_{sc}.

2.4 $$FF = \frac{P_{\max}}{V_{oc} \times J_{sc}}$$

The fundamental parameter of a solar cell that gives information on its performance is the efficiency η

2.5 $$\eta = \frac{V_{oc} J_{sc}}{P_{inc}} FF$$

Where V_{oc} is the open circuit voltage, J_{sc} is the short-circuit current density, FF is the fill factor, and P_{inc} is the incident solar power, which is the power of the incident radiation upon the cell. The most frequent conditions are air mass (AM) 1.5, irradiance 100 mW/cm^2. The use of this standard irradiance value is particularly convenient since the cell efficiency in percent is then numerically equal to the power output from the cell in mW/cm^2. Figure 3 shows a typical plot of an I-V curve and the parameters that can be obtained from it.

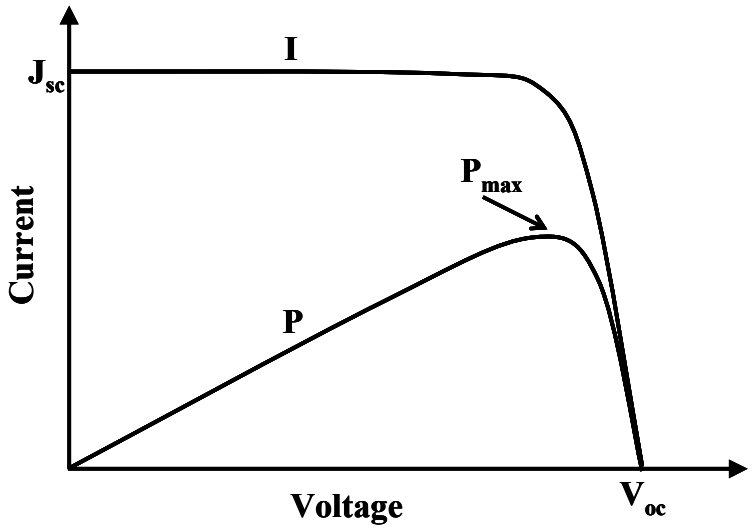

Figure 2.3 I-V curve showing current-voltage characteristic and power curve of a solar cell.

2.5 Optical absorbance

The optical absorbance of a solution is defined by the Beer Lambert law; [3]

2.6
$$A(\lambda) = -\log_{10} T(\lambda) = \log_{10} \frac{I_0}{I(\lambda)} = \varepsilon(\lambda) cl$$

Where $T(\lambda)$ is the transmittance, $I(\lambda)$ is the intensity of light a specified wavelength λ that has passed through a sample (transmitted light intensity) and of I_0 is the intensity of the light before it enters the sample (incident light intensity), $\varepsilon(\lambda)$ molar extinction coefficient (mol^{-1} dm^3 cm^{-1}) which is a quantity depending on the nature of the absorbing molecules and on the wavelength, c (mol dm^{-3}) the concentration of the sample and l (cm) is the length of light path through the sample.

A sensitizer in dye sensitized cells should have a high value of extinction coefficient and absorb broadly in the visible and near IR range of the electromagnetic spectrum. The light absorption process has to lead to the electron transfer to the semiconductor. The extinction coefficient is related to the dye chromophore oscillator strength (f) which is a measure of the intensity of a transition over a frequency range. In order to give an expression for the oscillator strength and to obtain the strength of the absorption band, a dye molecule can be replaced with a simple model of a classical oscillator of mass m_e and charge e. Maximum absorption is obtained when the frequency of the incident light approaches the resonance frequency of the oscillator. The oscillator strength can be calculated for a classical oscillator of mass m_e and charge e as follows (equation 2.7).[4]

2.7
$$f = \frac{\int_{band} \varepsilon \times d\nu}{\left(\int_{band} \varepsilon \times d\nu \right)_{classical(e,m_e)}} = \frac{4\varepsilon_0 2.303 m_e c_0}{N_A e^2} \times \int_{band} \varepsilon \times d\nu$$

$$= 1.44 \times 10^{-19} mol \times dm^{-3} \times cm \times s \times \int_{band} \varepsilon \times d\nu$$

In this equation c_0 is the speed of light ε_0 is the vacuum permittivity and N_A is the Avogadro constant.

High values of ε enable the use of thinner layers of TiO_2 compared with dyes with low ε where more dye is required in order to maximize the light harvesting. An example where ε =14200 $M^{-1}cm^{-1}$ is not very high is the ruthenium based dye N3 which has been the first successful in DSC.[2] For this, a 10 μm thickness of TiO_2 layer is required for efficient light harvesting. Among the ruthenium based dyes, N719 is the most important since has given the maximum value of a cell efficiency of 11% with ε=13900 $M^{-1}cm^{-1}$.[5] The amphiphilic Z907 with ε=12200 $M^{-1}cm^{-1}$ is another example.[6] In contrast, organic dyes usually have higher extinction coefficients compared to ruthenium based dyes. Organic indoline dyes which have been studied in this work, have very high extinction coefficients of D102 ε=55800 $M^{-1}cm^{-1}$,[7] D149 ε=68700 $M^{-1}cm^{-1}$,[8] D131 ε=48800 $M^{-1}cm^{-1}$,[9] D205 ε= 53000 $M^{-1}cm^{-1}$.[8] Recently a class of new Ru based dyes indentified as "C dyes" have been developed by Grätzel et al. with high ε. For example for the dye called C101 ε = 17500 M^{-1} cm^{-1} and for C102 ε=16800 M^{-1} cm^{-1}.[10]

The extinction coefficient can also be related to the absorption coefficient α. In dye cell often this quantity is used to relate to the concentration of a dye in a TiO_2 layer after desorption experiments. From Beer Lambert law we can work out α as follows

2.8 $$\log_{10} T = -\varepsilon \times c \times l$$

2.9 $$T = e^{-\alpha \times l}; \quad \ln T = -\alpha \times l$$

2.10 $$2.303 \log_{10} T = -\alpha \times l$$

2.11 $$\log_{10} T = -\frac{\alpha \times l}{2.303} = -\varepsilon \times c \times l$$

2.12 $$\alpha = 2.303 \times \varepsilon \times c$$

A value of α = 7320 cm^{-1} is obtained for N719 at 550 nm from ε = 10960 M^{-1} cm^{-1} and c = 0.29 mol dm^{-3} calculated from dye loading. From this the value of light harvesting efficiency could also be calculated as follows

2.13 $$\eta_{LHE} = 1 - e^{-\alpha \times d} = 1 - e^{-7320 \times 0.0003} = 0.9$$

Where the experimental *d*= 3 μm is the thickness of the TiO_2 film.

2.6 Electron transfer at electrode surfaces

Electron transfer at the surface of an electrode immersed in a solution containing a redox species can occur via a reducing agent which injects electrons into the electrode or an oxidizing agent which extracts electrons from the electrode. Associated to these two processes there are currents, called exchange currents, that flow in both directions electrode-solution and solution-electrode. When the currents are equal, the electrode is considered to be at equilibrium. If an overvoltage is applied, the equilibrium is altered and the potential of the system will shift promoting a net current which is the result of suppression of current flux in one direction and an increasing of current flux in the other direction. A cathodic current would imply that electrons must be captured, or holes injected, by an oxidizing agent in solution which would be reduced. Vice versa, an anodic current would imply that electrons must be injected and holes captured by reducing agents in solution, in order that anodic current can flow and the reducing agent is oxidized.[11]

For a simple redox reaction where O and R are the oxidized and reduced species

2.14 $$O + ne^- \rightarrow R$$

The Nernst equation can be derived in terms of electrochemical potential and written in the form of equation 2.15

2.15 $$E = E^{\circ'} + \frac{RT}{nF} \ln \frac{[O]}{[R]}$$

where E is the applied potential, $E^{\circ'}$ is the formal potential, R is the gas constant, T is the temperature, [O] and [R] are respectively the concentrations of the oxidized and reduced species. The electrochemical potential of the electron can be considered as equivalent to Fermi level of a redox system $E_{F,\,redox}$. On an absolute scale the Fermi energy level can be expressed as the "*electrical work required to take a test positive charge into the conductive phase of the electrode from a point in vacuo outside the system"* (Bard and Faulkner).[12] For practical reasons it is more convenient to talk about electrode potentials that are more easily measured and expressed on a relative scale. For example the potential corresponding to the Fermi level of a redox couple, can be measured against a reference electrode like the saturated calomel electrode (SCE).

The Marcus energy level model is an approach for the description of electron transfer between metal or semiconductor electrodes at the solution interface. The reason is that the properties of metal and semiconductor electrodes can be related to the properties of the solution only when both are described with the same model. One of the main characteristics of this model is that common factors present in all electrode reactions could be related. For example the fluctuation of the energy levels of ions in solution can be related to the Fermi distribution of electrons in the energy levels of the metal or semiconductor electrodes. The energy levels of the ion in solution fluctuate relative to the energy of the electron in the solid electrode, and the electron transfer occurs by tunnelling between levels of equal energies. Semiconductors electrodes are better described in terms of energy bands and energy levels for electrons.

Figure 2.4 shows the band diagram for a metal electrode at open circuit condition where no current flows and the exchange of electrons between the electrode and the redox couple in solution is at equilibrium. In this case the Fermi energy level is equal to the $E_{F,redox}$ of the redox couple and the exchange current is the same in each direction leading to a no net current flux through the surface.

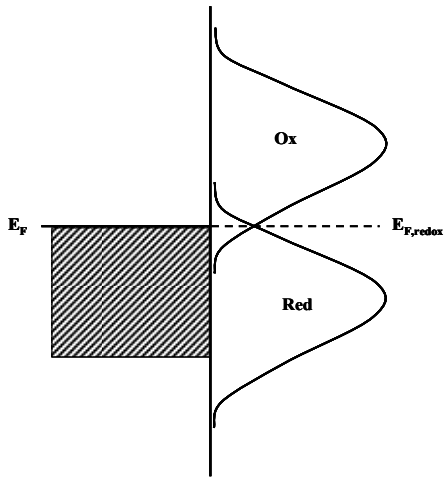

Figure 2.4 Band diagram for a metal electrode in contact with the solution at the equilibrium.

If the equilibrium is perturbed by an applied negative potential the Fermi level of the electrode will shift perturbing the equilibrium and leading, for the case where $E_F > E_{F,redox}$, to an increase of the cathodic current from the metal to the solution, and a decrease of the anodic current. This is because there is more overlap between the filled levels of the metal and levels of the oxidizing agent, and less overlap between the unoccupied levels in the metal and the levels of the reducing agent. (Figure 2.5)

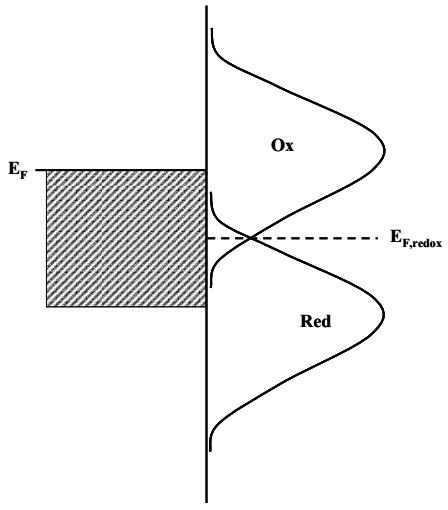

Figure 2.5 Band diagram for a metal electrode in contact with the solution under applied negative overpotential.

The behaviour of a semiconductor electrode is different from a metal electrode due to its different physical properties. For an intrinsic semiconductor, electronic states are delocalized just as in metals, and there are bands of allowed electronic energies. At 0 K, the bands are either completely filled or completely empty and so do not contribute to the conductivity. In semiconductors the current-carrying bands are separated by the *band gap* and do not overlap like in metals. The Fermi level is situated in this gap. The band above the Fermi level is called *conduction band* (CB) and is empty at T=0 and the band below the Fermi level is called *valence band* (VB) and is completely filled at T=0.

Intrinsic semiconductors are usually doped. This is a procedure which involves the addition of different elements to form p-type or n-type semiconductor. A p-type semiconductor is obtained adding a certain type of atoms (e.g. aluminum and gallium to silicon) in order to increase the number of free positive charge carriers called holes. Vice versa in an n-type semiconductor the addition of impurities (e.g. antimony and arsenic to silicon) greatly increases the conductivity of the semiconductor because the donor material provides electrons. In doped semiconductors the Fermi level is either close to the CB for an n-type semiconductor, or close to the VB for a p-type semiconductor.

When a semiconductor electrode is in contact with an electrolytic solution, a potential difference is established at the interface. This occurs mainly on the semiconductor side creating a region of potential variation close to its surface called the *space-charge region*. Here the behaviour of an n-type semiconductor electrode will be illustrated. In this case electrons are the majority carriers and holes are minority carriers. Figure 2.6a shows the band diagram before the semiconductor is in contact with an electrolytic solution and no potential is applied. When a potential is applied at a system of a semiconductor in contact to a solution, the semiconductor bands in the space charge region will bend based on the different potential applied. Different cases can be considered: (i) if there is no space region and the electrode is at flat band potential, bands will not bend (ii) there is an electron accumulation layer and bands will bend downwards. (iii) electrons are removed from the space charge

region and the bands will move upwards creating a depletion layer.[13] Figure 2.6 shows the cases of depletion and accumulation layers.

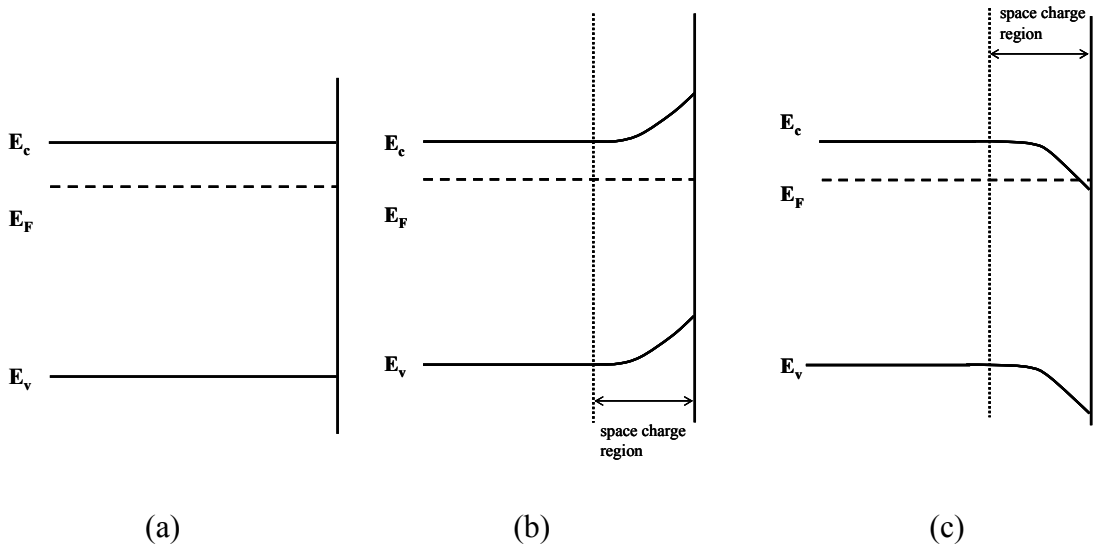

Figure 2.6 (a) Band diagram for an n-type semiconductor electrode, (b) depletion, (c) accumulation.

A case of a depleted layer of an electrode at equilibrium and with a negative overpotential applied is depicted in terms of Marcus theory in figure 2.7. At equilibrium the Fermi level of the semiconductor electrode equalizes with the redox Fermi level. When a negative overpotential is applied, the Fermi level will shift up and cathodic current may flow originating from electron transfer from the semiconductor conduction band to the overlapping unoccupied oxidizing agent level.

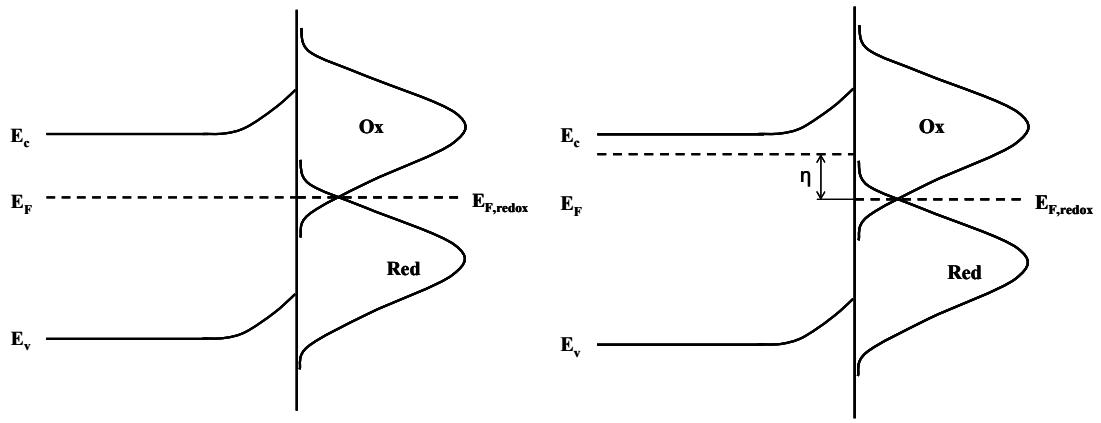

Figure 2.7 Marcus representation of a n-type semiconductor electrode in contact with an electrolytic solution under applied potential (a) at the equilibrium, (b) under a negative overpotential η applied.

Interaction between semiconductor and electrolyte solution is a very well studied phenomenon in DSCs. In particular the back reaction that occurs at the interface TiO_2 electrolyte containing the iodide /triiodide redox couple. This process should be minimised since the electrons which back react do not contribute to the photocurrent generated in a DSC.[14] This is due to a little band bending of the TiO_2 particles because the width of the space charge region is much greater than the particle size.

2.7 Diffusion

Diffusion, convection and migration, are the three modes of mass transport in electrochemical systems. It can be explained as the movement of chemical species (ions or molecule) under the influence of concentration difference. The species will move from the high concentration area to the low concentration area until the concentration is uniform in the whole phase. Diffusion is described by Fick's first and second law. Fick's first law in one dimension is represented by the equation 2.16

2.16
$$J = -D\frac{\partial c}{\partial x}$$

where J is the flux of species corresponding to the number of moles passing through a unit area as a function of time, D is the proportionality coefficient known as the diffusion coefficient, and the negative sign means that the flux is *down* the concentration gradient (typical values of D are 10^{-6}-10^{-5} cm^2 s^{-1}), $\frac{\partial c}{\partial x}$ represent the concentration gradient in direction x.

Fick's second law describe the variation of concentration with time and can be seen in figure 2.7 in a simple one dimension scheme of diffusion where the direction of diffusion opposes the concentration represented by equation 2.17

2.17

$$\frac{\partial c}{\partial t} = D\frac{\partial^2 c}{\partial^2 x}$$

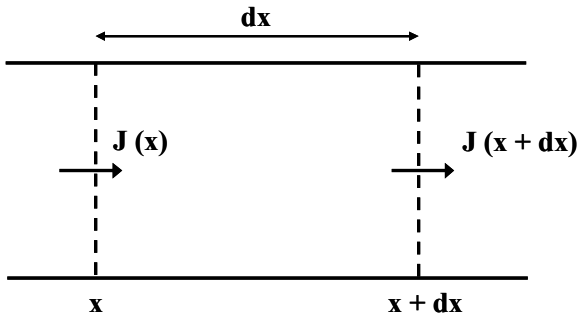

Figure 2.7 Representation of diffusion in one dimension.

This relationship for one dimension is relevant in electrochemistry since it predicts the concentration variation of an electroactive species close to the electrode surface in respect to both time and distance.

In order to obtain the concentrations of oxidized (O) and reduced (R) species, at a certain point x and time t, the partial differential equation should be solved. If the diffusion process is identified, the concentrations could be calculated when their initial values at t=0 and the values at certain position x (boundary conditions), are

known. For a homogeneous solution where only O is present the initial experimental conditions are

2.18 $C_O(x, 0) = C_O^*$

2.19 $C_R(x, 0) = 0$

Where C_O is the concentration of the oxidized species C_O^* is the concentration of oxidized species in the bulk solution and C_R is the concentration of the reduced species. The boundary conditions depend on the way the species diffuse and here two important cases can be mentioned; semi infinite-diffusion and limited diffusion.

In semi-infinite diffusion the conditions are

2.20 $\lim_{x\to\infty} c_O(x,t) = c_O^*$

2.21 $\lim_{x\to\infty} c_R(x,t) = 0$

Where $x \to \infty$ means that the concentration does not change during the experiment due to the large distance from the electrode. This condition applies to unstirred solutions.

Limited diffusion is the typical case of thin layer cell and electrochemically active species adsorbed at the surface of the electrode where

2.22 $c_O(x > L) = 0$

defining L as the layer thickness.

2.8 Electrocatalysis

Electrocatalysis is defined in its widest sense as the study of how reactions may be accelerated at electrodes. This often requires the surface of electrode to be modified in some way or for there to be a mediating molecule close to the electrode or in solution. These are called electrocatalysts or mediators. In DSCs electrocatalysis occurs between the Pt coated FTO counter electrode and triiodide species in the electrolyte solution, where Pt exhibits high electrocatalytic activity for triiodide reduction and, due to the high cost of Pt, it is important to look for alternatives. Recently Grätzel and co workers used CoS as electrocatalytic mediator obtaining good stability and performance for a DSC.[15] In the present work electrocatalysis was studied via cyclic voltammetry of N719 dye on FTO and FTO-TiO_2 electrodes in presence of low concentrations of iodine.

2.9 Cyclic voltammetry

Potential sweep methods are widely employed for the study of electrochemical systems. They consist of scanning a specific region of potential while measuring the current response resulting from the electron transfer to or from chemical species involved in the electrochemical reaction. Cyclic voltammetry is a potential sweep method which involves the use of a three electrode cell and a potentiostat which controls the potential and measures the current that flows between the electrodes.[16] The configuration of the cell foresees the use of the so called *working electrode (WE)*, *counter electrode (CE)*, and *reference electrode (RE)*. The working electrode is the electrode where the oxidation or reduction takes place, the counter electrode is used to pass the same current that is induced to flow through the working electrode (usually made of an inert metal such platinum), and the reference electrode is used as a reference point against which the potential of the working electrode can be measured. The electronics of the potentiostat ensure that no current flows between WE and RE because otherwise the RE could undergo chemical modifications which could cause its potential to change. The presence of the CE thus ensures that flux of current does not interfere with the RE chemical equilibrium. Figure 2.8a shows the potential waveform for cyclic voltammetry where the potential is swept from E_1 to E_2

as a function of time and swept back to E_1. In figure 2.8b is shown the graphical representation of a cyclic voltammetry. The experiment, related to a diffusive species at the surface of the electrode, shows a cyclic voltammogram where the curve represents the current response as a function of the potential applied to the electrochemical cell described above. Initially no current is flowing and when the potential where the electrode reaction begins is reached, the current start to rise until a certain point of a maximum value. The cyclic voltammogram in figure 2.8b is for a one electron transfer reversible reaction (those with fast electrode kinetics relative to the time-scale of the sweep), defined as a reaction that can proceed easily in either direction (oxidation and reduction) as the potential conditions change. Irreversible reactions are those in which, after the initial reduction or oxidation, the reaction cannot be reversed, so that the cyclic voltammogram shows a forward peak but no reverse peak.

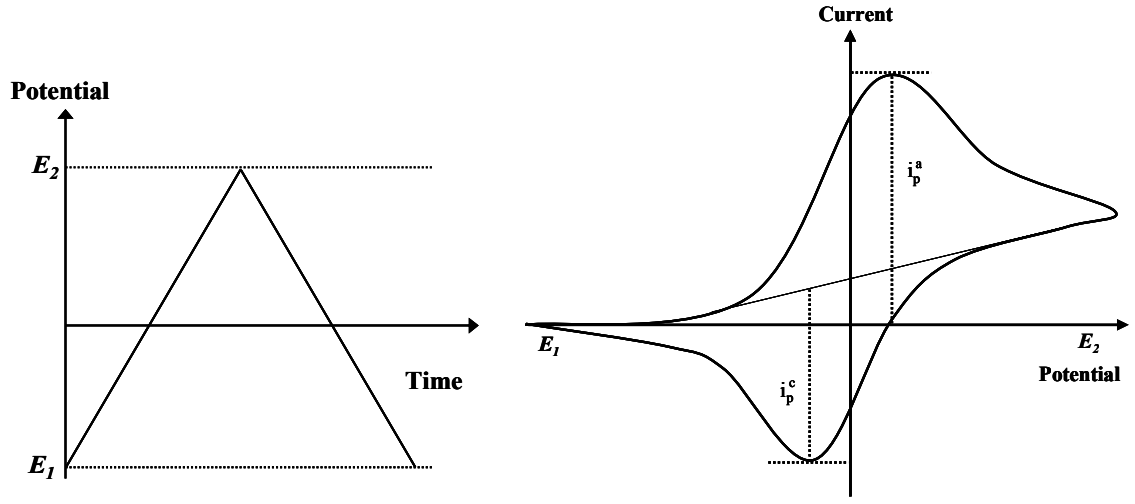

(a) (b)

Figure 2.8 (A) potential waveform of a cyclic voltammetry. (B) Cyclic voltammogram for reversible reduction and oxidation.

There are a few parameters that can be defined in order to better understand what information a cyclic voltammogram can give. The sweep rate at which the voltage is changed with the units of volt per second (Vs^{-1}), influences the shape of the cyclic voltammogram giving information on the properties of the system investigated.

Looking at the plot in figure 2.8b i_p^a and i_p^c are respectively the peak currents of anodic and cathodic processes, defined as

Anodic process $\quad R - e^- \rightarrow O$

Cathodic process $\quad O + e^- \rightarrow R$

Although the peaks have the same shape, the potentials at which they occur are different for the two processes (cathodic and anodic). As result, there is a peak-to-peak separation which is characteristically 59 mV for a reversible one-electron transfer at 25°C, independent of the scan rate. If we average the values of the potentials at which these processes occurs we find the mid-potential E_{mid} which is approximately equal to the standard potential of the reaction. Always in a three electrode cell, the potential is referred to a reference value, and in this work the Ag/AgCl (3M KCl) reference electrode has been used.

Cyclic voltammetry can be employed for the study of adsorbed redox active species immobilized at the surface of the working electrode. For a reversible one-electron transfer reaction, the ideal shape of a cyclic voltammogram is shown in figure 2.9 where it can be seen that the potential peak to peak separation is zero. This is due to the fact that no diffusion is present since the species is adsorbed at the electrode surface. An expression for i_p can be found from a derivative of the Nernst equation

2.23 $$i_p = \frac{n^2 F^2}{4RT} \nu A \Gamma_{total}$$

Where Γ is the surface coverage, ν is the scan rate, A is the active surface area of the electrode where the species is adsorbed and n is the number of electrons exchanged. The equation shows the direct proportionality of the peak current to the scan rate which is diagnostic of electrode reaction of adsorbed species.[17]

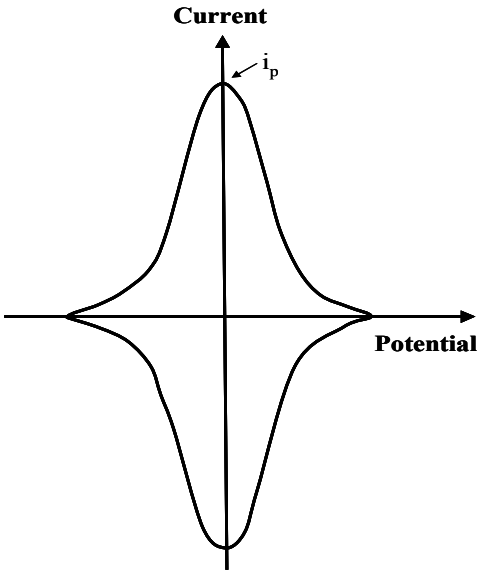

Figure 2.9 Ideal cyclic voltammogram for an adsorbed species under Nernstian conditions.

In this work, in order to investigate the adsorption process, we refer to the theory of the adsorption isotherm, specifically to the Langmuir isotherm. The Langmuir isotherm is based on three criteria: (i) adsorption cannot proceed beyond monolayer coverage, (ii) all surface sites are equivalent and can accommodate at most one adsorbed atom, (iii) the ability of a molecule to adsorb at a given site is independent of the occupation of neighbouring sites.[3] The calculation of the coverage of a monolayer at the active surface area of the electrode has been done as follows:

- calculation of the charge underneath the peak of a cyclic voltammogram using specific software for cyclic voltammetry experiments (Gpes Autolab)

- calculation of the moles corresponding to the charge (where it has been assumed that the process under investigation is a one-electron process and the charge is directly proportional to the concentration of molecules at the surface of the electrode)

$$n = \frac{Q}{F}$$

Where n is the number of moles, Q is the charge and F is the Faraday constant

- calculation of the total number of molecules, multiplying the number of moles by Avogadro's constant

$$molecules = n \times 6.022 \cdot 10^{23}$$

This simple procedure allows us to compare the number of molecules which could fit at the surface of the electrode active area, calculated from experimental data, with the theoretical number of sites available for monolayer coverage.

2.10 Coupled homogeneous reactions

It has been seen that cyclic voltammetry is useful to investigate processes at the electrodes surfaces of electro active species where (O) is converted in a heterogeneous electron transfer to a product (R).[18] There are also cases where the electron transfer reaction of species O or R is coupled with homogeneous chemical reaction. In this case what could happen is that an electron transfer gives a product that is unstable. If E represents an electron transfer at the electrode surface and C a homogeneous chemical reaction, is possible to define a two step process that is referred to as an EC reaction

E $\qquad O + ne^- \rightleftharpoons R$

C $\qquad R \longrightarrow X$

Where O and R are the oxidised and reduced species and X is the inactive product of the electrode reaction R which is not electro active at the potentials where O is active. Furthermore, if the chemical step that leads to an inactive product is irreversible, the label EC_{irr} is sometimes used.

The cyclic voltammogram for an EC reaction differs from that of a stable electrode reaction previously shown (figure 2.8b). For the EC reaction, R is unstable and decays. Although the peak of the forward scan (O to R) is similar for both reversible and EC reactions, as the potential is swept back from R to O, the reverse peak

disappears due to the fact that R has been destroyed through homogeneous reaction leading to the product X. Figure 2.10 shows the trend of cyclic voltammograms of an EC reaction generated with Digisim software. It shows the influence of increasing the rate constant for the forward processes k_f that leads to the loss of reversibility, where (i) $k_f = 10^6$ s^{-1} (ii) $k_f = 10^4$ s^{-1} (iii) $k_f = 10$ s^{-1}. If k_f is significantly fast, as soon as R is formed at the surface of the electrode, it disappears due to homogeneous reaction.

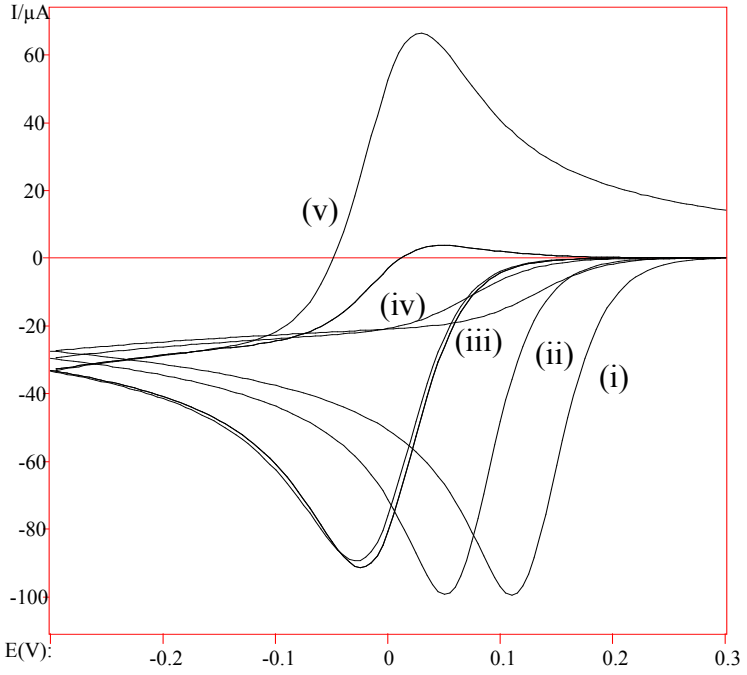

Figure 2.10 Cyclic voltammetry of an EC reaction generated with Digisim, increasing the rate constant k_f from (i) to (v). Values of 10^{-5} cm^2 s^{-1} were used for diffusion coefficients for all the species involved in the EC mechanism. Concentration were for O = 10^{-3} mol dm^{-3}; R = 0 mol dm^{-3}; X = 0 mol dm^{-3}.

Another mechanism among the coupled homogeneous reactions is the EC ' (catalytic mechanism) defined by the following scheme

E $\qquad\qquad$ $O + ne^- \rightleftarrows R$

C ' $R + Z \longrightarrow O + Y$

Where the product of the reaction R reacts with an electro-inactive species in order to regenerate O and an additional product Y. The term catalytic defines the processes where the homogeneous reaction regenerates the reagent of the electrode reaction. Figure 2.11 illustrates Digisim simulation for cyclic voltammograms of an EC ' mechanism. The current voltage curve with the lowest current corresponds to the case where no Z has been added to the solution and therefore no chemical reaction occurs. As soon as Z is added, the catalytic reaction can start and for a fixed scan rate and concentration of Z, the current will be higher than when no Z is present in solution. This is due to the fact that the reactant O is regenerated during the reaction and so that can react again at the electrode surface. As the quantity of Z is increased the current also increases since more chemical reaction occurs.

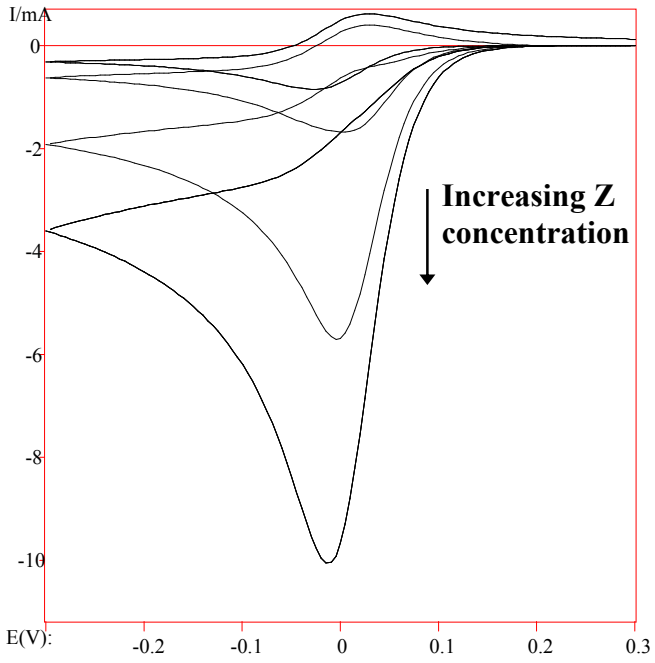

Figure 2.11 Digisim simulations for cyclic voltammograms representing an EC ' mechanism. The effect of the increase of species Z is shown. Diffusion coefficients used in this simulation were 10^{-5} cm^2 s^{-1} for all species involved in th EC' mechanism. Concentrations used in the simulation were O = 0.01 mol dm^{-3}, R = 0.05 mol dm^{-3}, Z = 0.1 mol dm^{-3}.

2.11 Spectroelectrochemistry

Spectroelectrochemistry is a coupled technique which involves the use of spectroscopic and electrochemical methods. Spectroscopy deals with the interaction of atoms ions and molecules with electromagnetic radiation, electrochemistry with charge transfer at the electrode surfaces. In general the electromagnetic radiation does not interfere with the electrochemical reaction giving as a result spectra that are related exclusively to the reaction occurring at the surface of the electrodes.[19] Spectroscopy in the UV-Vis range is the most common employed for the characterisation of the charge transfer in an electrochemical system due to the nature of species under investigation which are often coloured and with high extinction coefficient. In fact changes in Abs can be monitored when a species that is generated electrochemically undergo for example a reduction or oxidation, leading to a species which has changed its colour. The first and one of the most widely used technique for spectroelectrochemical experiments is related to the use of OTE (optically

transparent electrode),[20] which is usually made of a glass plate coated with conductive but optically transparent layer of either ITO (indium doped tin oxide) or FTO (fluorine doped tin oxide). The spectroelectrochemical cell set up is depicted in figure 2.12 where the OTE is used as working electrode, platinum wires as counter and reference electrodes, all immersed in a solution phase (electrolyte with redox system) contained in a standard cuvette.[21]

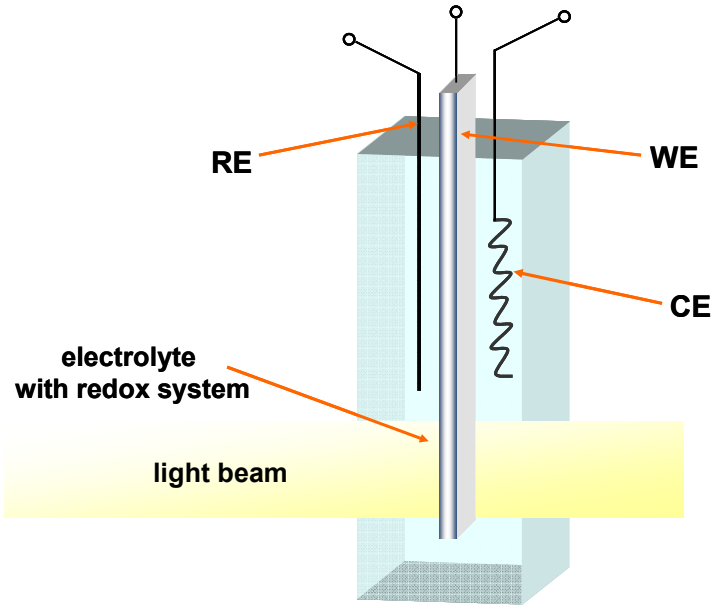

Figure 2.12 Spectroelectrochemical cell.

The cell is placed in a spectrometer in such a position that the light beam path is not obstructed by either CE or RE. Different electrochemical and spectroscopic techniques can be used to probe processes in both, solution and at electrode surfaces. In the present work a special spectroelectrochemical cell has been built (see chapter Experimental Techniques and Methods), in order to characterize the redox behaviour of dyes adsorbed at the surface of an optical transparent electrode. The experiment is conducted by applying an initial potential where the redox system does not react. Then a step potential is applied in the region in which the electrochemical conversion occurs. Spectra are recorded at regular time intervals monitoring qualitatively the course of the oxidation or reduction reactions, occurring at the surface of the working electrode.

References

1. Wang, P.; Zakeeruddin, S. M.; Comte, P.; Charvet, R.; Humphry-Baker, R.; Gratzel, M., *Journal of Physical Chemistry B* **2003,** *107* (51), 14336-14341.
2. Nazeeruddin, M. K.; Kay, A.; Rodicio, I.; Humphrybaker, R.; Muller, E.; Liska, P.; Vlachopoulos, N.; Gratzel, M., *Journal of the American Chemical Society* **1993,** *115* (14), 6382-6390.
3. Atkins, J. d. P. a. P., *Physical Chemistry*. Seventh ed.; Oxford University Press Inc.: New York, 2002.pag 491.
4. Forsterling, H. K. a. H.-D., *Principles of Physical Chemistry*. John Wiley & Sons Ltd: New York, 2000.
5. Nazeeruddin, M. K.; Zakeeruddin, S. M.; Humphry-Baker, R.; Jirousek, M.; Liska, P.; Vlachopoulos, N.; Shklover, V.; Fischer, C. H.; Gratzel, M., *Inorg. Chem.* **1999,** *38* (26), 6298-6305.
6. Wang, P.; Zakeeruddin, S. M.; Moser, J. E.; Nazeeruddin, M. K.; Sekiguchi, T.; Gratzel, M., *Nature Materials* **2003,** *2* (7), 498-498.
7. Schmidt-Mende, L.; Bach, U.; Humphry-Baker, R.; Horiuchi, T.; Miura, H.; Ito, S.; Uchida, S.; Gratzel, M., *Advanced Materials* **2005,** *17* (7), 813-+.
8. Kuang, D.; Uchida, S.; Humphry-Baker, R.; Zakeeruddin, S. M.; Gratzel, M., *Angewandte Chemie-International Edition* **2008,** *47* (10), 1923-1927.
9. Howie, W. H.; Harris, J. E.; Jennings, J. R.; Peter, L. M., *Solar Energy Materials and Solar Cells* **2007,** *91* (5), 424-426.
10. Gao, F.; Wang, Y.; Shi, D.; Zhang, J.; Wang, M. K.; Jing, X. Y.; Humphry-Baker, R.; Wang, P.; Zakeeruddin, S. M.; Gratzel, M., *Journal of the American Chemical Society* **2008,** *130* (32), 10720-10728.
11. Morrison, S. R., *Electrochemistry at Semiconductor and Oxidised Metal Electrodes*. Plenum Press: New York, 1980.
12. Bard, L. R. F. A. J., *Electrochemical Methodes Fundamaentals and Applications*. John Wiley & Sons Inc.: New York, 2001.
13. Christopher M. A. Brett, A. M. O. B., *Electrochemistry (Principles, Methods, and Applications)*. Oxford University Press: New York, 1993.
14. Peter, L. M.; Wijayantha, K. G. U., *Electrochimica Acta* **2000,** *45* (28), 4543-4551.
15. Wang, M. K.; Anghel, A. M.; Marsan, B.; Ha, N. L. C.; Pootrakulchote, N.; Zakeeruddin, S. M.; Gratzel, M., *Journal of the American Chemical Society* **2009,** *131* (44), 15976-+.
16. Compton, R. G., *Understanding Voltammetry*. World Scientific Publishing Co. Pte. Ltd.: 2009.
17. Christopher M. A. Brett, A. M. O. B., *Electroanalysis*. Oxford University Press: New York, 2005.
18. Fisher, A. C., *Electrode Dynamics*. Oxford University Press: New york, 2205.
19. Kavan, L.; Dunsch, L., *Chemphyschem* **2007,** *8* (7), 975-998.
20. Kuwana, T.; Heineman, W. R., *Accounts Chem. Res.* **1976,** *9* (7), 241-248.
21. Scholz, F., *Electroanalytical Methods*. Springer: 2005.

Chapter 3: Experimental Techniques and Methods

This chapter is divided in two main sections. One is related to the experimental techniques and the second is related to the methods for the preparation of electrodes, chemicals used, and the fabrication of DSCs discussed in this work.

3.1 Experimental techniques

3.1.1 Cyclic voltammetry

For voltammetric studies an Autolab potentiostat (PGSTAT 12 Ecochemie, Netherlands) was employed. A Pt foil counter electrode was employed with a surface area of 30 mm^2. The working electrode was a FTO (fluorine-doped tin oxide) coated glass from Asahi Glass Fabritech (AGC type U TCO glass, Japan). The grade of FTO was TEC 15 with resistance of 12-14 Ω/□. The active exposed surface area for the FTO electrodes was 9 mm^2 or 42 mm^2. The reference electrode employed was a Ag/AgCl (3 M KCl) from CH Instruments Inc which was connected to a home made luggin capillary. Experiments were conducted after thorough de-aerating with argon for at least 15 minutes. The temperature during the experiments was 20 ± 2 ^oC. Figure 3.1 shows a schematic representation of the electrochemical cell used in this work.

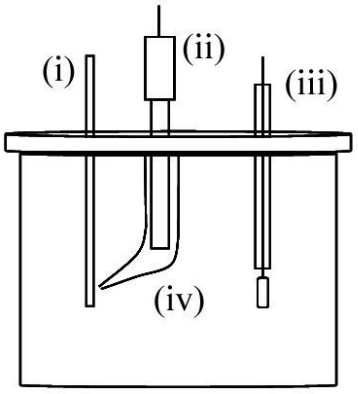

Figure 3.1 Electrochemical cell, (i) FTO working electrode, (ii) Ag/AgCl (3 KCl M) reference electrode, (iii) Pt foil counter electrode, (iv) Luggin capillary.

The value of ca. 300 Ω for the uncompensated resistance of this configuration can be calculated based on the resistance values of tetrabutyl perchlorate in ACN found in the literature.[1]

3.1.2 Spectroscopy and Spectroelectrochemistry

UV/VIS spectroscopic and spectroelectrochemical studies were carried out with Varian Cary 50 UV-Vis spectrophotometer. For spectroelectrochemical studies a potentiostat from Ivium Technologies (Compactstat electrochemical interface) was employed and experiments were conducted under constant argon flux. The working electrode was a FTO (fluorine-doped tin oxide). The active exposed surface area for the FTO electrodes was 42 mm^2. Counter electrode and reference electrodes were respectively Pt foil and Pt wire and a Luggin capillary was also used. The temperature during the experiments was $20 \pm 2\ ^oC$.

As a general consideration a cell for spectroelectrochemical studies should match the following requirements. It should guarantee good electrical properties in order to minimize the iR drop, should have a potentiostat system able to sustain potential steps and current transient without distortion, and a proper cell design so that CE and RE do not interfere with the electrochemical processes at WE, and neither with spectroscopic detection.[2]

In order to carry out spectroelectrochemical experiments, a special cell was built made of PTFE filled glass and fitted in the spectrometer using a special cell holder. The following figures (3.2-3.7) show in detail the different sides of the cell. The units are mm. The cell is made by two pieces connected together by four screws, the body and the lid (figure 3.2, 3.3). The body has a hole in the middle which allows light to go through; quartz lenses were used in order to contain the solution in the cell and being transparent to the light. The body has two chambers that can be seen from the top view in figure 3.6. The electrodes are fitted in the lid in two different ways. Counter electrode and reference electrode are inserted through holes in the lid whereas the working electrode is fixed by a screw in the internal part of the lid which can be seen in figure 3.5. The WE cannot be seen from the outside. The reason why is because with this approach the WE is not exposed to the air and moreover its

active area (where the dye is adsorbed) is not damaged by insertion through a tight hole. Connection to the WE was made internally by a Pt wire that can be seen in figure 3.3 in the lid. CE and RE are not in the light path to the WE.

The spectroelectrochemical cell was filled in the bigger chamber (figure 3.6) with a solution of acetonitrile and 0.1M NBu_4PF_6. The electrodes were fitted in the lid and then the lid fixed at the body by the 4 screws. Once sealed, the cell was placed in the spectrometer and kept in the dark. In order to ensure that no air would interact with the solution the cell was kept under argon flux. Connections to the electrodes were made through wires coming from the potentiostat and attaching to the cell inside the spectrometer.

The experiment was conducted applying a step potential initially in the potential region where the species adsorbed on the WE were not active then in the region where the redox processes were occurring. Usually the potential were scanned backward after ten minutes from the forward scan, due to the time to set up the potentiostat.

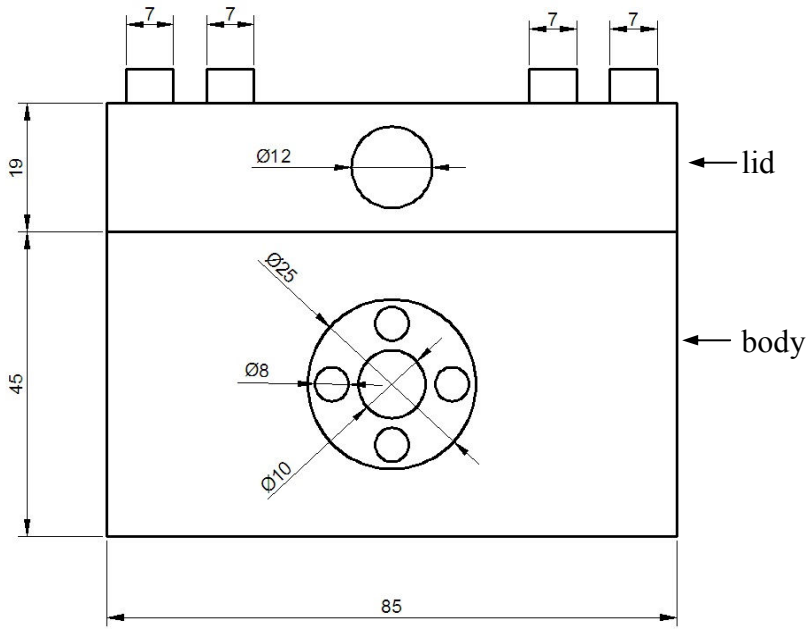

Figure 3.2 Front side.

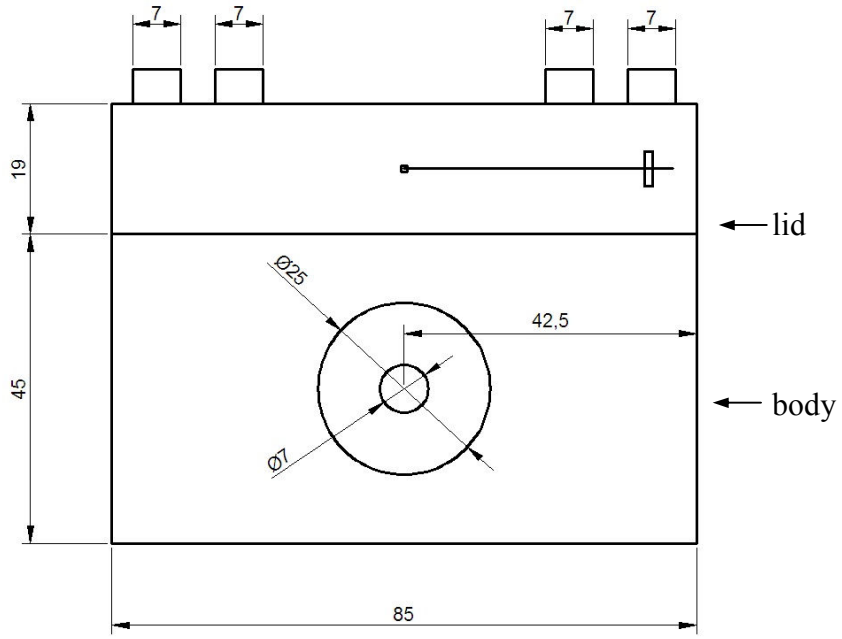

Figure 3.3 Back side.

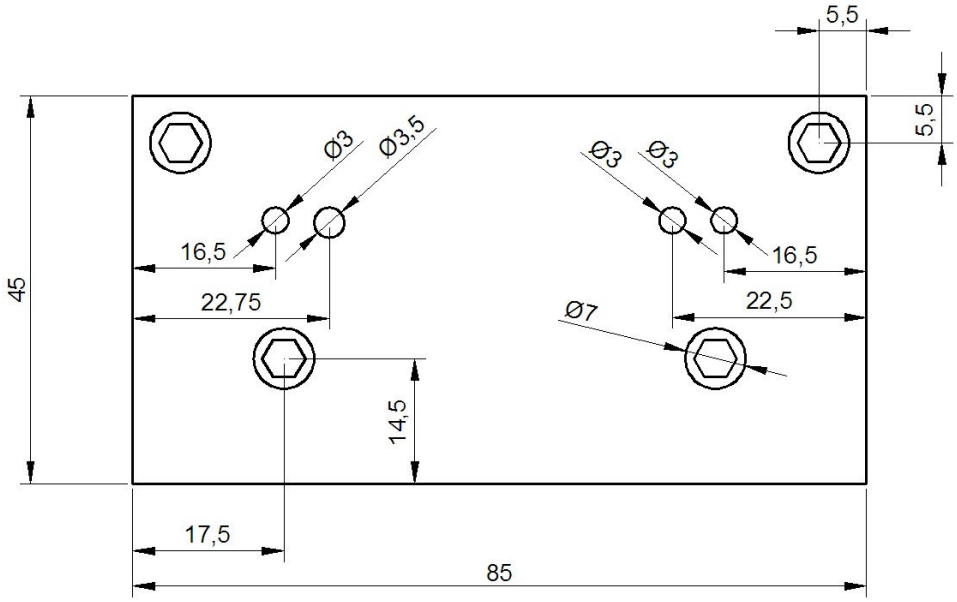

Figure 3.4 Top view.

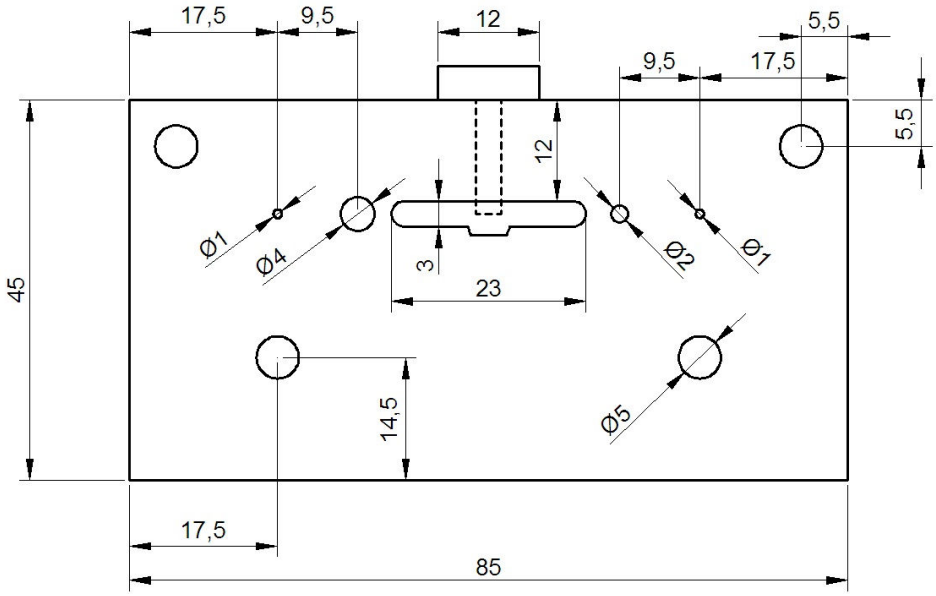

Figure 3.5 Internal side of the lid, the dashed line represents the screw which is used to fix the working electrode against the lid wall.

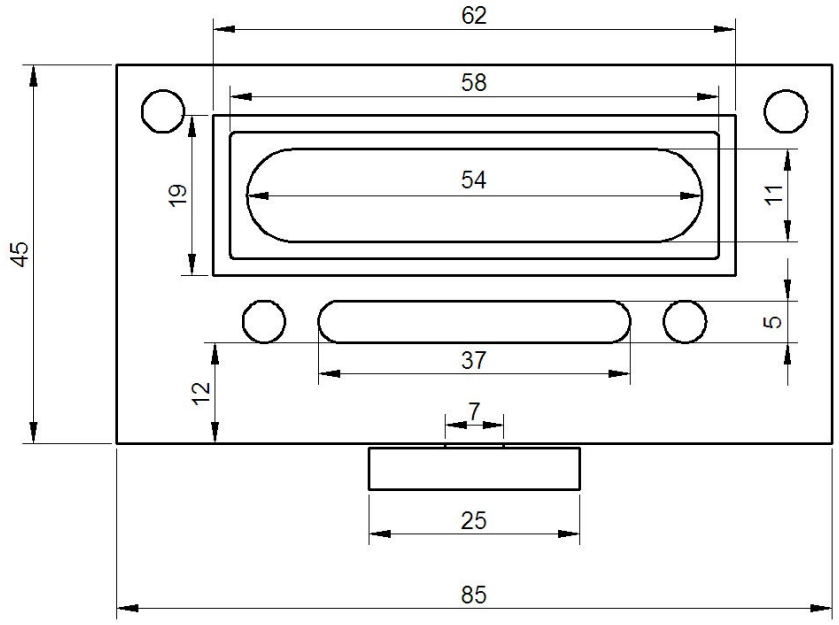

Figure 3.6 Top view of the body.

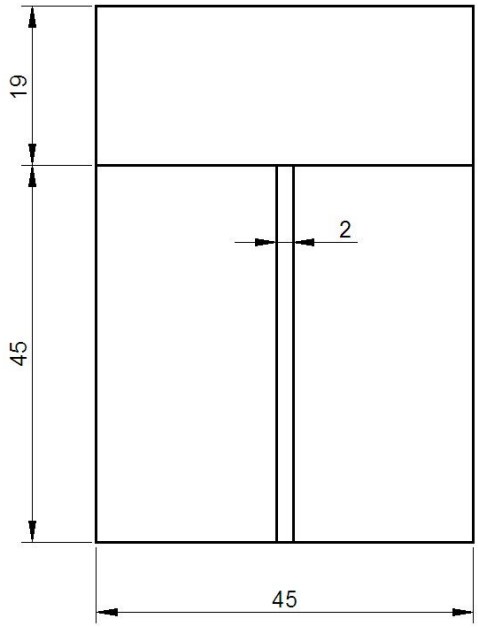

Figure 3.7 Side view (symmetric for both the two sides).

3.1.4 Incident photon-to-current conversion efficiency (IPCE)

In this work DSCs were made with organic dyes (see chapter 6) and the IPCE was measured with spectral resolution of 5nm using light from a xenon lamp and a Bentham monochromator in a spectral range of 400 to 800 nm. A yellow filter (Schott GG550) was used to remove the second-order light diffraction at wavelengths longer than 550 nm. The incident photon flux was measured with a calibrated Si photodiode under the same cell conditions, as a calibration to calculate the IPCE value of the DSC. Figure 3.8 shows the experiment set up. The lamp generates light in the visible spectrum and the monochromator, previously set, mechanically scans different wavelengths. The light beam is focused by a lens into the cell active area (approximately 1 cm^2). The generated current is sent to a potentiostat which transform the current into a potential, the value is read by the lock-in amplifier which filters out the components of the signal from the cell that do not correspond to the driving frequency. Finally the data are collected and saved by the computer.

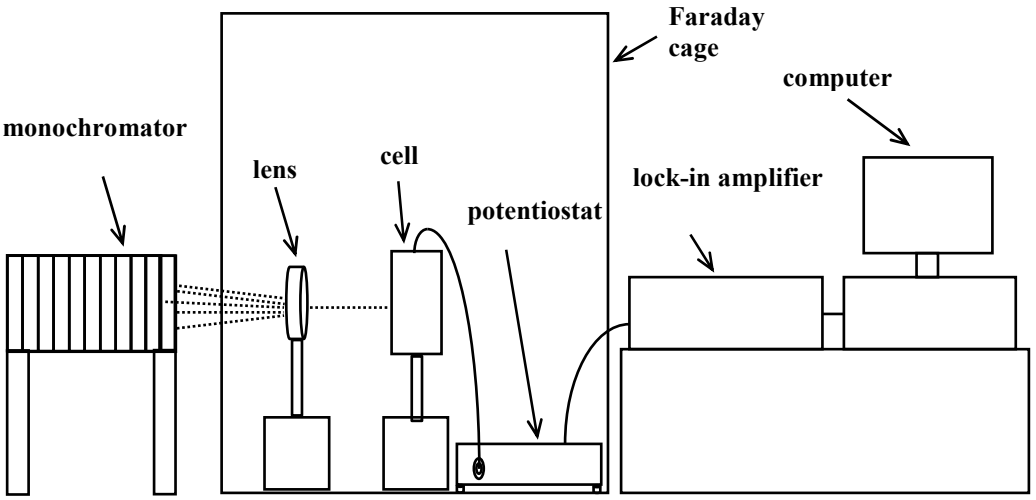

Figure 3.8 IPCE set up

3.1.5 Current-voltage characteristic

The schematic setup to measure the current-voltage response of the cell is shown in figure 3.9. The current-voltage characteristics of the cells were measured under simulated AM 1.5 illumination (100mWcm^{-2}) provided by a solar simulator (1kW Xe with AM 1.5 filter, Müller). A GaAs solar cell was used for calibration of the light intensity. The voltage applied to the cell was scanned cyclically from 0 to V_{OC}, whilst the current response was recorded.

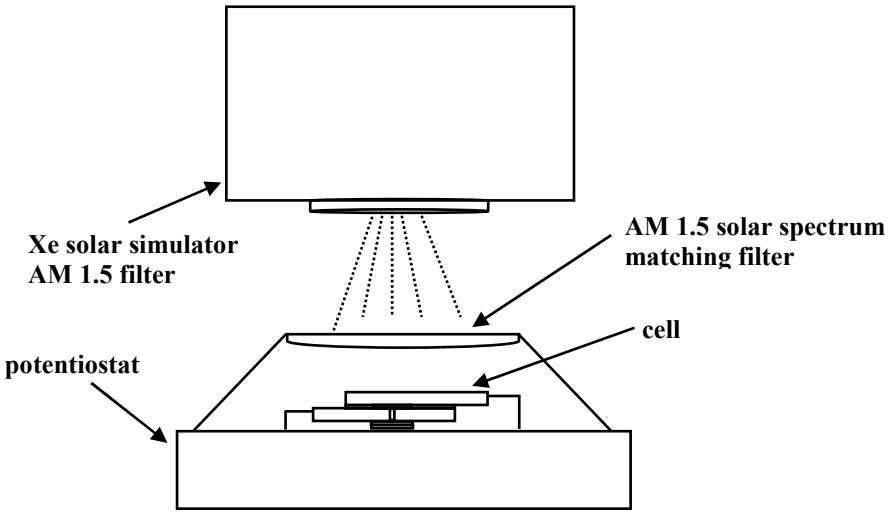

Figure 3.9 Current-voltage set up.

3.2 Methods

3.2.1 Chemical and reagents

All chemicals were used as received. Acetonitrile (HPLC grade) was obtained from Fisher Scientific. Tetrabutylammonium hexafluorophosphate (NBu_4PF_6, electrochemical grade), tetrabutylammonium iodide (puriss.) and tert.-butanol (ACS > 99.7% GC) were purchased from Fluka. LiI (anhydrous 99.99%) was obtained from Aldrich. 3-propyl-1-mithyl imidazolium (98%) from Merk. Tert butyl pyridine, valeronitrile and iodine were from Sigma-Aldrich. The dye Z907 *cis*-bis (isothiocyanato) - (2,2'-bipyridyl-4,4'-dicarboxylicacid)-(2,2'-bipyridyl-4,4'-dinonyl) ruthenium(II), TiO_2 HT colloid (9 nm average particle diameter), SX1170-25 hot-melt polymer spacer were purchased from Solaronix. The organic dyes D102, D131, D149, D205 where purchased from Chemicrea inc. (Japan). The metal complex $RuL(bipy)_2^{2+}$ with L=4,4'-dicarboxylic acid-2,2'-bipyridine was prepared following a literature procedure.[3] Sodium hydroxide (Sigma ultra minimum 98%) was obtained from Sigma-Aldrich. Ethanol (absolute) was purchased from Fisher Scientific. FTO (fluorine-doped tin oxide) coated glass from Asahi Glass Fabritech (AGC type U TCO glass, Japan).

3.2.2 Procedure for electrode preparation and dye adsorption

FTO slides were washed and sonicated (400 W Fisher ultrasound bath) 6 times for 15 minutes each in 5 % Deconex, water Milli-Q, ethanol, twice in isopropanol, and finally analytical grade ethanol. After cleaning a gold stripe was evaporated onto FTO electrodes (excluding active area) in order to reduce series resistance.

The electrodes were heated for 30 minutes at 450 °C on a hot plate, cooling down to 75 °C and then immersed in a dye bath. Electrode size for electrochemical experiments was 32x4 mm with active area of either 42 mm^2 or 9 mm^2. For spectroelectrochemical experiments was 42x7 mm with active area of 0.42 mm^2.

FTO-TiO_2 was prepared by "doctor blading" technique (uniformly spreading TiO_2 paste on a defined area of FTO glass with a glass bar), figure 3.10.

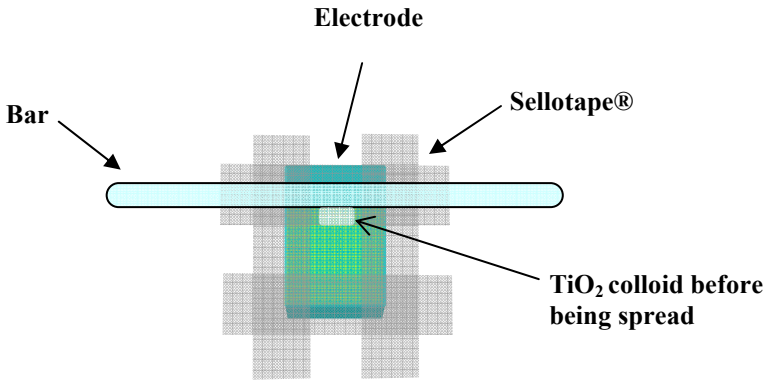

Figure 3.10 Electrode fixed by Sellotape®, a small amount of titanium dioxide is left on the top edge of Sellotape® and spread down by the bar.

The TiO_2 film thickness was measured by cross sectional SEM (Scanning Electron Microscopy). Electrodes were cut in order to expose the nano crystalline TiO_2 along the edge. The samples were then mounted so that the edge supporting the exposed TiO_2 was upwards. Gold was evaporated onto the surface to improve the SEM resolution.

Unless otherwise specified, the dyes were adsorbed on FTO and FTO-TiO_2 electrodes through immersion in 50% acetonitrile 50% *tert.*-BuOH solutions of ruthenium-based and organic dyes for a given time; typically one hour for experiment using FTO electrodes and 16 hours for FTO-TiO_2 electrodes. The concentrations of the dye baths varied according to the different experiments carried out (see chapter 4, 5 and 6).

3.2.3 Fabrication of DSCs

FTO electrodes were cleaned according to the procedure described above (3.2.2). The two slides were prepared differently based on the use as counter or photo electrode. The size of the electrodes was 25x15 mm.

3.2.3.1 Photoelectrode

A blocking layer[4-5] of titanium dioxide was deposited by spray pyrolysis[6] on the surface of the photo electrode using 0.2 M solution of titan(IV) bis(acetylacetonato)-diisopropylate in isopropanol (HPLC grade). Subsequently a layer of colloidal n-TiO_2 was spread on a defined area (usually 1 cm^2) employing the doctor blading technique (3.2.2). The electrode was then heated at 450°C for 30 minutes in a furnace and cooled down to 75°C and finally immersed in dye bath solution 50% acetonitrile 50% *tert.*-BuOH. Usual concentration of a dye bath for DSCs is 0.5 mM. Figure 3.11 shows the photo electrode after blocking layer and TiO_2 deposition.

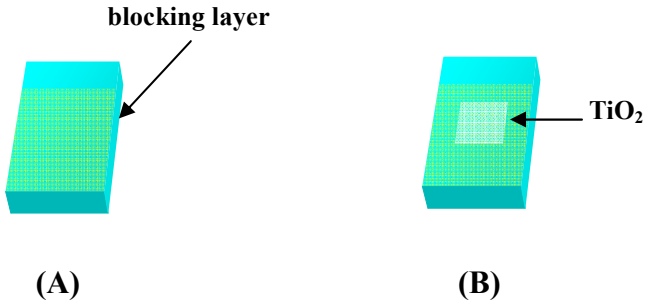

Figure 3.11 (A) Photo electrode showing the blocking layer, (B) after doctor blading with TiO_2 deposited.

3.2.3.2 Counter electrode

The counter electrode instead was treated with a platinum solution using approximately 15 µL of a 5 mM of hexachloroplatinate ($H_2PtCl_6 \cdot 6H_2O$) in iso-propanol onto the conducting surface. Subsequently the electrode was annealed to 400° C for 20 minutes resulting in a Pt coated FTO electrode. Two small holes were drilled previous to platinum deposition in order to facilitate the injection of the electrolyte via a syringe when the cell was completed.

3.2.3.3 Electrolyte

The electrolyte composition used in the cells made and reported in this work (see chapter 6) was; LiI 1.0 M, 3 propyl-1-methyl imidazolium iodide 0.6 M, I_2 0.05 M, tert-butyl pyridine 0.5 M in acetonitrile 50% and valeronitrile 50%.

3.2.3.4 Cell assembling

The two electrodes were then sandwiched together using the hot-melt spacer. Firstly the hot-melt was cut and shaped in the way that could seal and not cover the area where the dye was adsorbed. Secondly the spacer was placed on the dye sensitized photo electrode and then the platinised counter electrode was placed on top of it. The cell assembled was then moved and kept for a few seconds to a hot plate at 120°C, temperature which causes the hot-melt to melt and seal the cell.

Finally the cell was filled with the electrolyte through the counter electrode holes. After filling, the holes were sealed with pieces of glass microscope slide using hot-melt polymer. The exposed areas of FTO on each electrode were used to form external connections to the cell and were coated in a layer of conductive silver paint (RS).

References

1. House, H. O.; Feng, E.; Peet, N. P., *Journal of Organic Chemistry* **1971,** *36* (16), 2371-&.
2. Scholz, F., *Electroanalytical Methods*. Springer: 2005.
3. Pearson, P.; Bond, A. M.; Deacon, G. B.; Forsyth, C.; Spiccia, L., *Inorganica Chimica Acta* **2008,** *361* (3), 601-612.
4. Cameron, P. J.; Peter, L. M., *Journal of Physical Chemistry B* **2003,** *107* (51), 14394-14400.
5. Cameron, P. J.; Peter, L. M.; Hore, S., *Journal of Physical Chemistry B* **2005,** *109* (2), 930-936.
6. Kavan, L.; Gratzel, M., *Electrochimica Acta* **1995,** *40* (5), 643-652.

Chapter 4: Cis-bis(isothiocyanato)-bis(2,2'-bipyridyl-4,4'dicarboxylato)-Ru(II) (N719) dark-reactivity when bound to fluorine-doped tin oxide (FTO) or titanium dioxide (TiO_2) surfaces

Contents

The work presented in this chapter is based on a peer reviewed publication:

Cis-bis(isothiocyanato)-bis(2,20-bipyridyl-4,40dicarboxylato)-Ru(II) (N719) dark-reactivity when bound to fluorine-doped tin oxide (FTO) or titanium dioxide (TiO2) surfaces Alberto Fattori, Laurence M. Peter, Stephen R. Belding, Richard G. Compton, Frank Marken, Journal of Electroanalytical Chemistry 640, **2010** 61–67.

4.1 Abstract

The solar cell sensitizer *cis*-bis(isothiocyanato)-bis(2,2'-bipyridyl-4,4'dicarboxylato)-ruthenium(II) (N719) is adsorbed and investigated at two electrode surfaces: (i) at a bare fluorine-doped tin oxide (FTO) and (ii) at a nano-particulate anatase (TiO_2) film in contact with FTO. N719 is adsorbed from acetonitrile onto FTO surfaces giving poor quality partial or multi-layer coverage commencing at 10^{-7} molar concentration. In contrast, from 50% acetonitrile 50% ^{t}BuOH solution of N719 Langmuirian adsorption occurs with well-defined mono-layer coverage and a binding constant ca. 2×10^5 mol^{-1} dm^3. The adsorbed N719 exhibits voltammetric oxidation/back-reduction responses with $E_{mid} \approx 0.56$ (weaker) and 0.68 (dominant) V vs. Ag/AgCl (3 M KCl) and with chemically reversible characteristics at sufficiently high scan rates (ca. 16 Vs^{-1}). A chemical reaction step involving oxidized N719 at the electrode surface leads to the loss of electrochemical activity at slower scan rates with a first order chemical rate constant of ca. 2.4 s^{-1}. The electro-catalytic oxidation of iodide is demonstrated for both the intact metal complex N719 and the reaction product formed after oxidation. When adsorbed onto TiO_2 (porous films made from approximately 9 nm diameter TiO_2 particles, Langmuirian binding constant ca. 10^5 mol^{-1} dm^3), immersed in acetonitrile (0.1 M NBu_4PF_6), and at sufficiently fast scan rates (ca. 16 Vs^{-1}), the N719 metal complex exhibits reversible voltammetric responses (with $E_{mid} \approx 0.68$ V vs. Ag/AgCl (3 M KCl)). At slower scan rates, the voltammetric response again appears irreversible, however, this time *without* significant degradation of the N719 metal complex at the TiO_2 surface. It is shown that the conduction mechanism via electron hopping becomes ineffective due to degradation of FTO-adsorbed N719. In the presence of iodide, the electrocatalytic iodide oxidation process (dark electrocatalysis) is shown to occur predominantly at the N719-modified FTO electrode surface. Implications of this dark reactivity for the solar cell performance are discussed.

4.2 Introduction

As discussed in chapter 2.1, in a DSC upon a photon absorption an electron is excited from the HOMO to the LUMO of the dye, followed by ultrafast electron injection into the conduction band of the TiO_2.[1] Injected electrons accumulate in the TiO_2 and subsequently diffuse towards the FTO substrate where they are extracted into the external circuit.[2] Meanwhile, photo-oxidised dye molecules are reduced back to their original state by iodide species in the electrolyte (regeneration).[3-6] Several other processes can occur in the working solar cell: geminate recombination of injected electrons with oxidised dye molecules, transfer of conduction band electrons to oxidised electrolyte species, and degradation of the oxidised dye by undesirable side reactions before regeneration has taken place.[7] The competition between these processes (regeneration, recombination, and degradation) is important in determining the overall efficiency and useful lifetime of the solar cell.[8-9] Efficient regeneration of the dye is crucial to obtain a high turnover number for the sensitizer so that the lifetime is acceptably long.[10] The long-term stability of the DSCs has been estimated by real-time and accelerated aging experiments to be 5-10 years, although some disagreement still exists in the literature.[11-14] While these aging experiments are an important practical test of the solar cell, they provide no mechanistic information about the cause of any deterioration in performance. Detailed knowledge of the mechanisms and rates of regeneration and degradation of N719 (figure 4.1) is clearly important in order to predict and improve the long term stability of DSCs.

Various different techniques have been employed in order to determine the photophysical properties of dyes.[15-18] Electrochemical techniques such as cyclic voltammetry (chapter 2.9) are useful for investigating redox properties and determine reversible potentials of dyes. Previous electrochemical studies of the dye N719 have mainly focused on the dye in solution, using a range of different solvents and working electrodes.[19-21] Wolfbauer investigated the effect of deprotonation on the dye properties.[22] Bond et al. reported complex anodic redox chemistry for N719 in acetone or acetonitrile solution where the oxidation of the dye is accompanied by chemical processes in solution or adsorbed to the electrode surface.[19] Several types of electrodes including glassy carbon, platinum, and gold were employed and a second oxidation process associated with the adsorbed dye identified. The important

case of the electrochemistry of N719 adsorbed on FTO has not been investigated previously, although chemically more inert ruthenium metal complexes adsorbed onto FTO [23] and onto TiO_2 [24] surfaces have been well studied. Important information about the chemical rate constants for decay reactions involving N719 at oxide surfaces and their effects on surface conductivity have not been previously reported.

Redox active species when immobilized on inert metal oxide surfaces such as TiO_2 give rise to surface conduction phenomena via electron hopping.[25] This kind of mechanism is central to the reactivity of N719 and related dyes under conditions where redox cycling occurs driven by an applied electrode potential. For a range of dye systems including N719 Grätzel et al. have demonstrated that hopping conduction at the surface of TiO_2 is possible via charge percolation.[26] Importantly, the molecular structure of the dye and the mode of adsorption were shown to affect the rate of electron hopping. Typical hole hopping rates were reported in terms of the apparent diffusion rate 10^{-13} m^2s^{-1} for mesoporous TiO_2 electrodes immersed in acetonitrile. For the case of N719 irreversible behaviour was reported due to a chemical reaction step and the percolation of charge was observed to be impeded by (i) slower hole hopping due to poorly aligned thiocyanate ligands and (ii) lower conductivity due to the chemical degradation of N719 eliminating charge percolation pathways.

In the present work, the adsorption and electrochemical reactivity of N719 are revisited. First the adsorption and reactivity on FTO are studied and then adsorption and reactivity on nanoparticulate TiO_2 are investigated with the aims of (i) obtaining and comparing binding constants for adsorption, (ii) quantifying the electrochemical stability of the adsorbed N719 on FTO and on TiO_2, and (iii) investigating the dark electrocatalytic iodide oxidation at immobilized N719. The degradation and regeneration of oxidised N719 is studied using voltammetric techniques, and a rate constant for the degradation process in acetonitrile is estimated. It is also demonstrated that both electrochemically-active N719 and the electrochemically-inactive degradation product of N719 act as dark electro-catalysts for iodide oxidation. A potentially ***beneficial*** role of the N719 degradation process in suppressing dark recombination processes during DSC operation is proposed.

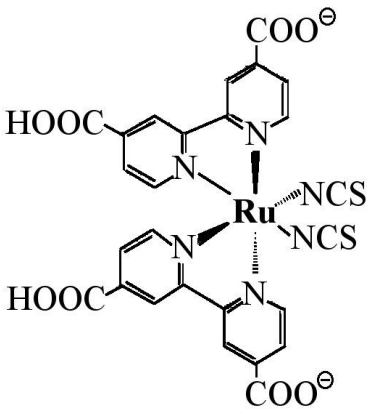

(N719)

Figure 4.1 Molecular structure of the solar cell dye *cis*-bis(isothiocyanato)-bis(2,2'-bipyridyl-4,4'dicarboxylato)-ruthenium(II) (N719).

4.3 Experimental

4.3.1 Instrumentation and chemicals

The description of the instrumentation and chemicals used for carry out the experiments reported in this chapter can be found in the chapter 3.1.1, 3.2.1.

4.3.2 Procedures for electrode preparation and dye adsorption

FTO slides were washed following the procedure explained in chapter 3.2.2. In order to reduce series resistance losses, a gold stripe was evaporated onto FTO electrode surface (not exposed to the solution). N719 dye adsorption on bare FTO was carried out in two procedures:

Procedure A: heating the electrodes for 30 minutes at 450 °C on a hot plate, cooling down to 75 °C and immersion into an acetonitrile solution of N719 dye in presence of 0.1 M NBu_4PF_6 for 1 hour. The presence of NBu_4PF_6 was found to enhance the adsorption of dye on FTO although N719 in acetonitrile is only poorly soluble and even for 10^{-4} M dye concentration incomplete dissolution of the dye in acetonitrile was observed.

Procedure B: heating the electrodes for 30 minutes at 450 °C on a hot plate, cooling down to 75 °C and immersion into a solution of N719 dye in 50% acetonitrile 50% ^{t}BuOH for 1 hour.

FTO-TiO_2 was prepared by "doctor blading" (see chapter 3.2.2). The FTO electrode is then left for 30 minutes on a hot plate at 450 ^{o}C in order to sinter the anatase crystals. N719 adsorption at these electrodes was achieved following procedure B with typically 10^{-4} M N719 dye in 50% acetonitrile 50% ^{t}BuOH over night (16 hours). Typical SEM images for the FTO surface (with a poor quality N719 film immobilised onto the surface with procedure A with 10^{-4} M N719; this solution was cloudy and contained dye particles) and a cross-sectional view of the FTO-TiO_2 electrode are shown in figure 4.2.

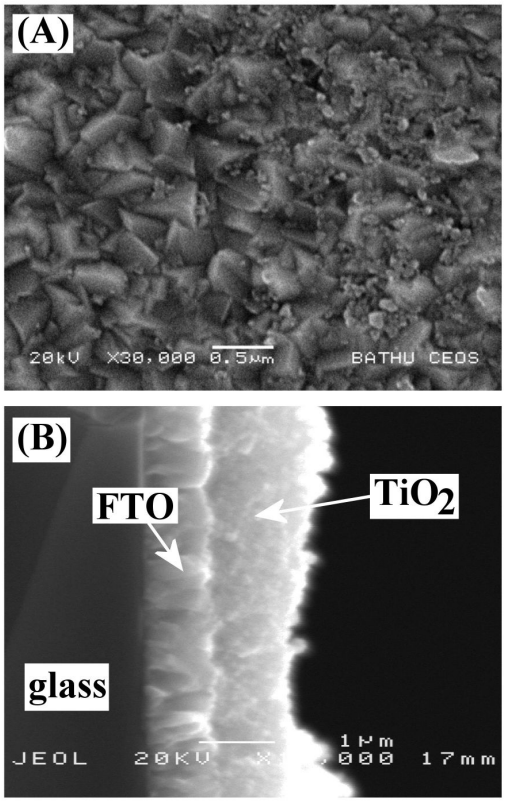

Figure 4.2 (A) Scanning electron micrograph (SEM) of an FTO electrode surface with N719 immobilised after immersion into a solution of 10^{-4} M N719 metal complex in acetonitrile for 12h. Multi-layer deposits have been formed and particulate deposits (presumably due to direct colloid particle adhesion) are visible as well as the underlying microcrystalline FTO substrate. (B) SEM of the cross section of a FTO electrode with a mesoporous TiO_2 film coating.

4.4 Results and Discussion

4.4.1 Adsorption and voltammetric oxidation of N719 at FTO electrode surfaces

The ruthenium metal complex N719 (see structure in figure 4.1) is only very sparingly soluble in acetonitrile. An FTO electrode (fluorine-doped tin oxide, poly-crystalline, see figure 4.2) immersed into a solution or suspension of 10^{-4} M N719 shows characteristic voltammetric responses consistent with the oxidation of adsorbed ruthenium metal complex (see figure 4.3A) rather than responses for the oxidation of dissolved N719. A chemically reversible (at sufficiently fast scan rates, vide infra) oxidation response is observed consistent with earlier literature reports.[19] The midpoint potential (see chapter 2.9 obtained as $E_{mid} = \frac{E_p{}^{ox} + E_p{}^{red}}{2}$) is approximately E_{mid} = 0.68 V vs. Ag/AgCl (3 M KCl). Closer inspection reveals the presence of two processes with midpoint potentials of 0.56 (weaker) and 0.68 (dominant) V vs. Ag/AgCl (3 M KCl). These values are consistent with the corresponding literature values reported by Nazeeruddin as 0.57V vs. SCE [20] for N719 in solution. Removal of the FTO electrode from the solution, rinsing, and re-immersion into acetonitrile with 0.1 M NBu_4PF_6 without dye results in similar voltammetric responses. This suggests that N719 adsorption onto FTO rather than diffusion in solution is the dominating factor in the voltammetric response. In acetonitrile adsorption of the N719 metal complex onto FTO occurs readily and the adsorption step can be carried out in a separate solution followed by voltammetric measurements in acetonitrile containing only 0.1 M NBu_4PF_6 supporting electrolyte.

The solubility of N719 in acetonitrile appeared to be poor (only ca. 10^{-6} M, literature reports suggest moisture is affecting the solubility)[19] and therefore two procedures for dye adsorption were employed. Adsorption experiments on FTO electrode surfaces were carried out (i) for N719 solutions in acetonitrile (procedure A) and (ii) for N719 solutions in 50% acetonitrile 50% ^{t}BuOH (procedure B, see experimental). In all cases adsorption is facile and voltammetric responses are observed. figure 4.3 summarises the experimental data.

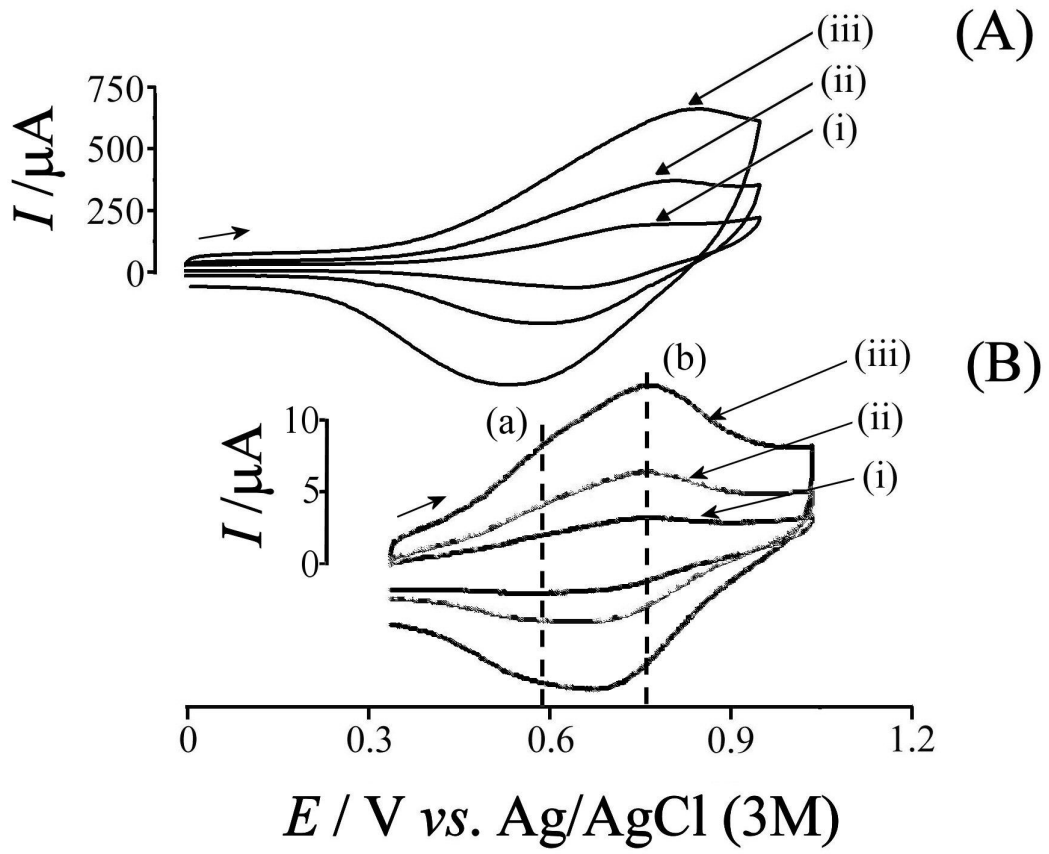

Figure 4.3 (A) Cyclic voltammograms (scan rate (i) 5, (ii) 15, and (iii) 30 Vs^{-1}) for the oxidation and back-reduction for N719 in saturated solution (10^{-4} M in acetonitrile / 0.1 M NBu_4PF_6) at a 42 mm^2 FTO electrode. (B) Cyclic voltammograms (scan rate (i) 1, (ii) 2, and (iii) 4 Vs^{-1}) for the oxidation and back-reduction of N719 adsorbed onto 42 mm^2 FTO (from 10^{-4} M N719 in 50% acetonitrile 50% ^{t}BuOH). The points (a) and (b) refer to the two distinct oxidation process with E_{mid} 0.56V and E_{mid} 0.68V vs. Ag/AgCl (3M).

When adsorbed from acetonitrile solution, N719 binding occurs between 10^{-7} and 10^{-6} M dye concentration in solution and mono-layer coverage appears to be achieved at ca. 10^{-6} M. However, multi-layer adsorption occurs (voltammetric peaks become broad and ill defined) and at higher N719 concentration even particulate deposits can be identified by SEM (see figure 4.2 A) due to poor solubility of N719 in acetonitrile and direct micro particle aggregation at 10^{-4} M dye bath concentration. The isotherm for the adsorption process clearly deviates from that expected for Langmurian binding (see figure 4.4 A, dashed line) and continues to rise beyond the

mono-layer level. In contrast, adsorption from a solution in 50% acetonitrile 50% ^{t}BuOH (procedure B) provides well-defined mono-layer coverage and the Langmurian binding constant can be estimated as 2×10^5 M^{-1}. For comparison the literature value for a similar dye system and for adsorption onto TiO_2 is 5×10^4 M^{-1}. [10] The observed monolayer coverage of ca. 4μC corresponds to $2.5x10^{13}$ molecules which is in good agreement with the theoretical of $3.38x10^{13}$ molecules, calculated taking into account the surface available of 42 mm^2, FTO glass surface roughness of 1,5 and dye molecular foot print of 180 $Å^2$ ca. $200x10^{-16}$ cm^2.

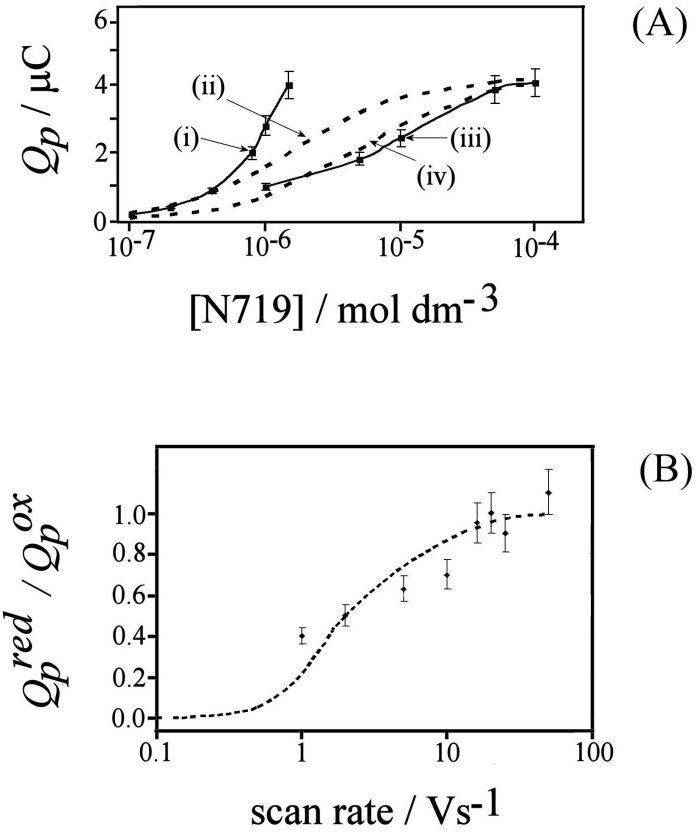

Figure 4.4 (A) Plot of the charge under the oxidation peak versus concentration of N719 metal complex during adsorption onto FTO for (i) the binding of N719 from acetonitrile onto FTO, (ii) the corresponding Langmuir isotherm with $K = 6 \times 10^5$ mol^{-1} dm^3, (iii) the binding of N719 from 50% acetonitrile 50% ^{t}BuOH onto FTO, and (iv) the corresponding Langmuir isotherm with $K = 2 \times 10^5$ M^{-1}. (B) Plot of the ratio of reduction charge to oxidation charge for cyclic voltammograms obtained with N719 adsorbed onto FTO from 50% acetonitrile 50% ^{t}BuOH dye bath (procedure B) and immersed in acetonitrile 0.1 M NBu_4PF_6. The dashed line indicates a calculated curve (generated using Digisim 2.0 assuming a thin layer EC_{irr} mechanism) for a chemical rate constant of $k = 2.4$ s^{-1}.

At sufficiently high scan rate the oxidation process for adsorbed N719 on FTO is fully reversible and a plot of peak current versus scan rate is approximately linear (not shown) in agreement with a surface-immobilised redox system. However, when going to lower scan rates the peak for the back-reduction of N719 is diminished and for scan rates lower than 0.2 Vs^{-1} the N719 oxidation process becomes chemically irreversible. The process can be interpreted in terms of an EC_{irr} mechanism. The rate constant for the chemical reaction step can be estimated by comparing the ratio of peak charges for oxidation and back-reduction, Q_p^{red}/Q_p^{ox}, with a simulated voltammetric response for a surface immobilized redox system (employing Digisim 2.0 and assuming thin film conditions so that diffusion effects are eliminated). The plot in figure 4.4 B shows experimental data points and the dashed line which has been calculated for the case of a chemical rate constant k = 2.4 s^{-1}. This corresponds to an approximate half life of 288 ms. A typical value for the degradation rate constant for a DSC in operation has been reported as 10^{-4} s^{-1} [27](corresponding to half life of ca. 7000s). The difference in half life can be rationalized based on (i) the nature of the substrate and (ii) the presence of iodide in high concentration in the DSC (vide infra).

4.4.2 Adsorption and voltammetric oxidation of N719 at TiO_2-modified FTO electrode surfaces

In dye-sensitised solar cell devices a film of nanoparticulate TiO_2 is used to effectively separate charges upon absorption of photons. The N719 sensitiser (introduced by Grätzel et al.)[28] is now commonly employed adsorbed on nanoparticulate TiO_2.[29] The adsorption of N719 onto TiO_2 was previously investigated by IR methods.[30] Here a film of ca. 1 μm thickness (see figure 4.2 B) prepared from TiO_2 nanoparticles is employed for the absorption of N719 dye and for electrochemical studies.

When immersed into a solution of 10^{-6} M N719 in acetonitrile, the TiO_2 film takes on a visible red colouration due to the adsorbed metal complex. In cyclic voltammetry experiments (see figure 4.5 A) a characteristic oxidation and back-reduction with E_{mid} = 0.68 V vs. Ag/AgCl (3 M KCl) is observed. When compared to data for FTO in figure 4.3 B, the peak current for the oxidation is reduced to about 40%, which may be attributed to the TiO_2 particles blocking part of the FTO electrode surface. Therefore voltammetric responses at high scan rate are essentially due only to the N719 metal complex adsorbed to FTO and no direct evidence for the N719 metal complex bound to TiO_2 is observed in spite of the visible coloration. It is likely that adsorption of N719 from acetonitrile solution does not yield uniform monolayer coatings and therefore electron conduction (via hopping across the TiO_2 insulator surface) is ineffective.

Next, experiments were conducted for the adsorption of N719 metal complex from a 50% acetonitrile 50% ^{t}BuOH solution (procedure B, see figure 4.5 B). Under these condition peak currents are considerably increased indicating successful electron hopping conduction into the TiO_2 film. The plot in figure 4.6 shows that at a concentration of 10^{-4} M N719 a substantial amount of dye is bound to the FTO-TiO_2 film electrode.

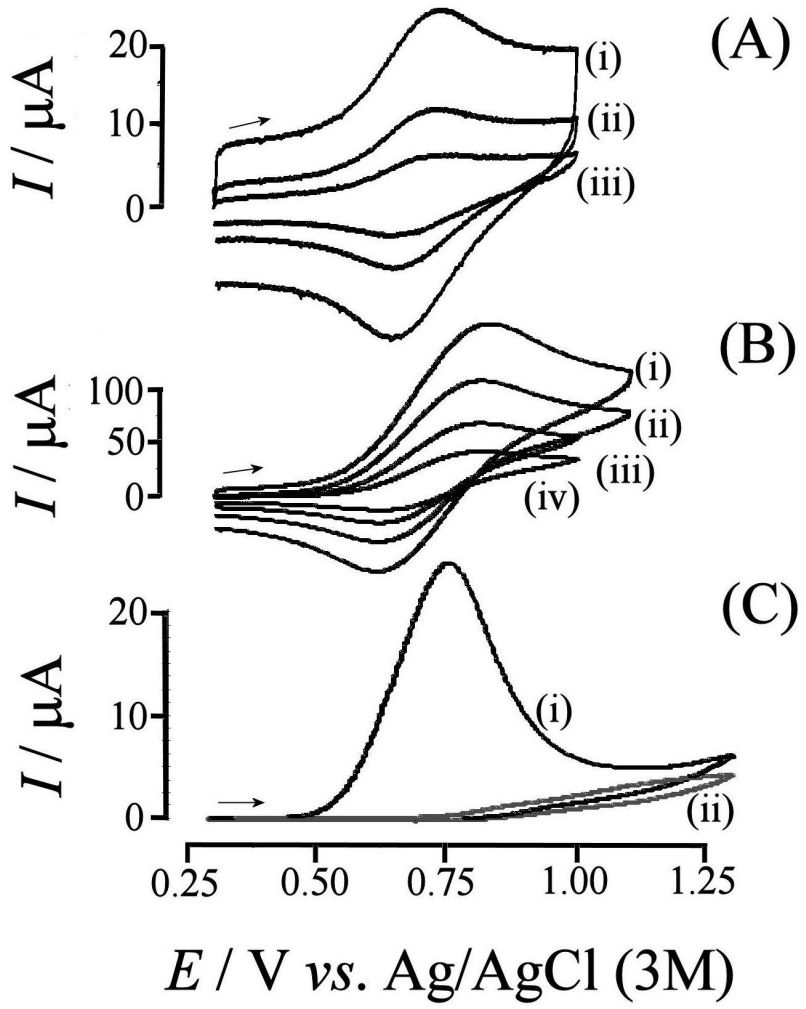

Figure 4.5 (A) Cyclic voltammograms (scan rate (i) 16, (ii) 8, and (iii) 4 Vs^{-1}) for the oxidation and back-reduction of N719 adsorbed on a 9 mm^2 FTO-TiO_2 film electrode (procedure A, 10^{-6} M N719) in acetonitrile 0.1 M NBu_4PF_6. (B) Cyclic voltammograms (scan rate (i) 16, (ii) 8, (iii) 4, and (iv) 1.6 Vs^{-1}) for the oxidation and back-reduction of N719 adsorbed on a 9 mm^2 FTO-TiO_2 film electrode (procedure B, 10^{-4} M N719) immersed in acetonitrile 0.1 M NBu_4PF_6. (C) Cyclic voltammograms (scan rate 0.016 Vs^{-1}, (i) first cycle, (ii) second cycle) for the oxidation of N719 adsorbed on a 42 mm^2 FTO-TiO_2 film electrode (procedure B 10^{-4} M N719) immersed in acetonitrile 0.1 M NBu_4PF_6.

The unusual shape of the experimental isotherm in figure 4.6 when compared to the approximate Langmuirian trend (see dashed line) is believed to be due to the percolation limit for hopping conduction through the adsorbed redox centers and the need for a high scan rate in these experiments. A typical slow scan rate voltammogram obtained with a scan rate of 16 mVs^{-1} is shown in figure 4.5 C.

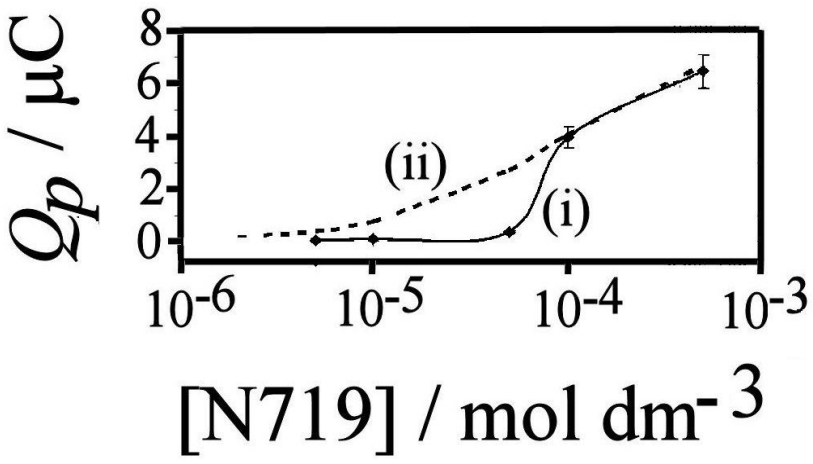

Figure 4.6 Plot of the charge under the oxidation peak (at a scan rate of 16 Vs^{-1}) versus the concentration of N719 (procedure B). The dashed line shows the corresponding Langmuir isotherm with $K = 1 \times 10^4\ M^{-1}$.

Not surprisingly, the oxidation is effective (the charge under the oxidation peak is 390 μC, which is approximately 100 × the charge of a mono-layer (see figure 4.4 A). There is no back-reduction peak and in the second potential cycle the oxidation peak is absent. It is possible to scan the potential to more negative potentials where TiO_2 films become electrically conducting[31] and this will in theory re-reduce any remaining oxidized N719 metal complex within the TiO_2 film. But in this case negative potentials also do not lead to the recovery of the voltammetric response for the oxidation (not shown). It is most likely (and consistent with the report by Wang et al.)[26] that the oxidized form of the N719 metal complex has chemically reacted and the pathway for hopping conduction across the mono-layer is interrupted.

The red coloration of the TiO_2 film electrode with adsorbed N719 (procedure B) is consistent with that for the solution phase N719 metal complex. UV/Vis spectra in figure 4.7 A and 4.7 B compare the optical absorption in solution and when adsorbed on TiO_2 and clearly the main absorption band at 540 nm is observed in both spectra. The electrochemical oxidation of the N719 metal complex adsorbed onto FTO-TiO_2 film does not lead to a significant change in colour, and indeed the UV/Vis spectrum of the sample after oxidation still shows a strong band for the parent compound (see

figure 4.7 C). In addition, new weaker absorption bands appear at 470 nm and 645 nm. Desorption of the N719 metal complex into 0.1 M KOH followed by UV/Vis analysis confirms that most of the ruthenium complex (ca. 80%) remains intact even after exhaustive oxidation and only ca. 20% close to the FTO surface is converted.

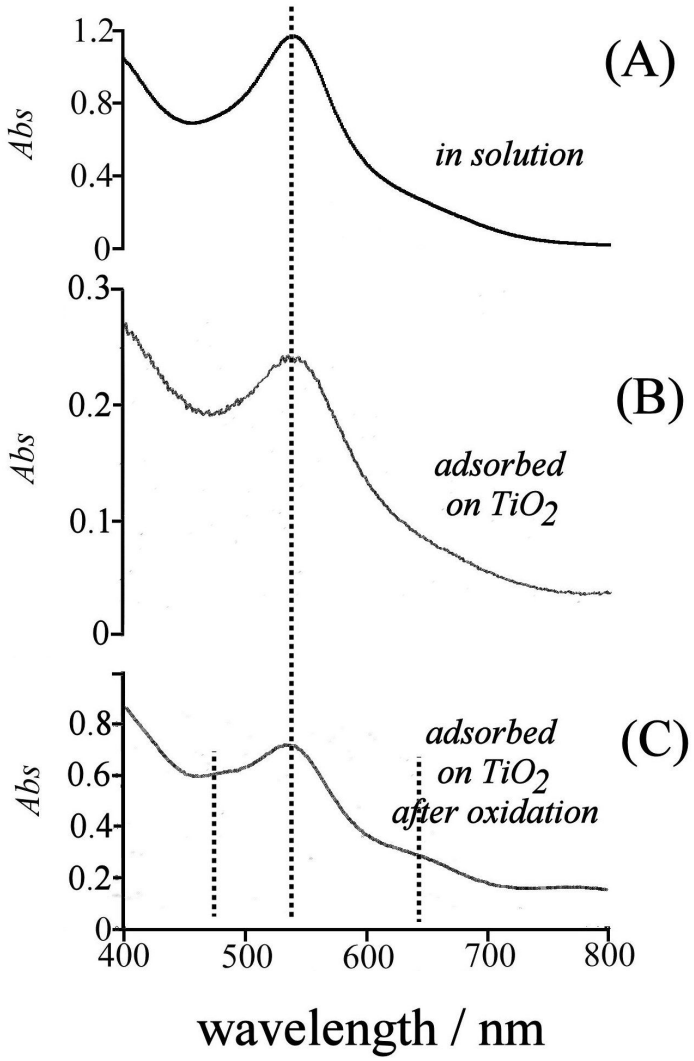

Figure 4.7 (A) UV/Vis absorption spectrum for 10^{-4} M N719 in 50% acetonitrile 50% ^{t}BuOH. (B) UV/Vis absorption spectrum for N719 metal complex adsorbed onto a FTO-TiO_2 film electrode (procedure B). (C) UV/Vis spectrum of the sample in (B) after applying a potential of 1 V vs. Ag/AgCl(3 M KCl) in acetonitrile 0.1 M NBu_4PF_6 and exhaustive oxidation.

In order to fully explain the experimental findings the following model is proposed (see figure 4.8). Oxidation of N719 adsorbed onto FTO occurs followed by electron hopping to and from neighboring N719 sites. The oxidized state of the N719 metal complex (mainly at the FTO electrode surface) undergoes an irreversible chemical transformation leading to an electrochemically apparently inactive species (vide infra) and this causes the electron hopping transport to halt. In figure 4.5 B it can be seen that at a scan rate of ca. 1.6 Vs^{-1} a significant degree of irreversibility is observed and this is due to a sufficient but diminishing number of N719 metal complexes close to the FTO electrode surface. Exhaustive oxidation under these conditions will occur only until conductivity fails and this is the reason for the incomplete oxidation and back-reduction of N719 adsorbed onto the TiO_2 film. The rate of the loss of conductivity (e.g. the scan rate at which irreversibility becomes important) is in good agreement with the rate for the chemical reaction observed for N719 metal complex adsorbed onto FTO which is $k = 2.4\ s^{-1}$ (see figure 4.4 B).

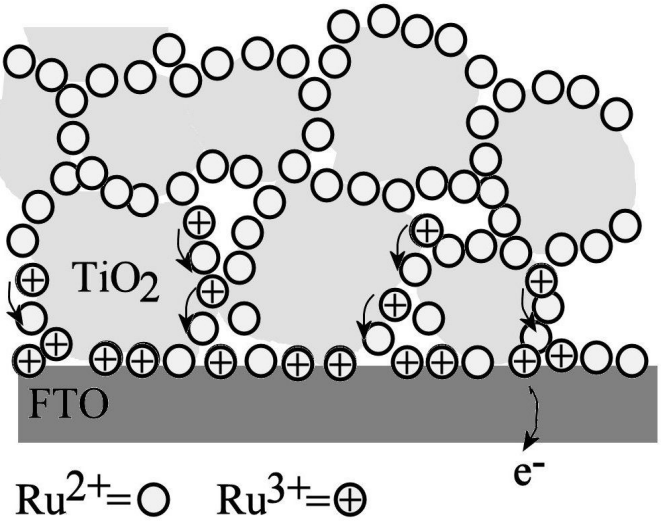

Figure 4.8 Schematic representation of the electron hopping process during oxidation of N719 metal complex adsorbed into a FTO-TiO_2 film electrode.

This mechanistic model allows the rate of electron transport through Ru(III/II) centers adsorbed onto the TiO_2 film to be estimated. The reaction layer $\delta_{reaction}$ within the TiO_2 film can be expressed approximately as in equation 4.1.

4.1

$$\delta_{reaction} = \sqrt{\frac{D_{electron}}{k}}$$

Where D is the apparent diffusion coefficient and k is the chemical rate constant and its value k = 2.4 s^{-1} (vide supra), the estimated reaction layer $\delta_{reaction}$ = 0.2 μm (assuming 20% of a 1 μm thick film has been converted, vide supra) the apparent diffusion coefficient for the hopping of electrons in Ru(III/II) redox centers be obtained as $D_{electron}$ = 10^{-13} m^2s^{-1}. This value is realistic and in excellent agreement with the apparent diffusion coefficients evaluated by Grätzel et al. for structurally similar dyes on TiO_2 surfaces.[26]

4.4.3 Voltammetric oxidation of N719 at FTO electrode surfaces in the presence of iodide

In dye-sensitized solar cells, the electrolyte solution often consists of acetonitrile containing a LiI (typically in 1 M concentration) redox system to allow holes generated photochemically within the N719 dye layer to recapture an electron from iodide.[5-6] The process leads to the formation of I_3^- anions which then diffuse to the collector electrode. The transfer of electrons from iodide to the adsorbed N719 metal complex is studied here in order to reveal the kinetics of electron transfer.

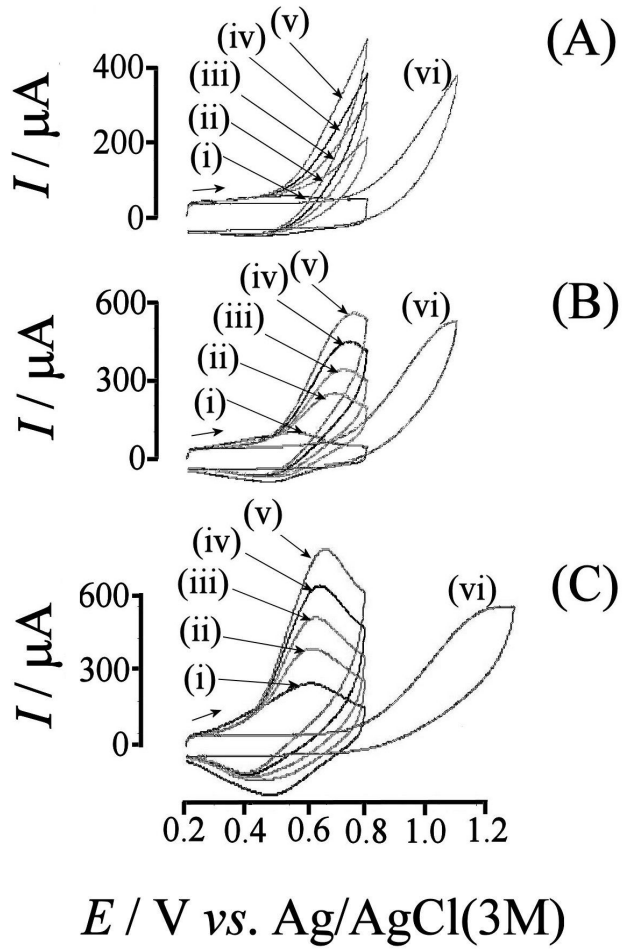

Figure 4.9 Cyclic voltammograms (scan rate 16 Vs^{-1}) obtained with a 42 mm^2 FTO electrode with N719 metal complex adsorbed and immersed in acetonitrile containing 0.1 M NBu_4PF_6 and (i) 0, (ii) 100, (iii) 200, (iv) 300, and (v) 400 μM LiI. In (vi) the effect of having no N719 metal complex adsorbed is shown. The adsorption of N719 was based on 1 h immersion of the FTO electrode into (A) 0.1 μM, (B) 0.4 μM, (C) 1 μM N719 metal complex in acetonitrile.

Figures 4.9 and 4.10 show cyclic voltammograms obtained with FTO electrodes as a function of the coverage with N719 metal complex. In figure 4.9 A it can be seen that in the oxidation of iodide on a bare FTO electrode is inhibited (see figure 4.9 Avi). The presence of even low coverage N719 immediately increases the iodide oxidation current. Figure 4.9 A to 4.9 C demonstrate the effect of the N719 coverage showing that for a complete monolayer of N719 metal complex the iodide oxidation occurs at ca. 0.6 V vs. Ag/AgCl (3 M KCl) as an essentially diffusion controlled process (anodic peak currents are approximately consistent with values estimated based on the Randles-Sevcik equation[32] and the rate constant for bimolecular electron transfer cannot be obtained). In the absence of N719 metal complex the oxidation peak is observed at ca. 1.2 V vs. Ag/AgCl (3 M KCl). The fact that the electro-catalytic iodide oxidation in the presence of N719 is diffusion controlled suggests very fast interfacial electron transfer. The lowering of the N719 coverage on the FTO surface causes the peak to become more irreversible with the peak shifting positive.

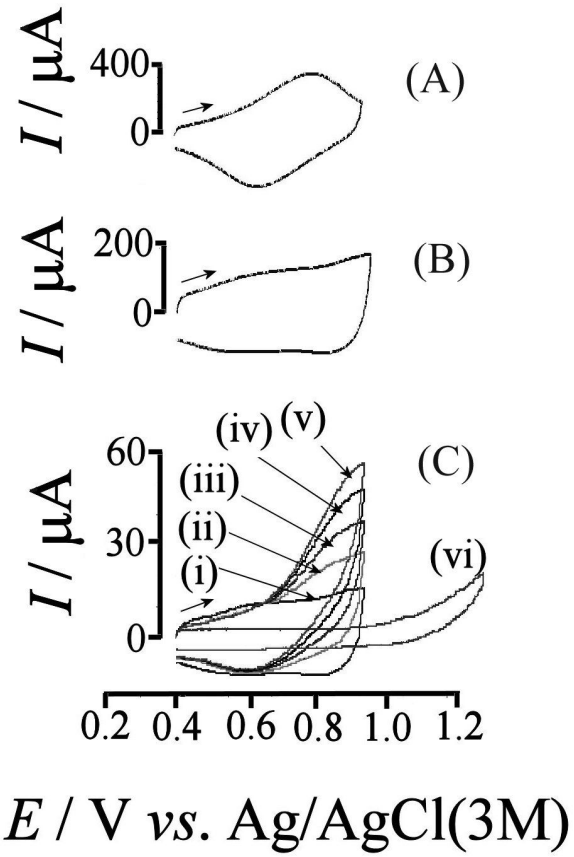

Figure 4.10 (A) and (B) 1 µM dye bath, the N719 metal complex was irreversibly oxidised prior to the experiment by cyclic voltammetry with a scan rate of 5 mVs^{-1} and it can be seen that even after irreversible oxidation the electrocatalytic effect remains (C)

This may be interpreted as a rate-limitation by a potential driven reaction step e.g. the transfer of electrons from the FTO to the N719 system (see figure 4.11, note that step 1 is rate limiting). Based on the cyclic voltammetry evidence (vide supra), there are two distinct ways for the dye to be adsorbed on FTO which leads to two electrochemical responses at 0.56 V and at 0.68 V vs. Ag/AgCl (3M KCl) midpoint potential. Careful inspection of figures 4.9 B and 4.9 C suggests that only the second type of adsorbed N719 metal complex with $E_{mid} \approx 0.68$ V vs. Ag/AgCl (3 M KCl) is electro-catalytically active for the iodide oxidation.

Perhaps surprisingly after irreversible oxidation of the N719 dye at the FTO electrode surface, electrocatalysis for the iodide oxidation is still observed (see figure 4.10 A-C). This can be rationalised by assuming an oxidation product formed irreversibly from N719 without a peak-shaped response in the voltammogram but with a broad capacitive response (similar to ruthenium oxide films).[33]

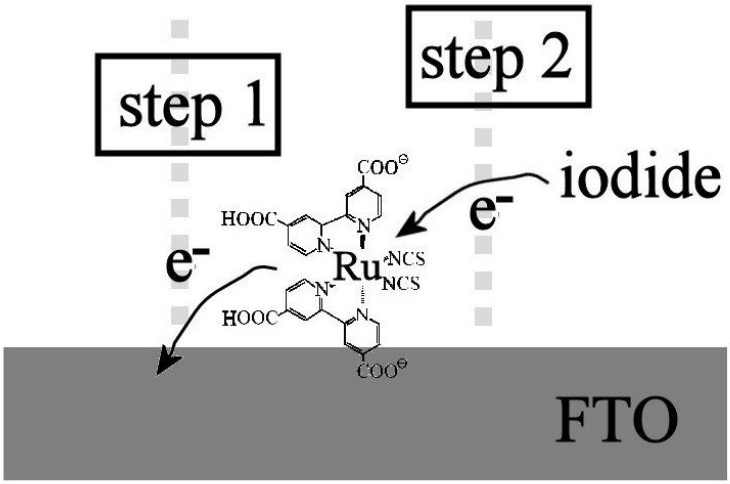

Figure 4.11 Schematic representation of a possible two step electrocatalytic oxidation of iodide.

4.4.4 Voltammetric Oxidation of N719 at TiO_2-Modified FTO Electrode Surfaces in the Presence of Iodide

In order to explore the electron transfer from the N719 metal complex adsorbed onto TiO_2 to iodide, experiments were conducted with FTO-TiO_2 film electrodes. Voltammograms shown in figure 4.12 A demonstrate the electro-catalytic effect of N719 adsorbed onto the FTO-TiO_2 electrode.

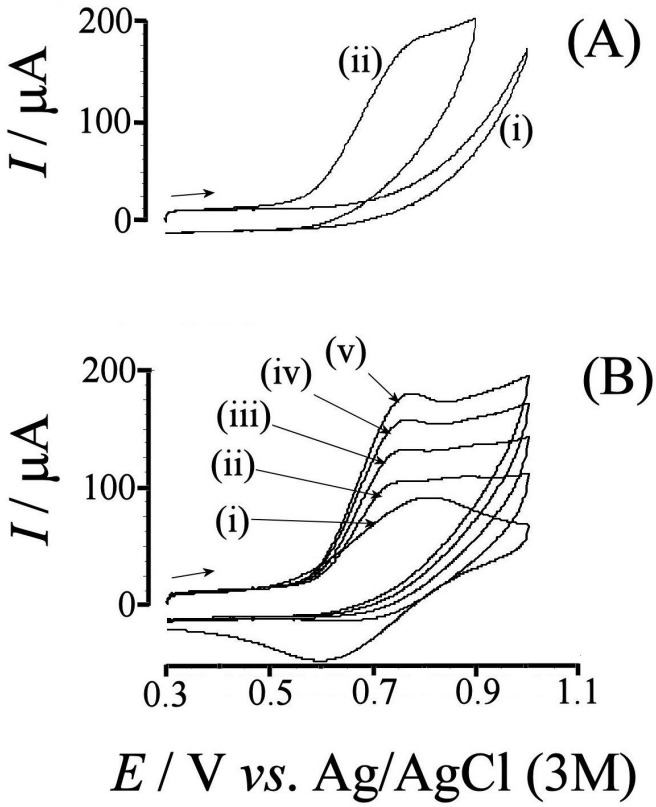

Figure 4.12 (A) Cyclic voltammograms (scan rate 16 Vs^{-1}) for the oxidation of 2.7 mM iodide (LiI) in acetonitrile 0.1 M NBu_4PF_6 at a 9 mm^2 FTO-TiO_2 film electrode: (i) bare FTO-TiO_2 electrode and (ii) FTO-TiO_2 electrode with N719 metal complex adsorbed (procedure B). (B) Cyclic voltammograms (scan rate 16 Vs^{-1}) for the oxidation of (i) 0, (ii) 1.0, (iii) 1.6, (iv) 2.2, and (v) 2.7 mM iodide (LiI) in acetonitrile 0.1 M NBu_4PF_6 at a 9 mm^2 FTO-TiO_2 film electrode with N719 adsorbed (procedure B).

In the absence of N719 dye only the onset of the iodide oxidation can be seen but in the presence of N719 a clear peak response is obtained at a potential of 0.77 V vs. Ag/AgCl (3 M KCl). The addition of iodide leads to the loss of the back-reduction peak and to a corresponding increase in the oxidation peak (see figure 4.12 B). It is possible to analyse the resulting peak currents based on a planar diffusion layer model. Iodide in contact to both FTO surface and TiO_2 film will react with the oxidized form of the N719 dye and based on the earlier results (see figure 4.5) it appears most likely that at high scan rate (16 Vs^{-1}) the process directly at the FTO surface dominates. The peak current density normalized for the electro-catalytic oxidation of a 1 mM iodide solution at a plane FTO electrode at a scan rate of 16 Vs^{-1} can be extrapolated as ca. 2.4 mA cm^{-2} based on data in figure 4.9 C.

In comparison, data in figure 4.12 B suggest a peak current density of 0.4 mA cm^{-2} under the same conditions but in the presence of the mesoporous TiO_2 film. The reduction in peak current density is consistent with (i) a reduced active surface area due to blocking of FTO with TiO_2 particles and (ii) a reduced rate of diffusion of iodide in the porous film. The diffusion layer thickness $\delta_{diffusion}$ for iodide diffusion under the conditions employed in this experiment can be estimated based on equation 4.2.

4.2

$$\delta_{diffusion} = \sqrt{\frac{DRT}{vF}}$$

Where D (m^2s^{-1}) is the diffusion coefficient, R the gas constant (J K^{-1} mol^{-1}), T the absolute temperature (K), v the scan rate (Vs^{-1}), and F the Faraday constant ($Cmol^{-1}$). Assuming an estimated diffusion coefficient of ca. 1×10^{-9} m^2s^{-1} for iodide in the porous film the value obtained for $\delta_{diffusion}$ is 1.2 μm. This value is comparable to the thickness of the TiO_2 film and therefore diffusion of iodide within the porous film is dominating this process. Note also that the diffusion of charge carriers via electron hopping is considerably slower when compared to diffusion of iodide in the porous film. In order to observe the direct electro-catalytic oxidation of iodide directly at the N719 metal complex modified TiO_2 surface, the scan rate has to be reduced and this would result in the loss of the FTO surface conductivity due to oxidation of the N719 dye. Alternatively, the iodide concentration could be increased (leading to high

currents) or decreased (leading to a higher extent of surface charge conduction but diminished kinetic information). Therefore, currently this dark process cannot be fully resolved by the methods employed in this study. Figure 4.13 shows a schematic representation of iodide oxidation at the FTO electrode.

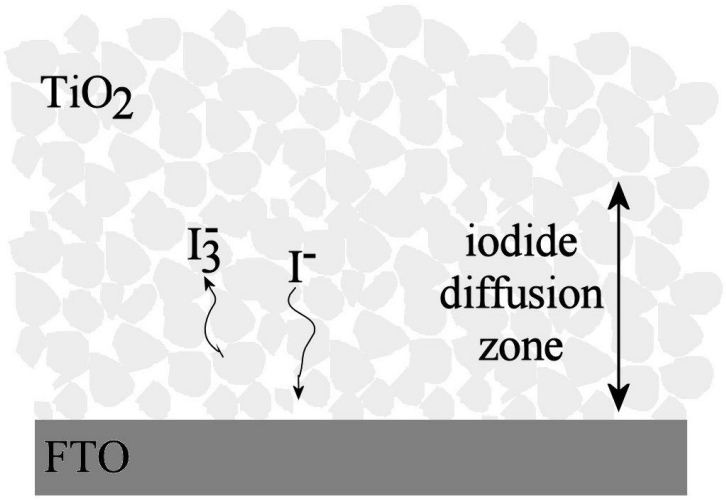

Figure 4.13 Schematic representation of the iodide oxidation at the FTO electrode surface and a diffusion layer within the TiO_2 film.

In a DSC operating in sunlight the presence of I^- ions in high concentration continuously regenerates the dye. In our experiment the rate of this regeneration cannot be directly observed due to the lower concentration of I^-.[2] Furthermore, it has been shown that under dark conditions the electron transfer step from N719 to oxide substrate becomes rate limiting. Most importantly, the N719 degradation after oxidation has been shown to occur close to the positively polarized FTO substrate without affecting N719 within the mesoporous TiO_2 film. During operation of the DSC hole hopping conduction to the FTO electrode surface provides a detrimental recombination pathway and ***the degradation of the dye at the FTO surface is likely to be beneficial. The success of N719 as a DSC dye may be linked to the reduced hole-electron recombination.*** The lifetime of DSCs based on N719 can be extended even if partial or complete dye degradation occurs close to the FTO substrate or when blocking layers are introduced.[34] Deterioration of solar cell performance is probably occurring only after a much more substantial amount of N719 is degraded.

4.5 Conclusions

1. The adsorption of N719 metal complex onto FTO and TiO_2 occurs from acetonitrile solution (with 0.1 M NBu_4PF_6) even at 10^{-7} M concentration. However, aggregate and multi-layer formation occurs due to insufficient solubility of N719 in acetonitrile. A well-defined adsorption process occurs in 50% acetonitrile 50% ^{t}BuOH with a Langmuirian constant of ca. 2×10^5 M^{-1}.

2. It has been shown that the N719 ruthenium complex employed in dye-sensitized solar cells is a potent electro-catalyst for the transfer of electrons from iodide into the positively polarized electrode. Even after chemical degradation of N719 (after remaining in the Ru(III) state for more than the half life $\tau_{1/2}$ = 288 ms) the electro-catalytic effect is still observed (although weakened).

3. The iodide oxidation process (in the dark) in the presence of oxidised N719 can be understood as a two step process with (i) a slow transfer of one electron from the Ru(II) metal complex into the FTO film followed by (ii) a fast transfer of one electron from iodide into the transient Ru(III) species.

4. The hopping conduction of electrons responsible for the voltammetric response for the oxidation and back-reduction of N719 adsorbed into the FTO-TiO_2 film electrode is strongly affected by the chemical degradation of N719 in the oxidised form. Only a partial oxidation of the dye adsorbed into the TiO_2 film occurred under exhaustive electrolysis conditions. The Ru(II/III) redox system at the FTO electrode surface is required as a "conduit" for electrons. The apparent diffusion coefficient for the hopping transport of electrons through Ru(III/II) sites in a monolayer in the dark is estimated as 10^{-13} m^2s^{-1}.

5. Degradation of N719 at the FTO substrate is likely to suppress hole-electron recombination and therefore is in part responsible for the high light harvesting efficiency of this particular molecular structure. However, degradation of N719 at the TiO_2 substrate may also cause detrimental effects and therefore more experimental work exploring the chemical reactivity of N719 on TiO_2 will be required.

In future, further experimental studies (in particular based on spectro-electrochemical methods) will be required to further resolve the effects of binding site and binding mode of adsorption on the reversible potential and reactivity of immobilized N719 and similar metal complexes.

References

1. Tachibana, Y.; Moser, J. E.; Gratzel, M.; Klug, D. R.; Durrant, J. R., *Journal of Physical Chemistry* **1996,** *100* (51), 20056-20062.
2. Lindstrom, H.; Rensmo, H.; Sodergren, S.; Solbrand, A.; Lindquist, S. E., *Journal of Physical Chemistry* **1996,** *100* (8), 3084-3088.
3. Clifford, J. N.; Palomares, E.; Nazeeruddin, M. K.; Gratzel, M.; Durrant, J. R., *Journal of Physical Chemistry C* **2007,** *111* (17), 6561-6567.
4. Montanari, I.; Nelson, J.; Durrant, J. R., *Journal of Physical Chemistry B* **2002,** *106* (47), 12203-12210.
5. Nasr, C.; Hotchandani, S.; Kamat, P. V., *Journal of Physical Chemistry B* **1998,** *102* (25), 4944-4951.
6. Walter, B. J.; Elliott, C. M., *Inorg. Chem.* **2001,** *40* (23), 5924-5927.
7. Bisquert, J.; Cahen, D.; Hodes, G.; Ruhle, S.; Zaban, A., *Journal of Physical Chemistry B* **2004,** *108* (24), 8106-8118.
8. Gratzel, M., *Inorg. Chem.* **2005,** *44* (20), 6841-6851.
9. Bach, U.; Lupo, D.; Comte, P.; Moser, J. E.; Weissortel, F.; Salbeck, J.; Spreitzer, H.; Gratzel, M., *Nature* **1998,** *395* (6702), 583-585.
10. Hagfeldt, A.; Gratzel, M., *Accounts Chem. Res.* **2000,** *33* (5), 269-277.
11. Nour-Mohhamadi, F.; Nguyen, S. D.; Boschloo, G.; Hagfeldt, A.; Lund, T., *Journal of Physical Chemistry B* **2005,** *109* (47), 22413-22419.
12. Hinsch, A.; Kroon, J. M.; Kern, R.; Uhlendorf, I.; Holzbock, J.; Meyer, A.; Ferber, J., *Progress in Photovoltaics* **2001,** *9* (6), 425-438.
13. Gratzel, M., *Comptes Rendus Chimie* **2006,** *9* (5-6), 578-583.
14. Grunwald, R.; Tributsch, H., *Journal of Physical Chemistry B* **1997,** *101* (14), 2564-2575.
15. Wang, P.; Zakeeruddin, S. M.; Moser, J. E.; Humphry-Baker, R.; Gratzel, M., *Journal of the American Chemical Society* **2004,** *126* (23), 7164-7165.
16. Kawano, R.; Nazeeruddin, M. K.; Sato, A.; Gratzel, M.; Watanabe, M., *Electrochemistry Communications* **2007,** *9* (5), 1134-1138.
17. Boschloo, G.; Hagfeldt, A., *Inorganica Chimica Acta* **2008,** *361* (3), 729-734.
18. Haque, S. A.; Tachibana, Y.; Klug, D. R.; Durrant, J. R., *Journal of Physical Chemistry B* **1998,** *102* (10), 1745-1749.
19. Bond, A. M.; Deacon, G. B.; Howitt, J.; MacFarlane, D. R.; Spiccia, L.; Wolfbauer, G., *J. Electrochem. Soc.* **1999,** *146* (2), 648-656.
20. Nazeeruddin, M. K.; Zakeeruddin, S. M.; Humphry-Baker, R.; Jirousek, M.; Liska, P.; Vlachopoulos, N.; Shklover, V.; Fischer, C. H.; Gratzel, M., *Inorg. Chem.* **1999,** *38* (26), 6298-6305.
21. Cecchet, F.; Gioacchini, A. M.; Marcaccio, M.; Paolucci, F.; Roffia, S.; Alebbi, M.; Bignozzi, C. A., *Journal of Physical Chemistry B* **2002,** *106* (15), 3926-3932.
22. Wolfbauer, G.; Bond, A. M.; Deacon, G. B.; MacFarlane, D. R.; Spiccia, L., *Journal of the American Chemical Society* **2000,** *122* (1), 130-142.
23. Forster, R. J.; Pellegrin, Y.; Keyes, T. E., *Electrochemistry Communications* **2007,** *9* (8), 1899-1906.
24. Trammell, S. A.; Meyer, T. J., *Journal of Physical Chemistry B* **1999,** *103* (1), 104-107.

25. Bonhote, P.; Gogniat, E.; Tingry, S.; Barbe, C.; Vlachopoulos, N.; Lenzmann, F.; Comte, P.; Gratzel, M., *Journal of Physical Chemistry B* **1998,** *102* (9), 1498-1507.
26. Wang, Q.; Zakeeruddin, S. M.; Nazeeruddin, M. K.; Humphry-Baker, R.; Gratzel, M., *Journal of the American Chemical Society* **2006,** *128* (13), 4446-4452.
27. Gratzel, M., *Progress in Photovoltaics* **2006,** *14* (5), 429-442.
28. Nazeeruddin, M. K.; Kay, A.; Rodicio, I.; Humphrybaker, R.; Muller, E.; Liska, P.; Vlachopoulos, N.; Gratzel, M., *Journal of the American Chemical Society* **1993,** *115* (14), 6382-6390.
29. Wang, Z. S.; Kawauchi, H.; Kashima, T.; Arakawa, H., *Coordination Chemistry Reviews* **2004,** *248* (13-14), 1381-1389.
30. Nazeeruddin, M. K.; Humphry-Baker, R.; Liska, P.; Gratzel, M., *Journal of Physical Chemistry B* **2003,** *107* (34), 8981-8987.
31. Milsom, E. V.; Novak, J.; Green, S. J.; Zhang, X. H.; Stott, S. J.; Mortimer, R. J.; Edler, K.; Marken, F., *Journal of Solid State Electrochemistry* **2007,** *11* (8), 1109-1117.
32. Scholz, F., *Electroanalytical Methods*. Springer: 2005.
33. McKenzie, K. J.; Marken, F., *Electrochemical and Solid State Letters* **2002,** *5* (9), E47-E50.
34. Cameron, P. J.; Peter, L. M., *Journal of Physical Chemistry B* **2005,** *109* (15), 7392-7398.

Chapter 5: Adsorption and Redox Chemistry of *cis*-$RuLL'(SCN)_2$ with L=4,4'-Dicarboxylic acid-2,2'-bipyridine and L'=4,4'-Dinonyl-2,2'-bipyridine (Z907) at FTO and TiO_2 Electrode Surfaces

Contents

The work presented in this chapter is based on a peer reviewed publication:

Adsorption and Redox Chemistry of cis-RuLL'$(SCN)_2$ with L=4,4'-Dicarboxylic acid-2,2'-bipyridine and L'=4,4'-Dinonyl-2,2'-bipyridine (Z907) at FTO and TiO_2 Electrode Surfaces Alberto Fattori, Laurence M. Peter, Keri L. McCall, Neil

Robertson, and Frank Marken Journal of Solid State Electrochemistry (accepted for publication).

5.1 Abstract

The electrochemical and spectroelectrochemical properties of the sensitizer dye Z907 (*cis*-RuLL'(SCN)$_2$ with L=4,4'-dicarboxylic acid-2,2'-bipyridine and L'=4,4'-dinonyl-2,2'-bipyridine) adsorbed on fluorine-doped tin oxide (FTO) and TiO_2 surfaces have been investigated. Langmuirian binding constants for FTO and TiO_2 are estimated to be 3×10^6 M^{-1} and 4×10^4 M^{-1}, respectively. The Ru(III/II) redox process is monitored by voltammetry and by spectro-electrochemistry. For Z907 adsorbed onto FTO, a slow EC-type electrochemical reaction is observed with a chemical rate constant of ca. $k = 10^{-2}$ s^{-1} leading to Z907 dye degradation of a fraction of the FTO-adsorbed dye. The Z907 adsorption conditions affect the degradation process. No significant degradation was observed for TiO_2-adsorbed dye. Degradation of the Z907 dye affects the electron-hopping conduction at the FTO-TiO_2 interface.

5.2 Introduction

As mentioned in the previous chapters (1 and 2), the understanding of the redox properties and chemical stability of the oxidized form of the dye is of crucial importance for the optimization of long-lived DSCs.

In order to guarantee a long lifetime of a DSC, the dye should be able to undergo millions of redox cycles before degradation occurs. Important parameters that influence the long-term stability of a DSC are the ability of a dye to survive elevated temperatures and to exhibit a sufficiently stable Ru(III) oxidised form. Dyes like *cis*-RuLL'(SCN)$_2$ with L=4,4'-dicarboxylic acid-2,2'-bipyridine and L'=4,4'-dinonyl-2,2'-bipyridine (also known has Z907; see figure 5.1) are reported to fulfil these requirements (chapter 1.3.1.1).[1-2] One very successful approach for avoiding the photochemical degradation of dye systems has been to alter the ligand structure. In the dye Z907, one bipyridyl ligand has been modified by attaching two nonyl hydrocarbon chains.[8] This modification has been reported to significantly enhance

the chemical stability in the oxidised form, and no direct observation of chemical degradation processes have been reported to date.

The way in which the sensitizer is attached to the semiconductor surface may affect reactivity and the electron injection kinetics.[3] In order for the dye to attach to the TiO_2 semiconductor substrate, functional groups such as carboxylate are required to form a strong bond (chapter 1.3.1.1).[4] Grätzel and coworkers[5] have reported that for 3 poly-pyridyl ruthenium dyes (including Z907) attached on TiO_2, charge transport may occur via Ru(III/II) electron hopping. This mechanism is effective if there is good electronic interaction associated with close packing of the dye molecules on the oxide surface. Typical electron diffusion coefficients are 10^{-13} m^2 s^{-1}. Although this Ru(III/II) charge hopping process may be of only secondary importance for solar cell operation, it could lead to electron/Ru(III) recombination at the FTO back electrode.

Previous studies on the DSC sensitizer *cis*-bis(isothiocyanato)-bis(2,2'-bipyridyl-4,4'dicarboxylato)-ruthenium(II) (or N719) have shown that electron hopping between adsorbed dye molecules is strongly affected by the chemical degradation of the oxidised sensitizer (see chapter 4). The study of N 719 adsorbed at the surface of FTO and FTO-TiO_2 electrodes immersed in acetonitrile electrolyte revealed EC-type degradation with k = 2.4 s^{-1}. [6] N719 is a highly successful dye because the degradation process is many orders of magnitude slower than regeneration by electron transfer from iodide. Degradation predominantly affects FTO-adsorbed dye, and this could even result in a beneficial effect since it retards electron/Ru(III) recombination at the FTO-TiO_2 interface by suppressing electron hopping.

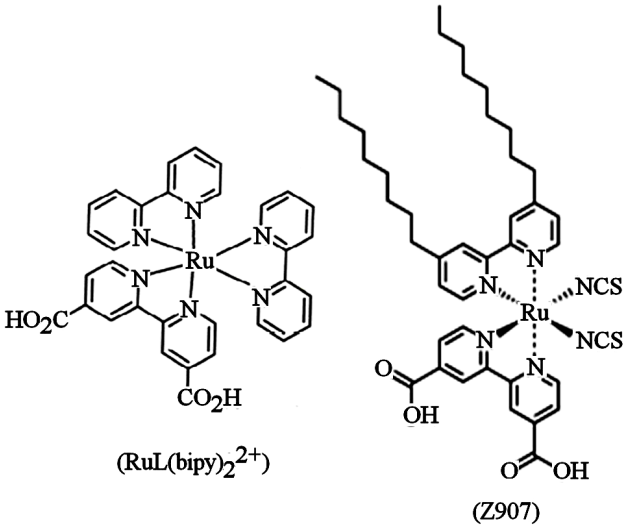

Figure 5.1 Molecular structures for $RuL(bipy)_2^{2+}$ and for Z907 (*cis*-$RuLL'(SCN)_2$ with L=4,4'-dicarboxylic acid-2,2'-bipyridine and L'=4,4'-dinonyl-2,2'-bipyridine)

In the present study, surface redox processes were investigated first for a fully chemically reversible surface redox system - $RuL(bipy)_2^{2+}$ (with L=4,4'-dicarboxylic acid-2,2'-bipyridine) - and then for the more reactive Z907 redox system (see figure 5.1). Cyclic voltammetry revealed that the dye adsorption conditions influence the chemical stability of Z907 film. The degradation rate for the oxidised Z907 adsorbed on FTO was found to be approximately two orders of magnitude slower compared to that determined previously for the oxidised N719. [7]

5.2 Experimental

5.2.1 Instrumentation and chemicals

The description of the instrumentation and chemicals used to carry out the experiments reported in this chapter can be found in the chapter 3.1.1, 3.2.1.

5.2.2 Preparation of FTO-TiO_2 film electrodes

FTO slides were washed according to the procedure in chapter 3.2.2. In order to reduce series resistance losses, a gold stripe was evaporated onto FTO electrode surface (not exposed to the solution). FTO-TiO_2 films were prepared by "doctor blading" (chapter 3.2.2). The electrodes active area was either 9 or 42 mm^2. The FTO electrode was then left for 30 minutes on a hot plate at 450 ^oC in order to sinter the anatase crystals. Z907 dye adsorption on bare FTO or on FTO-TiO_2 film electrodes was carried out by heating the electrodes for 30 minutes at 450 °C on a hot plate, cooling down to 75 °C, and immersion into a solution of Z907 dye in 50% acetonitrile 50% *tert.*-BuOH for a given time (typically with 10^{-4} M Z907 dye in 50% acetonitrile 50% *tert.*-BuOH for a period of 16 h).

5.3 Results and Discussion

5.3.1 Adsorption and Redox Chemistry of $RuL(bipy)_2^{2+}$ with L=4,4'-dicarboxylic acid-2,2'-bipyridine at FTO Thin Film Electrode Surfaces

A chemically stable model redox system, $RuL(bipy)_2^{2+}$ with L=4,4'-dicarboxylic acid-2,2'-bipyridine was employed initially to demonstrate well-defined redox processes at FTO film electrodes without the complication of additional chemical follow-up processes. Adsorbed monolayers of the Ru(III/II) system $RuL(bipy)_2^{2+}$ at FTO surfaces have been studied previously for application in electroluminescence analysis, and stable redox chemistry in aqueous media was reported. [8]

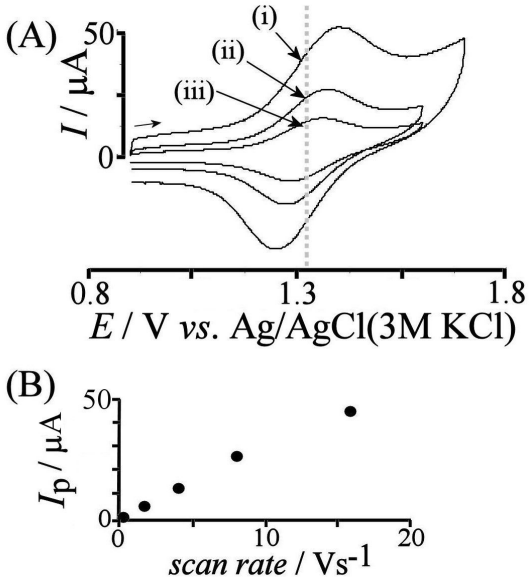

Figure 5.2 (A) Cyclic voltammograms (scan rate (i) 16, (ii) 8, and (iii) 4 Vs^{-1}) for the oxidation and back-reduction of $RuL(bipy)_2^{2+}$ (with L = 4,4'-dicarboxylic acid-2,2'-bipyridine) adsorbed onto a 9 mm^2 FTO electrode (1 hour in 10^{-5} M dye solution) and immersed in acetonitrile/0.1 M NBu_4PF_6. (B) Plot of the peak current for the oxidation peak versus scan rate.

Figure 5.2 A shows cyclic voltammograms for the oxidation of $RuL(bipy)_2^{2+}$ adsorbed onto FTO. The reversible potential for the Ru(III/II) process is ca. 1.34 V vs. Ag/AgCl(3M KCl). A plot of the oxidation peak current versus scan rate (see Figure 5.2B) is linear and consistent with a surface-immobilised redox system. Analysis of the charge under the cyclic voltammetric response, corresponding to 4.4 μCcm^{-2}, can be compared with the theoretical value for monolayer adsorption. Taking an area of ca. 2 nm^2 occupied by each $RuL(bipy)_2^{2+}$, [9] and a roughness factor of 1.5, the theoretical monolayer coverage is estimated as 12 μCcm^{-2}, which suggests that close packing is not achieved experimentally. The peak width at half height for the voltammetric signal is approximately 110 mV compared to the ideal theoretical value of 91 mV at 25 ^oC.[10] The peak-to-peak separation for the cyclic voltammograms shown in figure 5.2 A are most likely indicative of a slow interfacial electron transfer. The voltammetric responses remained unchanged over many experiments and therefore demonstrate the chemical inertness of the $RuL(bipy)_2^{2+}$ redox system. Next, the electrochemical characteristics are compared to Z907 adsorbed onto FTO electrodes.

5.3.2 Adsorption and Redox Chemistry of cis-RuLL'(SCN)$_2$ with L=4,4'-dicarboxylic acid-2,2'-bipyridine and L'=4,4'-dinonyl-2,2'-bipyridine (Z907) at FTO Thin Film Electrode Surfaces

The Z907 sensitizer dye (see figure 5.1) has been thoroughly studied [2] and employed in solar cell devices. However, there is no previous study of the chemical reactivity of Z907 immobilised by adsorption onto FTO, which is commonly employed as a substrate in solar cell assemblies. The voltammograms shown in figure 5.3 A demonstrate the facile adsorption of Z907 onto FTO surfaces and the resulting well-defined oxidation and reduction processes with a reversible potential of ca. 0.68 V vs. Ag/AgCl (3M KCl). The charge under the oxidation peak is approximately 11 μCcm^{-2} which is in excellent agreement with the theoretical prediction (vide supra).

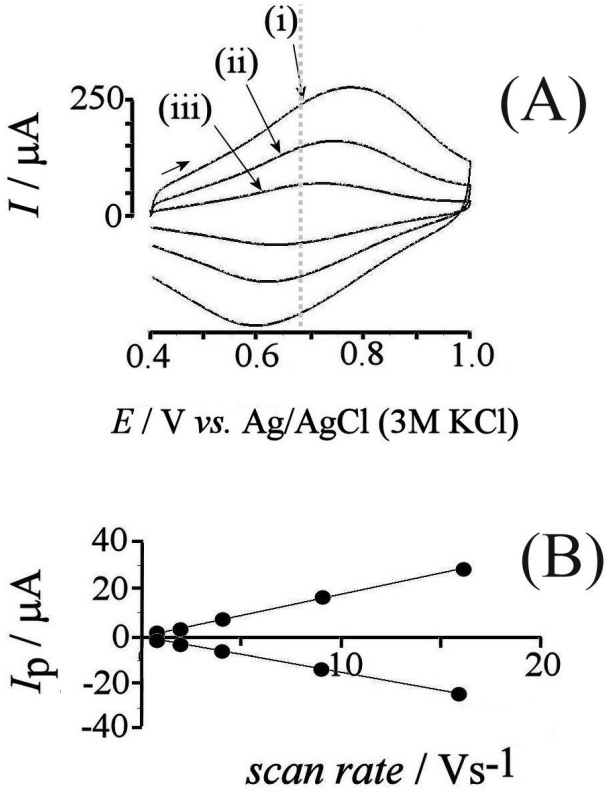

Figure 5.3 (A) Cyclic voltammograms (scan rate (i) 16, (ii) 8, (iii) 4 Vs^{-1}) for the oxidation and back-reduction for Z907 adsorbed on a 42 mm^2 FTO electrode (1 hour in 10^{-6} M dye solution) and immersed in acetonitrile/0.1 M NBu_4PF_6. (B) Plot of the peak currents versus scan rate.

A plot of the charge under the oxidation peak versus the Z907 concentration during the adsorption process shows Langmuirian characteristics (see figure 5.4) with an estimated binding constant of $K = 3 \times 10^6$ M^{-1}.

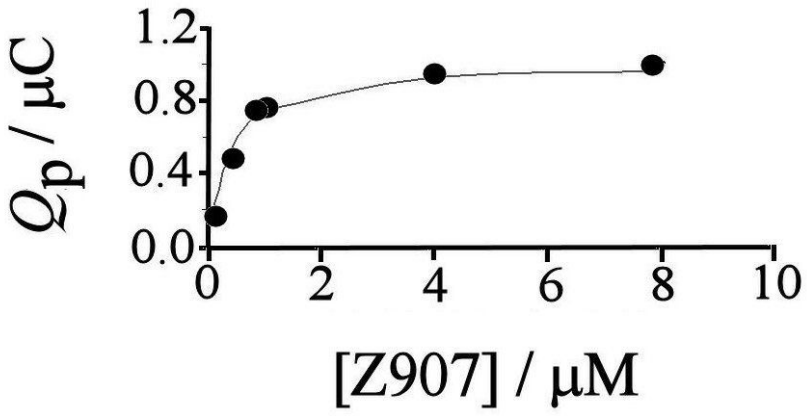

Figure 5.4 Plot of the charge under the oxidation peak (scan rate 16 Vs^{-1}) versus concentration of Z907 in the dye solution. The line corresponds to a Langmuirian binding constant of $K = 3 \times 10^6$ M^{-1}. The electrodes used in this experiment had an active surface area of 9 mm^2.

The shape of the voltammetric responses is broad (width at half height approximately 250 mV) indicating either different types of binding sites, intermolecular interactions, or different binding modes (orientations). The peak-to-peak separation of the cyclic voltammograms in figure 5.3 A appear very similar to that in figure 5.2 A and is therefore again attributed predominantly to slow electron transfer kinetics. The peak-to-peak separation of ca. $\Delta E_p = 180$ mV at a scan rate of $v = 16$ Vs^{-1} can be used to estimate the standard rate constant for interfacial electron transfer, $k_e \approx 2 \times 10^3$ s^{-1}, based on the expression 5.1.

5.1
$$\frac{\Delta E_p}{2} = \frac{RT}{\alpha F} \ln\left(\frac{RTk_e}{\alpha F v}\right) \quad \text{with } \alpha = ½ \text{ assumed.}^{11}$$

Where α is the transfer coefficient R the gas constant (J K^{-1} mol^{-1}), T the absolute temperature (K), v the scan rate (Vs^{-1}), and F the Faraday constant ($Cmol^{-1}$).
Closer inspection of the voltammetric data obtained at slower scan rates reveals a loss of charge sequentially cycle-by-cycle (see figure 5.5). The fast cyclic

voltammogram (scan rate 16 Vs^{-1}) was used as a probe measurement, and a slow cyclic voltammogram (not shown, scan rate 10 mVs^{-1}) was employed to enhance the loss effects which are attributed here to a chemical degradation process similar to that observed for the structurally related N719 dye.[7] The alternative mechanism of a loss of Z907 caused by simple desorption cannot be entirely ruled out but appears less likely (vide infra).

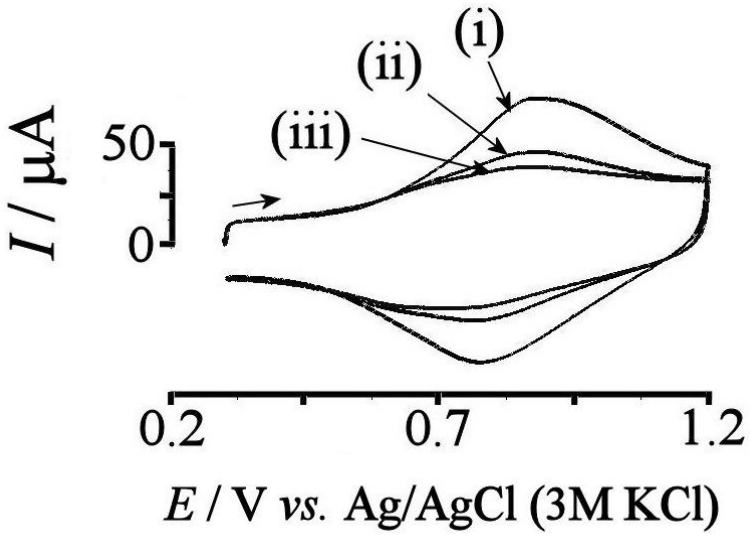

Figure 5.5 Cyclic voltammograms (scan rate 16 Vs^{-1}) for the oxidation and back-reduction of Z907 adsorbed onto a 9 mm^2 FTO electrode (1 hour in 10^{-6} M dye solution) and immersed in acetonitrile/0.1 M NBu_4PF_6. The three cyclic voltammograms represent (i) the first potential cycle, (ii) the potential cycle recorded after a slow potential cycle at 10 mVs^{-1} (not shown), and (iii) the potential cycle after a further slow potential cycle (not shown).

The chemical degradation of Z907 was followed as a function of the number of slow potential cycles (see figure 5.6 A-C). Interestingly, the loss of the Z907 response caused by slow scan rate experiments was found to depend on the conditions during the adsorption process. Data in figure 5.6 A to C have been obtained for two different Z907 concentrations and for two different equilibration times. In order to analyse these "decay curves", first order decay kinetics has been assumed with only a fraction of the adsorbed Z907 chemically reactive. In particular, for higher Z907 concentrations and for extended equilibration times a fraction of the Z907 complex appeared to be inert. The expression for fitting the decay curves (see figure 5.6 A-C)

has therefore two terms for (i) inert Z907 with a surface concentration [Z_0^{inert}] and (ii) reactive Z907 with an initial surface concentration [$Z_0^{reactive}$] (see equation 5.2).

5.2 $$[Z(t)] = [Z_0^{inert}] + [Z_0^{reactive}]e^{-kt_{ox}}$$

In this expression the chemical rate constant k can be obtained when the oxidation time (the time during slow scan cyclic voltammograms with applied potential positive of the reversible Ru(III/II) potential) is estimated (here t_{ox} = 112 s). The surface concentration of Z907 is expressed in terms of the charge under the oxidation response. Figure 5.6 A shows the data obtained for Z907 adsorption for 1 hour from a 10^{-6} M solution. The fraction of reactive Z907 is estimated to be 90%, and the decay rate constant $k = 1.1 \times 10^{-2}$ s^{-1}. In contrast, in figure 5.6 B (adsorption for 1 hour from 0.5×10^{-3} M solution) the fraction of reactive Z907 is 98% and the decay rate constant $k = 0.8 \times 10^{-2}$ s^{-1}. Finally, in figure 5.6 C (adsorption for 16 hours from 0.5×10^{-3} M solution) the fraction of reactive Z907 is 82% and the decay rate constant $k = 0.5 \times 10^{-2}$ s^{-1}.

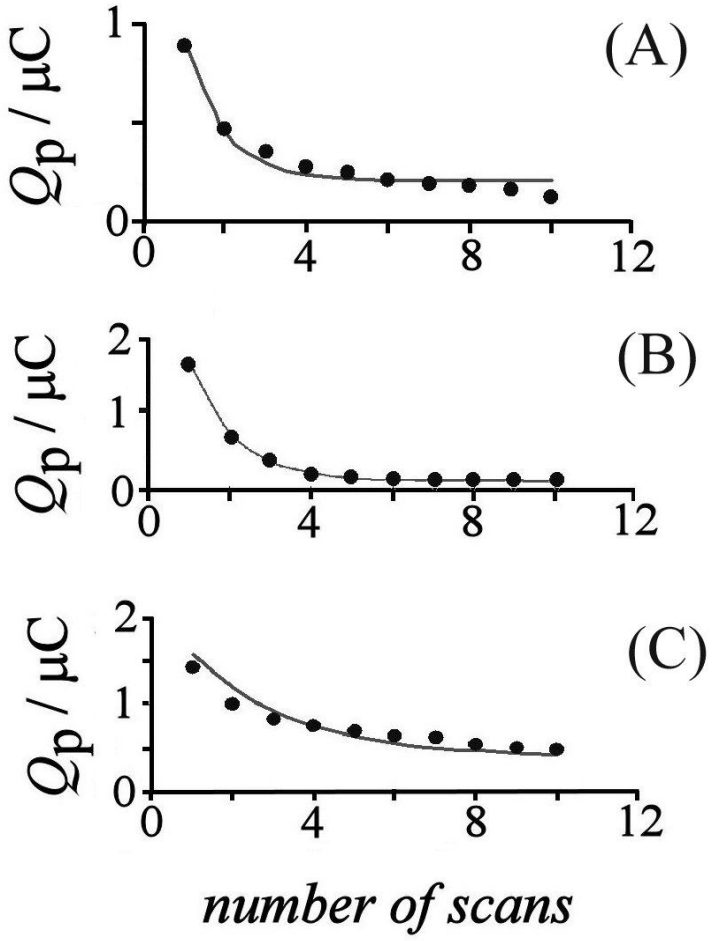

Figure 5.6 (A) Plot of the charge under the oxidation peak, Q_p (recorded at 16 Vs^{-1}), versus the number of slow potential cycles (10 mVs^{-1}) for Z907 adsorbed onto FTO (1 hour in a 10^{-6} M dye solution). The line shows a theoretical decay for a chemical rate constant $k = 1.1\times10^{-2}$ s^{-1}. Electrode area was 9 mm^2. (B) As before (1 hour in a 0.5×10^{-3} M dye solution). The line shows a theoretical decay for a chemical rate constant $k = 8\times10^{-3}$ s^{-1}. Electrode area was 9mm^2 (C) As before (16 hours in a 0.5×10^{-3} M dye solution). The line shows a theoretical decay for a chemical rate constant $k = 5\times10^{-3}$ s^{-1}. Electrode area was 9mm^2

Although the variation in the rate constant is small, there is a clear trend of slower decay with higher Z907 concentration and with a prolonged adsorption time. More importantly, the fraction of inert Z907 on the electrode surface can be increased by a longer adsorption period and this impacts on the initial rate of decay (see figure 5.6 C).

The decay rate constant for Z907, $k = 0.5 \times 10^{-2}$ s^{-1}, is more than two orders of magnitude slower compared to the value[14] of $k = 2.4$ s^{-1} observed for the related dye N719 (which has the same molecular structure, but without nonyl functionalities). For structurally closely related Ru complexes a degradation reaction via ligand loss has been proposed.[12] The retardation of the degradation process is likely to arise from the steric hinderence effect introduced by the packing of nonyl functionalities. The decrease in reactivity when a longer period of adsorption is employed is consistent with improved ordering of the adsorbed Z907 on the FTO electrode surface. Figure 5.7 summarises the idea of ordering and steric shielding.

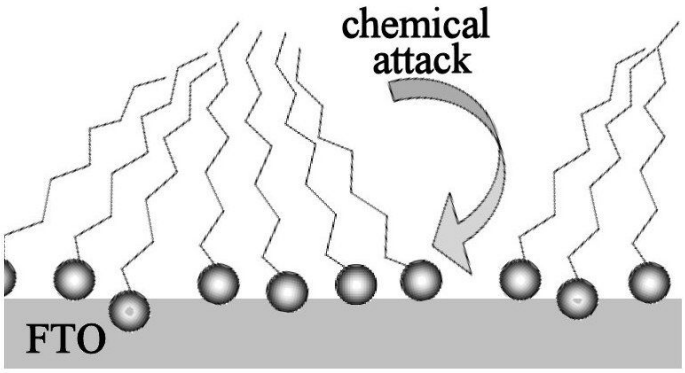

Figure 5.7 Schematic drawing of the orientation of immobilised Z907 dye molecules at the FTO electrode surface and possible nucleophilic attack for example by H_2O (see text).

5.3.3 Adsorption and redox chemistry of cis-RuLL'$(SCN)_2$ with L=4,4'-dicarboxylic acid-2,2'-bipyridine and L'=4,4'-dinonyl-2,2'-bipyridine (Z907) at FTO-TiO_2 thin film electrode surfaces

Z907 was adsorbed onto FTO-TiO_2 electrodes with a thin mesoporous TiO_2 film of approximately 3 μm thickness. The cyclic voltammograms shown in figure 5.8 A show a substantial increase in current and in the charge under the voltammetric response in the presence of the TiO_2. The peak current at fast scan rate (16 Vs^{-1}) is increased by a factor ten (see figure 5.3A and figure 5.5A), and the charge under the oxidation process can reach 600 μC (compared to ca. 1 μC for bare FTO). It can be seen that the peak-to-peak separation is widened which is not surprising given the higher peak current. The resistance causing this effect can be obtained as $R = \frac{\Delta E_p - 0.057}{\Delta I_p} = \frac{10 - 0{,}0057}{3.3x10^{-3}} = 285\Omega$. This value is in good agreement with the FTO thin film resistance.

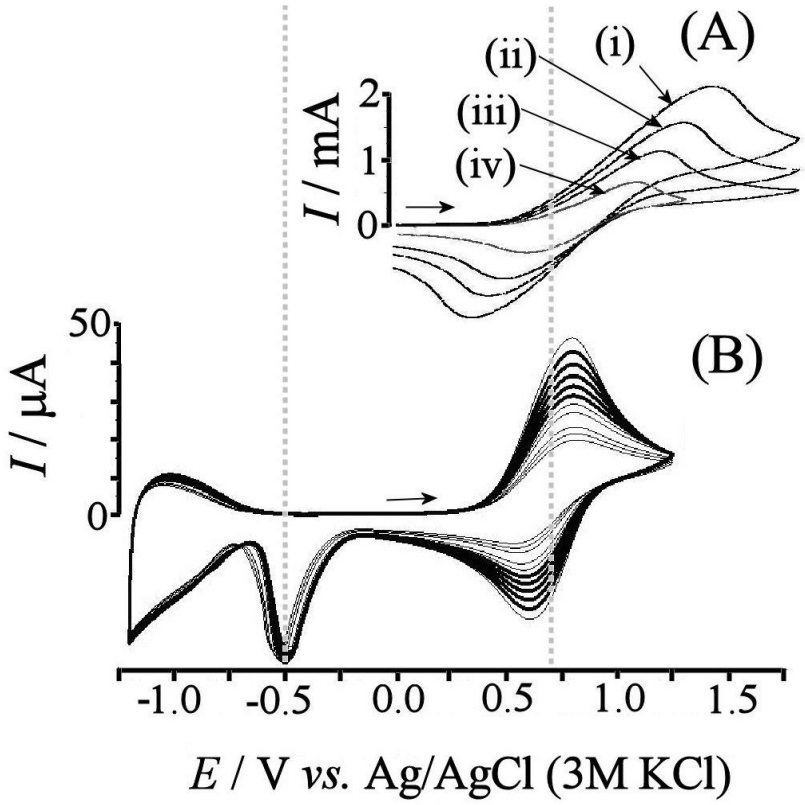

Figure 5.8 (A) Cyclic voltammetry (scan rates (i) 16, (ii) 8, (iii) 4, and (iv) 1.6 Vs^{-1}) for the oxidation and back-reduction of Z907 adsorbed onto a FTO-TiO_2 film electrode (16 hours in 10^{-4} M dye solution) immersed in acetonitrile/0.1 M NBu_4PF_6. (B) Multi-scan cyclic voltammetry (scan rate 0.1 Vs^{-1}) for the oxidation and re-reduction of Z907 adsorbed onto a FTO-TiO_2 film electrode (16 hour in 10^{-4} M dye solution) immersed in acetonitrile/0.1 NBu_4PF_6.

Due to slow electron diffusion within the film, a slow scan rate was required in order to determine the overall charge. Typical apparent diffusion coefficients for charge hopping are reported to be D ≈ 10^{-13} m^2s^{-1},[5] which leads to an estimated diffusion layer thickness[10] (equation 4.2) of

5.3
$$\delta = \sqrt{\frac{DRT}{vF}} = \sqrt{\frac{10^{-13} \times 8.31 \times 293}{0.016 \times 96487}} = 0.4 \mu m$$

Assuming a scan rate of $v = 0.016$ Vs^{-1}. Therefore, the limiting charge in figure 5.9 A is substantial and may approach exhaustive oxidation. The data in figure 5.9 A and

5.9 B demonstrate the effect of scan rate on the binding isotherms derived from the voltammograms. Reassuringly, the approximate Langmuirian binding constant, $K = 4 \times 10^4$ M^{-1}, is independent of the scan rate.

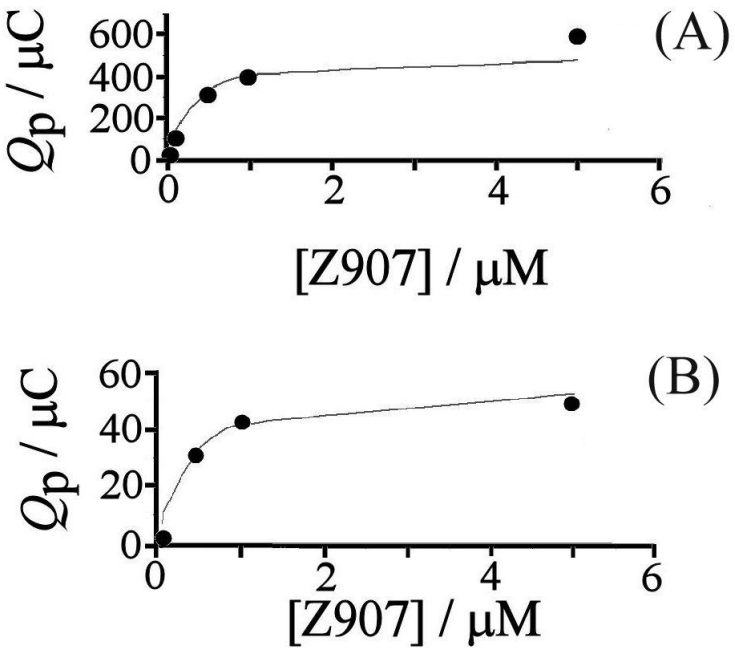

Figure 5.9 (A) Plot of the charge under the oxidation peak versus concentration of Z907 during dye adsorption (16 hours in dye solution). Scan rate: 16 mVs^{-1}. The line corresponds to a Langmuirian binding constant $K = 4\times10^4$ M^{-1}. (B) As before but with a scan rate: 16 Vs^{-1}. The line corresponds to a Langmuirian binding constant $K = 4\times10^4$ M^{-1}.

Loss of Z907 at the FTO electrode surface can impede the flow of electrons to and from the TiO_2 via hopping, and this can reduce the peak current for Z907 adsorbed onto TiO_2. When the potential is cycled over a wider potential range, it appears that the remaining oxidised dye at the TiO_2 surface which cannot communicate with the substrate by electron hopping can be reduced at a more negative potential due to the onset of bulk conduction due to electron injection into the TiO_2 film.[5] Figure 5.8 B shows a new peak response at -0.5 V vs. Ag/AgCl (3 M KCl) which has been attributed to a direct Ru(III/II) reduction for immobilised Z907 via electron conduction through TiO_2.[5] In spite of this reduction, the voltammetric response at more positive potentials for the immobilised Z907 dye continues to decay and this can primarily be ascribed to the chemical degradation of the Z907 dye at the FTO

electrode surface. Interestingly, the peak current for the cathodic response at -0.5 V vs. Ag/AgCl (3 M KCl) remains almost constant which could be interpreted as an insignificant degradation of Z907 on the TiO_2 surface.

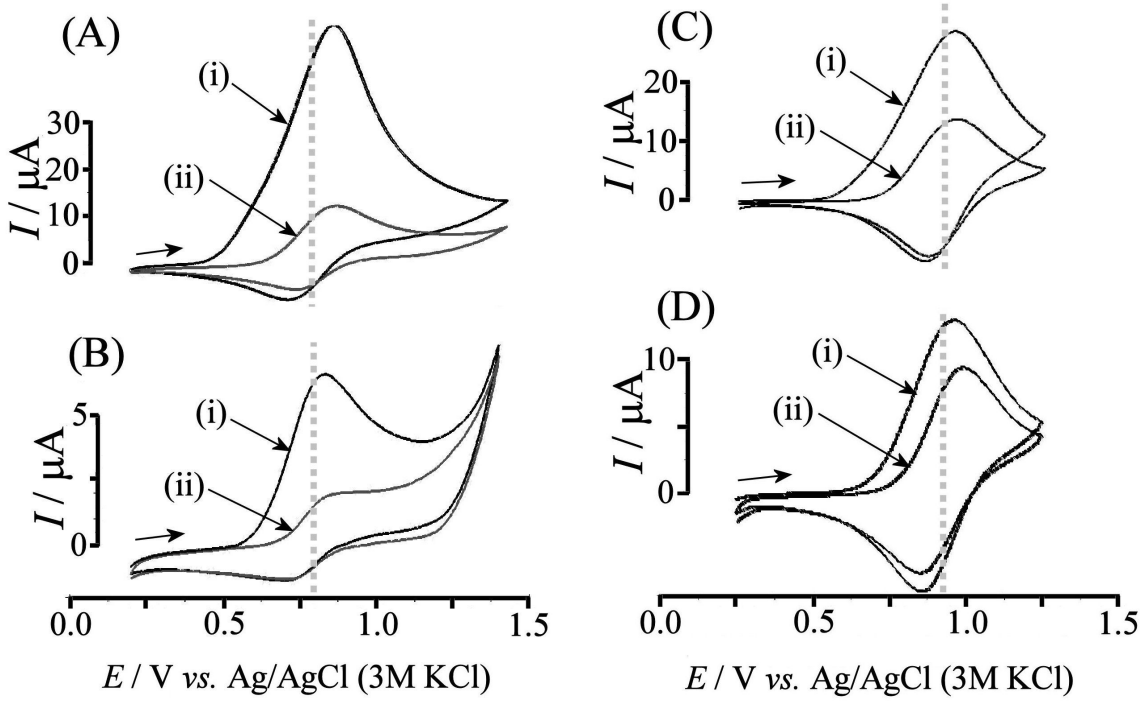

Figure 5.10 (A) Cyclic voltammograms (scan rate 16 mVs^{-1}, (i) first and (ii) second potential cycle) for the oxidation and back-reduction of Z907 adsorbed onto a FTO-TiO_2 film electrode (16 hours in 10^{-4} M dye solution) immersed in acetonitrile/0.1 M NBu_4PF_6. Electrode area was 9 mm^2. (B) As above showing (i) potential cycle 3 and (ii) potential cycle 4 recorded after a delay of 10 minutes. Electrode area was 9 mm^2. (C) Cyclic voltammograms (scan rate 16 mVs^{-1}, (i) first and (ii) second potential cycle) for the oxidation and back-reduction of Z907 adsorbed onto a FTO-TiO_2 film electrode (16 hours in 0.5×10^{-3} M dye solution) immersed in acetonitrile/0.1 M NBu_4PF_6. Electrode area was 9 mm^2. (D) As above showing (i) potential cycle 3 and (ii) potential cycle 4 recorded after a delay of 10 minutes. Electrode area was 9 mm^2.

The loss of the oxidation response for Z907 adsorbed onto FTO-TiO_2 is shown in figure 5.10. Consecutive cyclic voltammograms at slower scan rate clearly demonstrate the loss of oxidation response (in part due to loss of electron hopping conductivity at the FTO electrode surface and in part due to Ru(III) centres in the

TiO_2 which in electron hopping communication with the substrate). When changing the conditions for the Z907 adsorption procedure, again a marked change in the behaviour is observed. The decay of the oxidation response appears much slower when a 16 h deposition and equilibration time in 0.5×10^{-3} M Z907 bath were employed (see figure 5.10 C and 5.10 D). The rate of decay of the voltammetric response for the Ru(III/II) redox process on FTO and on FTO-TiO_2 are very similar which suggests that chemical degradation occurs rather than simple desorption. In the latter case the availability of more weakly bound Z907 from the TiO_2 surface should suppress the loss. This is not observed.

5.3.4 Spectroelectrochemistry of cis-RuLL'$(SCN)_2$ with L=4,4'-dicarboxylic acid-2,2'-bipyridine and L'=4,4'-dinonyl-2,2'-bipyridine (Z907) at FTO-TiO_2 thin film electrode surfaces

Further insight into the electrochemical and chemical processes for Z907 dye immobilised onto a FTO-TiO_2 film electrode was obtained by spectro-electrochemistry. First, the uptake of Z907 dye into the TiO_2 film was studied by UV/Vis absorption. The resulting coloured FTO-TiO_2 were immersed in aqueous/ethanolic (50:50) 0.1 M NaOH to desorb the Z907. The UV/Vis spectra of the solution after desorption were used to determine the absolute amount of adsorbed Z907. Figure 5.11 shows that again approximate Langmuirian characteristics are observed with a binding constant of ca. $K = 4 \times 10^4$ M^{-1} in agreement with data obtained by voltammetry (vide supra).

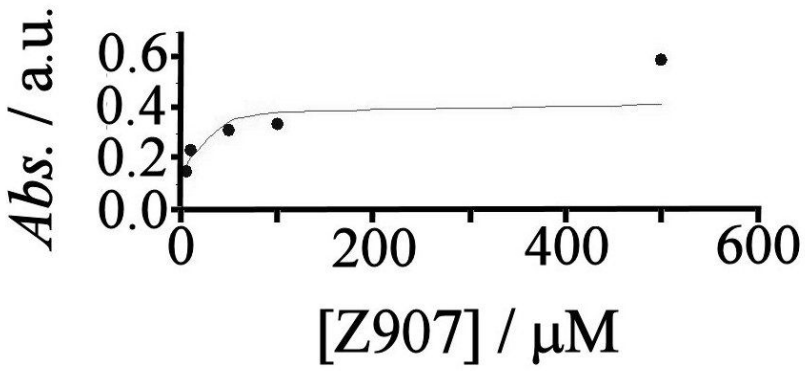

Figure 5.11 Plot of absorbance for Z907 on FTO-TiO_2 (at 510 nm) versus Z907 concentration during adsorption onto FTO-TiO_2 film electrodes (16 hours in dye solution). The line corresponds to a Langmuirian binding constant $K = 4\times10^4$ M^{-1}

The Z907 dye adsorbed onto TiO_2 shows an absorption maximum at ca. 520 nm (see figure 5.12 A). This apparent contradiction to cyclic voltammetry data in figure 5.10 A, is likely to be caused by a much higher uncompensated resistance distortion for the large area of the electrode employed in spectroelectrochemical experiments. When the applied potential is made more positive than the Ru(III/II) potential, this absorption peak shifts to longer wavelengths and decreases in strength. Simultaneously a new absorption appears at 780 nm, which is characteristic of the oxidised Z907 Ru(III) system.[5] In the case of a freshly prepared electrode, this process is almost fully reversible as reported in the literature.[5] Figure 5.12 B shows the return of the absorption peak at 520 nm when the potential is cycled back to 0.3 V vs. Ag/AgCl(3M KCl). When multiple slow scan rate potential cycles are carried out corresponding to exhaustive oxidation conditions the visual appearance of the Z907 modified FT-TiO_2 electrode does not change significantly, but the voltammetric response is diminished as discussed in the previous section. Subsequent desorption of the Z907 dye (after exhaustive potential cycling) into aqueous/ethanolic (50:50) 0.1 M NaOH followed by UV/Vis spectroscopy suggests that only minor chemical changes have occurred (see figure 5.12 C). It seems therefore likely that the chemical degradation of Z907 occurs predominantly at the FTO electrode surface and only to an insignificant extent on the TiO_2 surface. The stronger binding of Z907 onto FTO (compared to TiO_2) is likely to result in less mobility, less ordering, and a higher strain on the molecules all of which may

contribute to the degradation of $Z907^+$. From the UV/Vis data in figure 5.12 C the "molecular footprint" for Z907 on TiO_2 can be estimated as 2 nm^2 (assuming 9 nm diameter particles) in excellent agreement with a densely packed surface (vide supra).

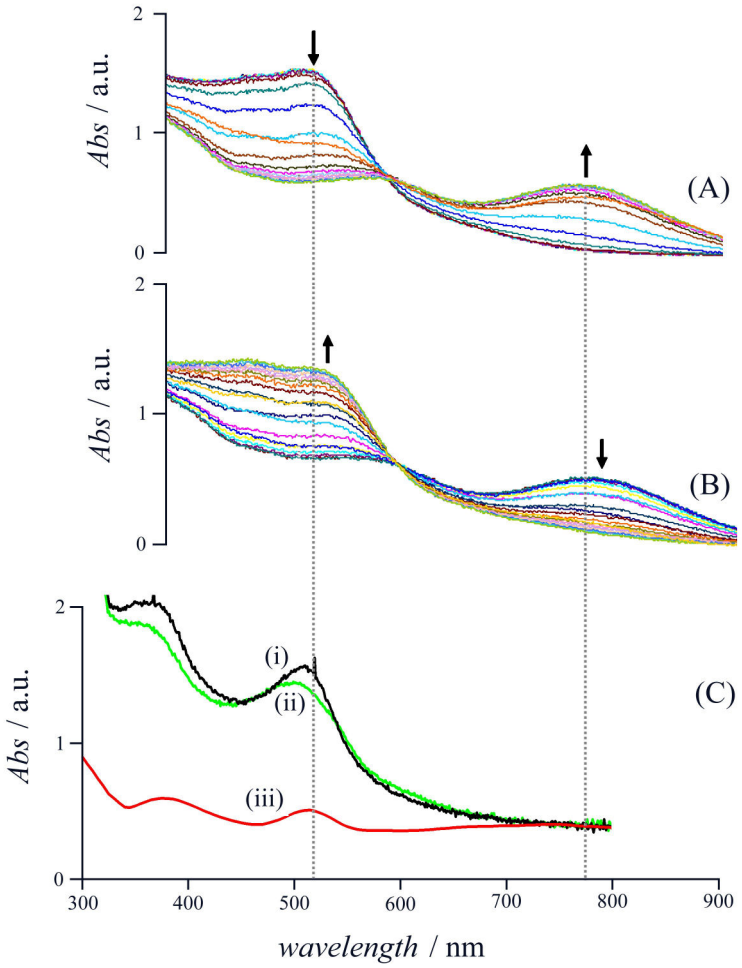

Figure 5.12 . (A) UV-Vis spectroelectrochemical data (potential range from 0.3 V to 1.1 V, stepped by 50 mV every 5 s) for the oxidation of Z907 adsorbed onto a FTO-TiO_2 film electrodes (16 hours in 0.5×10^{-3} M dye solution) immersed in acetonitrile/0.1 M NBu_4PF_6. (B) As before but for the reduction of Z907 (potential range from 1.1 V to 0.3 V, stepped by -50 mV every 5 s). (C) UV/Vis spectra for Z907 desorbed from a FTO-TiO_2 electrode into a solution of 0.1 M NaOH in aqueous ethanol (50:50). (i) Z907 on FTO-TiO_2 (16 hours in 10^{-4} M dye solution), (ii) Z907 on FTO-TiO_2 electrode after running a 20 cyclic voltammograms (10 mVs^{-1}), and (iii) difference spectrum.

Changes observed in voltammetric responses for the Ru(III/II) system are dominated by the electron hopping process directly at the FTO electrode surface (see figure

5.13). Degradation of Z907 at the FTO electrode surface causes a lower rate of hopping conduction and this suppresses the Ru(III/II) surface redox process.

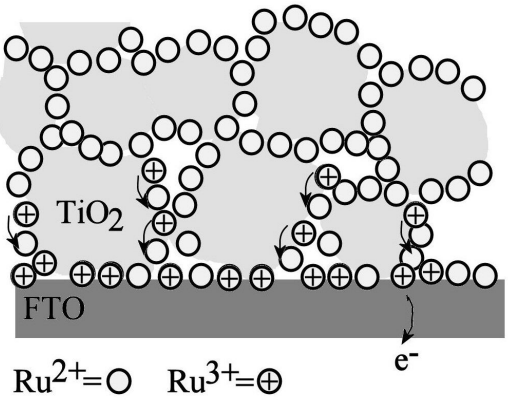

Figure 5.13 Schematic representation of the electron hopping mechanism responsible for the Z907 surface electrochemistry on FTO-TiO_2 film electrodes.

5.4 Conclusions

It has been demonstrated that for the Z907 dye system Ru(III/II) direct redox chemistry can be observed on FTO and on FTO-TiO_2 electrode surfaces. The binding constant for Z907 on FTO is significantly higher compared to that on TiO_2 although the molecular "footprints" for mono-layer adsorption are very similar. A fraction of Z907 adsorbed onto FTO undergoes a slow EC-type chemical degradation after oxidation. The dye adsorption conditions allow this fraction to be somewhat reduced. No significant degradation of oxidised Z907 occurs on TiO_2.

The Z907 degradation at the FTO electrode surface could have a small beneficial effect on the operation of solar cells due to a reduced rate of recombination processes (of Ru(III) and electrons[13]) at this interface. However, the absence of chemical Z907 degradation processes on the TiO_2 surface is important for a long operational lifetime under solar cell operation conditions. Further studies of the effects of (i) the solvent environment, (ii) other substrates, and (iii) temperature on the chemical Z907 degradation process will be required and the nature of the degradation product needs to be identified.

References

1. Zakeeruddin, S. M.; Nazeeruddin, M. K.; Humphry-Baker, R.; Pechy, P.; Quagliotto, P.; Barolo, C.; Viscardi, G.; Gratzel, M., *Langmuir* **2002,** *18* (3), 952-954.
2. Kroon, J. M.; Bakker, N. J.; Smit, H. J. P.; Liska, P.; Thampi, K. R.; Wang, P.; Zakeeruddin, S. M.; Gratzel, M.; Hinsch, A.; Hore, S.; Wurfel, U.; Sastrawan, R.; Durrant, J. R.; Palomares, E.; Pettersson, H.; Gruszecki, T.; Walter, J.; Skupien, K.; Tulloch, G. E., *Progress in Photovoltaics* **2007,** *15* (1), 1-18.
3. Shklover, V.; Ovchinnikov, Y. E.; Braginsky, L. S.; Zakeeruddin, S. M.; Gratzel, M., *Chemistry of Materials* **1998,** *10* (9), 2533-2541.
4. Finnie, K. S.; Bartlett, J. R.; Woolfrey, J. L., *Langmuir* **1998,** *14* (10), 2744-2749.
5. Wang, Q.; Zakeeruddin, S. M.; Nazeeruddin, M. K.; Humphry-Baker, R.; Gratzel, M., *Journal of the American Chemical Society* **2006,** *128* (13), 4446-4452.
6. Fattori A, P. L., Belding SR, Compton RG, Marken F, *Journal of Electroanalytical Chemistry* **2010**.
7. Pearson, P.; Bond, A. M.; Deacon, G. B.; Forsyth, C.; Spiccia, L., *Inorganica Chimica Acta* **2008,** *361* (3), 601-612.
8. Dennany, L.; O'Reilly, E. J.; Keyes, T. E.; Forster, R. J., *Electrochemistry Communications* **2006,** *8* (10), 1588-1594.
9. Fillinger, A.; Parkinson, B. A., *J. Electrochem. Soc.* **1999,** *146* (12), 4559-4564.
10. Scholz, E. F., *Electroanalytical Methods*. Springer: 2005.
11. Bard, L. R. F. A. J., *Electrochemical Methodes Fundamaentals and Applications*. John Wiley & Sons Inc.: New York, 2001.
12. Wolfbauer, G.; Bond, A. M.; MacFarlane, D. R., *Inorg. Chem.* **1999,** *38* (17), 3836-3846.

Chapter 6: Redox chemistry of indoline solar cell dyes immobilized at fluorine-doped tin oxide (FTO) and at TiO_2 surfaces

Contents

The work presented in this chapter is based on a forthcoming publication:

Redox Chemistry and Fast Hole Conduction Observed for Indoline Sensitizer Dyes Immobilised at Fluorine-Doped Tin Oxide (FTO) and TiO_2 Surfaces Alberto Fattori, Laurence M. Peter, Hongxia Wang, Hidetoshi Miura, and Frank Marken. To be submitted.

6.1 Abstract

The indoline dyes D102, D131, D149, and D205 are characterized when adsorbed on fluorine-doped tin oxide (FTO) and TiO_2 electrode surfaces. Adsorption from 50:50 acetonitrile – tert.-butanol onto fluorine-doped tin oxide (FTO) allows approximate Langmuirian binding constants of 6.5×10^4 mol^{-1} dm^3, 2.0×10^3 mol^{-1} dm^3, 2.0×10^4 mol^{-1} dm^3, and 1.5×10^4 mol^{-1} dm^3 (respectively) to be determined. Voltammetric data obtained in acetonitrile 0.1 M NBu_4PF_6 suggest reversible one-electron oxidation at E_{mid} = 0.94, 0.91, 0.88, and 0.88 V vs. Ag/AgCl(3M KCl), respectively, with aggregation (at high coverage) causing additional peak features at more positive potentials. Slow chemical degradation processes and electron transfer catalysis for iodide oxidation are observed for all four oxidized indolinium cations. When adsorbed onto TiO_2 nanoparticle films (ca. 9 nm particle diameter and ca. 3 μm thickness on FTO), reversible voltammetric responses with E_{mid} = 1.08, 1.16, 0.92, and 0.95 V vs. Ag/AgCl(3M KCl), respectively, suggest unusually fast electron/hole hopping diffusion (with $D_{app} > 5 \times 10^{-9}$ m^2s^{-1}) for all four indoline dye surface aggregates. Slow dye degradation is shown to affect charge transport via electron hopping. Spectro-electrochemical data for the adsorbed indoline dyes on FTO-TiO_2 suggests a red-shift of absorption peaks after oxidation and the presence of a strong charge transfer band in the near IR. Implications for solar cell devices are discussed.

6.2 Introduction

As discussed in the previous chapters, in order to improve DSCs efficiency, studies have been focused on the optimization of the device components such as electrolyte, semiconductor and dyes.[1-2] Solar cell dyes are crucial elements that influence significantly the DSC power conversion as well as its stability.[3] So far the most favoured sensitizers in DSCs have been ruthenium-based complexes, and among these particular attention has been given to *cis*-bis(isothiocyanato)-bis(2,2'-bipyridyl-4,4'dicarboxylato)-ruthenium(II)[4] also known as N719 and (*cis*-RuLL'$(SCN)_2$ with L=4,4'-dicarboxylic acid-2,2'-bipyridine and L'=4,4'-dinonyl-2,2'-bipyridine) known as Z907 [5-6] and phthalocyanine-ruthenium(II).[7] Since ruthenium based dyes are expensive, research moved towards the synthesis and investigation of metal-free organic dyes such as indoles,[8] hemicyanines,[9] anthocyanines,[10] coumarins,[11] and porphyrins.[12] More recently indoline[13-14] dyes have attracted attention due to their particular structure, their cheap and easy synthesis, and their high molar extinction coefficient.[15] Indoline dyes have several advantages as photosensitizers for DSCs:

(1) They have larger extinction coefficients (attributed to a strong intramolecular π-π^* transitions)[16] compared to metal-complex photosensitizers (which exhibit MLCT absorption).[17] These large extinction coefficients lead to efficient light harvesting properties in very thin films.

(2) The variety in their structures provides ample possibilities for molecular design, e.g. the introduction of substituents allows the control of their absorption spectra and aggregation properties. Sometimes co-adsorbers are used to allow further control in dye assembly process.[18]

(3) There are no concerns about resource limitations, because organic dyes do not contain noble metals such as ruthenium.

The main disadvantage of organic sensitizers is a tendency to undergo molecular aggregation leading to intermolecular quenching, faster electron-hole recombination, and potentially poor connection between the dye molecules and the semiconductor[19] which in turn may slow down the electron injection into the conduction band of the

titanium dioxide. A way to overcome the aggregation is by introducing long alkyl chains or aromatic groups in the molecular structure.[20]

Indoline dyes with increased π-conjugation have given high cell efficiencies. For example, the dye D205 gave a 7.2% power conversion efficiency.[19] The series "D" of indoline dyes such as D102, D131, D149, D205 (see figure 6.1), has attracted considerable attention due to their high extinction coefficients and excellent performance as sensitizers.[21] The adsorption of indoline dyes on TiO_2 nanoparticles and nanotubes[22] has been investigated experimentally and by computer simulation. Howie et al. showed that indoline dyes D102 D131 and D149 attach to the semiconductor surface via bidentate binding and with different orientation (parallel or vertical) to the substrate surface.[23]

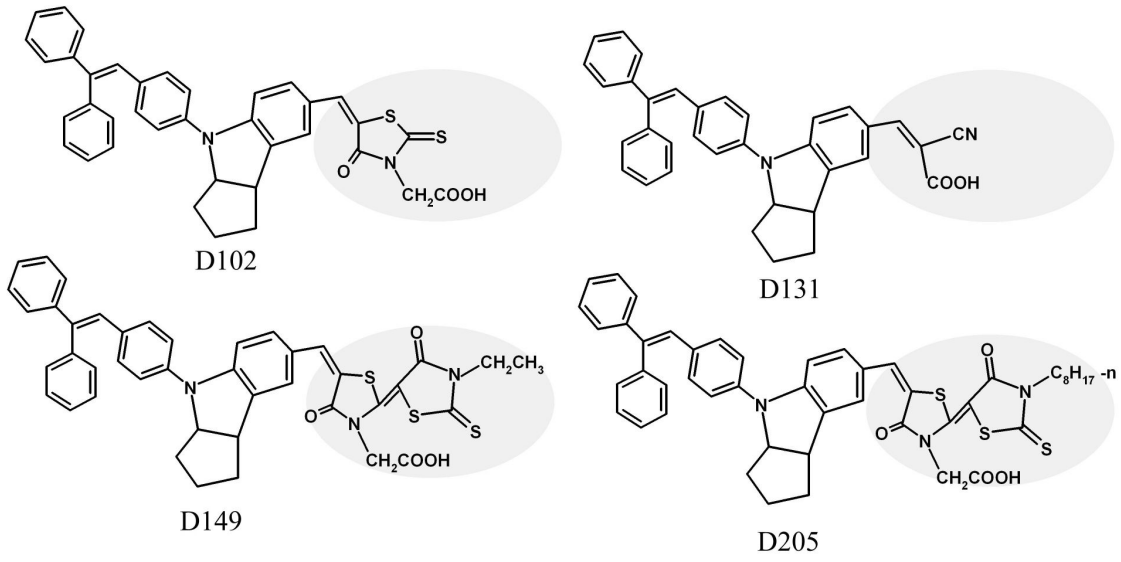

Figure 6.1 Molecular structures for indoline dyes D102, D131, D149, and D205.

It has been previously demonstrated for ruthenium dyes that the electron transfer between dye molecules when adsorbed on FTO- TiO_2 substrates occurs via electron hopping[24] with a typical apparent diffusion coefficient of $D_{app} = 10^{-13}$ m^2s^{-1} (see chapter 4).[25] In this chapter, it is shown that the same mechanism is responsible for charge percolation between the indoline/indolinium dye molecules. However, in the case of indoline dyes, due to dye aggregation (J-aggregate formation)[13] and charge delocalization, a much faster rate of electron hopping (with $D_{app} > 5 \times 10^{-9}$ m^2s^{-1}) is

observed. As a result charge diffusion in solar cell absorber layers is predicted to be significantly faster compared to ion diffusion in the surrounding organic solution phase. Electrochemical and spectroelectrochemical studies are reported for the four indoline dyes adsorbed at the surface of FTO and FTO-TiO_2 substrates. The electrocatalytic oxidation of iodide in the presence of indoline dyes is demonstrated, and the link between dye structure, dye degradation, and solar cell performance is discussed.

6.3 Experimental

6.3.1 Instrumentation and chemicals

The description of the instrumentation and chemicals used for conducting the experiments reported in this chapter can be found in Chapter 3 Experimental Techniques and Methods.

6.3.2 Methodologies

FTO slides were washed following procedure reported in chapter 3.2.2. In order to reduce series resistance losses, a gold stripe was evaporated onto FTO electrode surface (not exposed to the solution). Indoline dyes adsorption on bare FTO and FTO-TiO_2 was carried out by heating the electrodes for 30 minutes at 450 °C on a hot plate, cooling down to 75 °C, and immersion into a solution of dye in 50% acetonitrile 50% ^{t}BuOH (for 1 hour for electrochemical studies and 16 hours for spectroelectrochemical studies).

FTO-TiO_2 films were prepared by "doctor blading" (chapter 3.2.2). The FTO electrode is then left for 30 minutes on a hot plate at 450 ^{o}C in order to sinter the anatase crystals. Unless stated otherwise D102, D131, D149, D205 adsorption at these electrodes, was achieved using a dye bath of $5x10^{-5}$ M for voltammetric studies, and $5x10^{-4}$ M for spectroelectrochemical studies. The solvent was 50% acetonitrile 50% ^{t}BuOH.

6.4 Results & Discussion

6.4.1 Adsorption and oxidation of indoline dyes at FTO electrode surfaces

The indoline dyes used in this study feature a carboxylate functionality to facilitate binding to inorganic oxide surfaces. A fluorine-doped tin oxide (FTO) electrode surface immersed into a solution of indoline dye (in 50:50 acetonitrile:tert.-butanol) readily binds these dyes, and the resulting modified electrode can be studied by cyclic voltammetry in acetonitrile 0.1 M NBu_4PF_6.

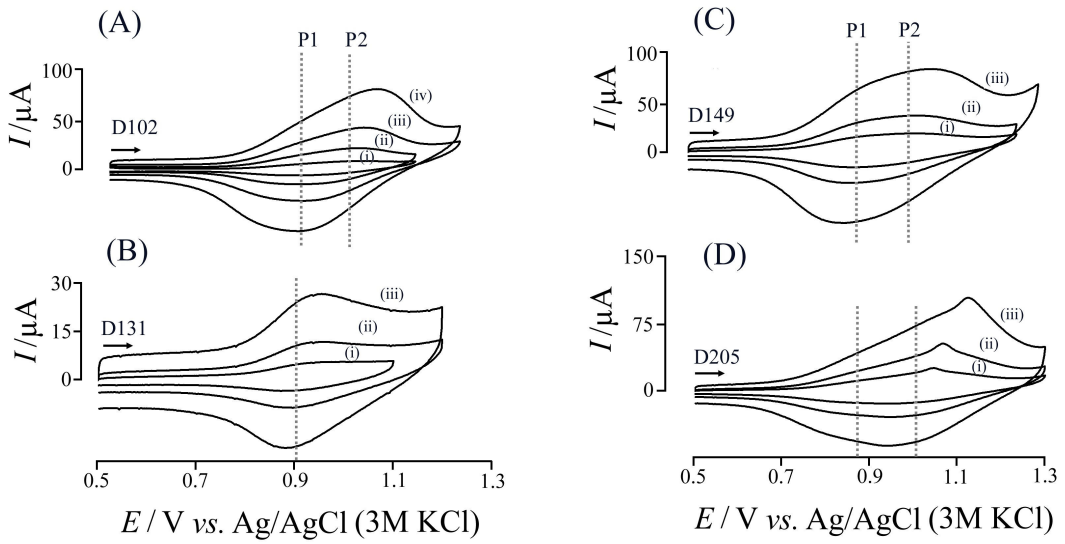

Figure 6.2 Cyclic voltammograms (scan rate (i) 1.6, (ii) 4, (iii) 8, and (iv) 16 V s^{-1}) for the oxidation of D102 (A), D131(B), and D149 (C) and D205 (D) adsorbed onto FTO (area 9 mm^2, from a 5×10^{-5} M dye bath) and immersed in acetonitrile 0.1 M NBu_4PF_6.

Figure 6.2 A-D shows typical voltammetric responses for the oxidation and back-reduction of D102, D131, D149 and D205 adsorbed onto FTO. The oxidation appears chemically reversible (at high scan rate) and it is apparent that there are probably two (or more) redox systems present (indicated as dashed lines P1 and P2). For D102, the presence of two separate redox systems separated by ca. 90 mV is attributed here to aggregation of the dye molecules at the electrode surface. Non-quenching aggregation of indoline dyes adsorbed onto electrode surfaces has been reported previously[26] and configurational isomers such as planar and perpendicular

to the electrode surface ("lying down" and "standing up") have been discussed.[23] For D102 the two midpoint potentials can be estimated as 0.94 V vs. Ag/AgCl (P1) and 1.03 V vs. Ag/AgCl (P2, see Table 1). For an aggregated dye, the formation of radical cations during oxidation can result in a repulsive interaction between oxidized D102 molecules and this will lead to broadening of the voltammetric response and appearance of additional features at high coverage. Similar experiments were carried out with the indoline dyes D131, D149, and D205 (figure 6.2 B-D) and generally very similar redox behaviour was observed (see Table 1). The dye D131 appears to be structurally distinct with the carboxylate group attached to a carbon – carbon double bond. Presumably due to a lower surface coverage, for D131 only one reversible redox system at E_{mid} = 0.91 V vs. Ag/AgCl and with a peak width at half height of ca. 150 mV (at a scan rate 16 Vs^{-1}) is observed. When plotting the peak current versus scan rate (see figure 6.3 A-D) a linear dependence consistent with an adsorbed redox system is observed for all four dyes.

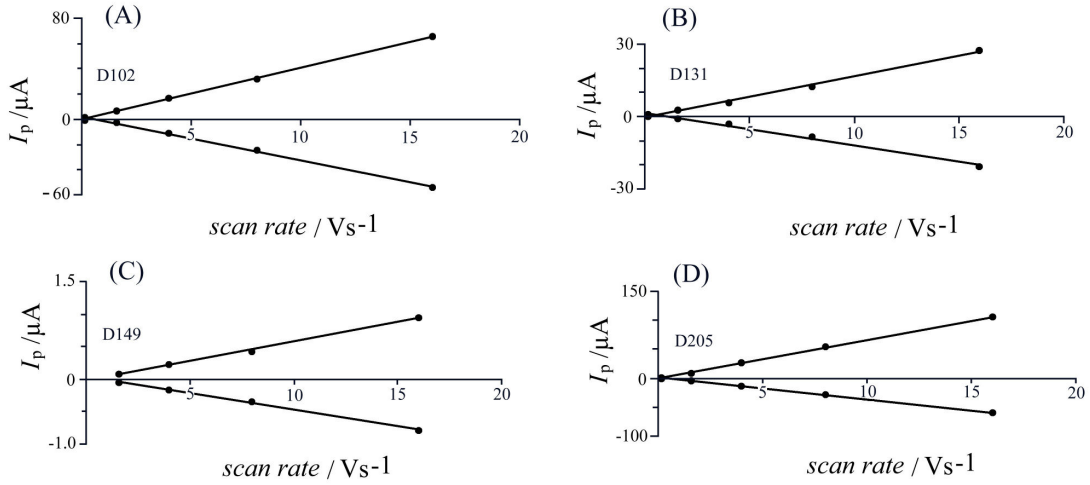

Figure 6.3 (A-D) Plot of the peak current (I_p) versus scan rate for the oxidation and back-reduction of D102 (A), D131 (B), D149 (C), D205 (D) adsorbed onto FTO.

In summary, it is observed that FTO-immobilized indoline dyes are oxidized in a chemically reversible process (see equation 6.1) at a sufficiently fast scan rate.

6.1 $$D(FTO) \rightleftharpoons D^{+}(FTO) + e^{-}$$

Next, experiments were carried out as a function of dye bath concentration in order to evaluate the adsorption characteristics. Figure 6.4 A-D shows the typical limiting behaviour for a plot of peak charge versus dye bath concentration and a Langmuir line indicating the theoretically expected behaviour for a mono-layer charge density which was for D102 (figure 6.4 A) of 11 μC cm^{-2} (measured on a 9 mm^2 electrode) and a binding constant of $K_{D102} = 6 \times 10^4$ mol^{-1} dm^3. Figure 6.4 B shows the Langmuirian curve for D131 with 11 μC cm^{-2} and a binding constant $K_{131} = 2 \times 10^3$ mol^{-1} dm^3. Values for D149 are shown figure 6.4 C with a charge of 11 μC cm^{-2} and $K_{149} = 5 \times 10^4$ mol^{-1} dm^3. For D205 the charge is 11 μC cm^{-2} and binding constant is $K_{205} = 6 \times 10^4$ mol^{-1} dm^3. The mono-layer coverage of ca. 11 μC cm^{-2} (corresponding to 6.8×10^{13} molecules cm^{-2}) is not very well defined (probably ± 25 % error) but it is very much consistent with the anticipated molecular "footprint" of approximately 2×10^{-18} m^2 per dye molecule[25] (corresponding to 7.4×10^{13} molecules cm^{-2}, (see Table 1).

Very similar results have been observed for the four dyes except that D131 appears to bind more weakly with $K_{D131} = 2 \times 10^3$ mol^{-1} dm^3 and therefore giving cyclic voltammetry data consistent with only partial surface coverage. The data shown in figure 6.2 B for example correspond to a surface coverage of only ca. 11%. Importantly, for all dyes cyclic voltammograms recorded with only partial surface coverage (not shown) results in a simple redox system consistent with process P1 (see Table 1) and therefore the more complex behaviour in process P2 is due to surface aggregation at high coverage and interaction of dye radical cations during oxidation (possibly including interactions introduced by the PF_6^- counter anions). The strongest binding constant of the four dyes is observed for D102 and D205.

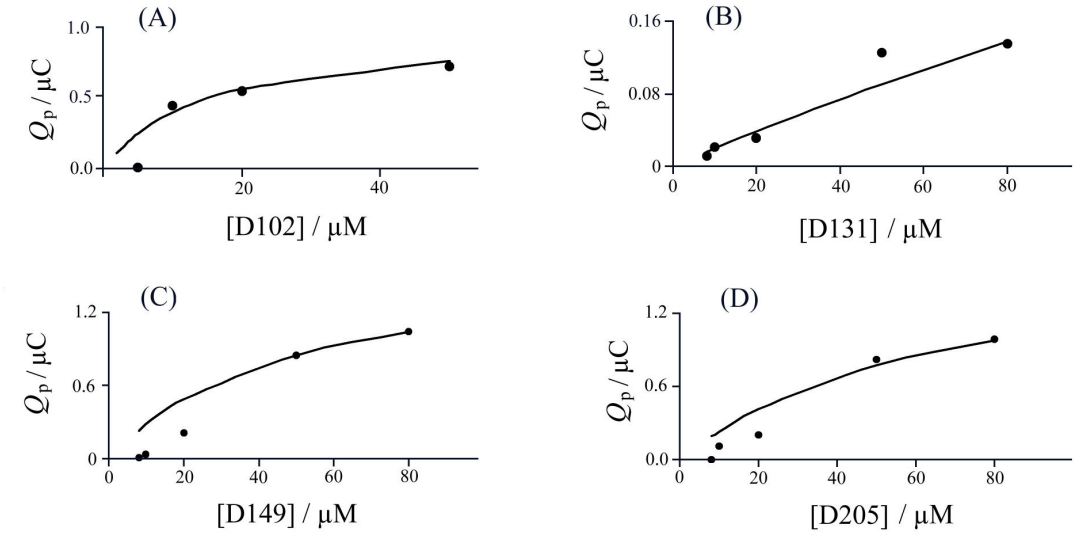

Figure 6.4 (A-D) Plot of the oxidation peak charge density (Q_p) versus concentration of indoline dyes in dye bath. Electrodes left 1 hour in a dye bath acetonitrile ^{t}BuOH (50:50). The line has been approximately fitted as a Langmuir isotherm with (A) D102 Q_0 = 11 μC cm^{-2} and K_{D102} = 6 × 10^4 mol^{-1} dm^3; (B) D131 Q_0= 11 μC cm^{-2} and K_{131}= 2 × 10^3 mol^{-1} dm^3; (C) D149 Q_0 = 11 μC cm^{-2} K_{149}= 5 × 10^4 mol^{-1} dm^3; (D) D205 Q_0 = 11 μC cm^{-2} and K_{205}= 6 × 10^4 mol^{-1} dm^3.

When slow scan rate cyclic voltammograms are recorded, the indoline dyes appear to lose electrochemical reactivity. It has recently been reported that indolinium cations indeed are prone to decarboxylation for example in the presence of base e.g. amines.[27] Figure 6.5 (A-C) shows a comparison, of cyclic voltammogram for D102, D149 and D205 obtained for a freshly prepared electrode at 16 Vs^{-1} and a cyclic voltammogram obtained under the same conditions but after recording a cyclic voltammogram at 0.04 Vs^{-1} (not shown). Clearly a major decrease in electrochemical response is observed, and this is attributed here to a chemical reaction rather than to diffusional losses of dye into the solution. From consecutive cyclic voltammograms the chemical rate constant for the chemical reaction step, k_{D102} = 10^{-1} s^{-1}, k_{149} = 6 × 10^{-2} s^{-1}, k_{205} = 10^{-1} s^{-1} can be estimated following the same procedure used in chapter 5 (eq. 5.2).[28] A comparison of this chemical rate constant describing loss for the different dyes (see Table 1) shows very similar behaviour with a trend of faster reaction for D131 and slower reaction for D149. For D131 only a lower limit for the chemical rate constant is obtained due to the fact that complete degradation occurred

already after cycling once at 0.04 Vs^{-1}. Generally, however, the degradation of the oxidized dye in acetonitrile 0.1 M NBu_4PF_6 appears to be slow when compared to ruthenium-based solar sensitizer dyes (see chapter 4 and 5).[25, 28] For indoline dyes, it has recently been shown that chemically irreversible degradation for the indolinium cation is observed when this experiment is carried out in the presence of the base tert.-butylpyridine.[27] In the processes investigated here adventitious traces of water in acetonitrile solvent may also affect the reactivity of indolinium cations.

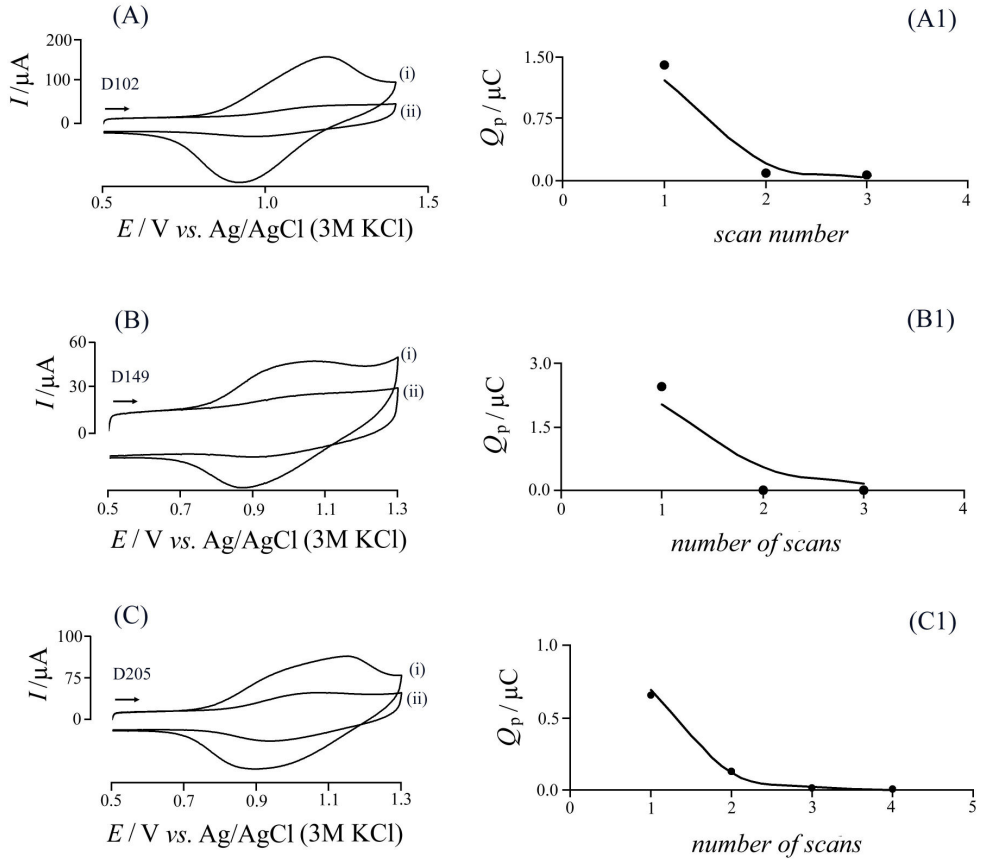

Figure 6.5 Cyclic voltammograms (scan rate 16 V s^{-1}) for the oxidation of (A) D102, (B) D149, (C) D205, adsorbed on FTO (0.5×10^{-3} M dye bath) and immersed in acetonitrile 0.1 M NBu_4PF_6 (i) before and (ii) after conducting a slow scan rate experiment with 0.04 Vs^{-1}. (A1), (B1), (C1), show the plot of Q_p vs number of scans of D102, D149, D205 adsorbed on FTO electrode form a 0.5×10^{-3} M dye bath in acetonitrile ^{t}BuOH (50:50), electrode left 16 hours in dye bath. Data has been estimated by cycling the potential alternately at scan rates of 16 and 0.04 Vs^{-1}. Experimental points are shown with theoretical line based on equation 5.2.

Experiments have been conducted by cycling the potential alternately at 16 and 0.04 Vs^{-1} three times. The data points indicate experimental data and the full line correspond to a theoretical line. The chemical rate constant can be calculated according to equation 5.2 (see chapter 5).

In the operating dye sensitized solar cell the indolinium produced after photo-excitation and electron transfer into the FTO-TiO_2 substrate is quickly reduced back to indoline by electron transfer from the iodide/tri-iodide redox system.[29] The solar cell sensitizer dye N719 has been demonstrated[25] to act as effective catalysts for the oxidation of iodide to tri-iodide and the rate of this reaction may be crucial in protecting the dye against degradation in the operating solar cell (see chapter 4). Cyclic voltammetry experiments were carried out to also investigate the catalytic ability of indoline dyes. Figure 6.6 (A-D) shows typical cyclic voltammograms for indoline dyes D102, D131, D149, and D205 adsorbed onto FTO and immersed into acetonitrile 0.1 M NBu_4PF_6. Gradual addition of LiI into the solution is shown to lead to a new oxidation peak at ca. 1.0 V for D102, ca. 1.1 V for D131, ca. 1.1 V for D149 and ca. 1.0 V vs. Ag/AgCl for D205 in the presence of 0.2 mM LiI. In the absence of the indoline dye the oxidation of iodide occurs at considerable more positive potentials (not shown). All four indoline dyes are potent catalysts (based on process P1) for the oxidation of iodide which is seen to occur with essentially diffusion controlled rate similar to that observed for the N719 dye in chapter 4.4.3 (based on approximately consistent values of anodic peak current calculated using the Randles-Sevcik equation).[28]

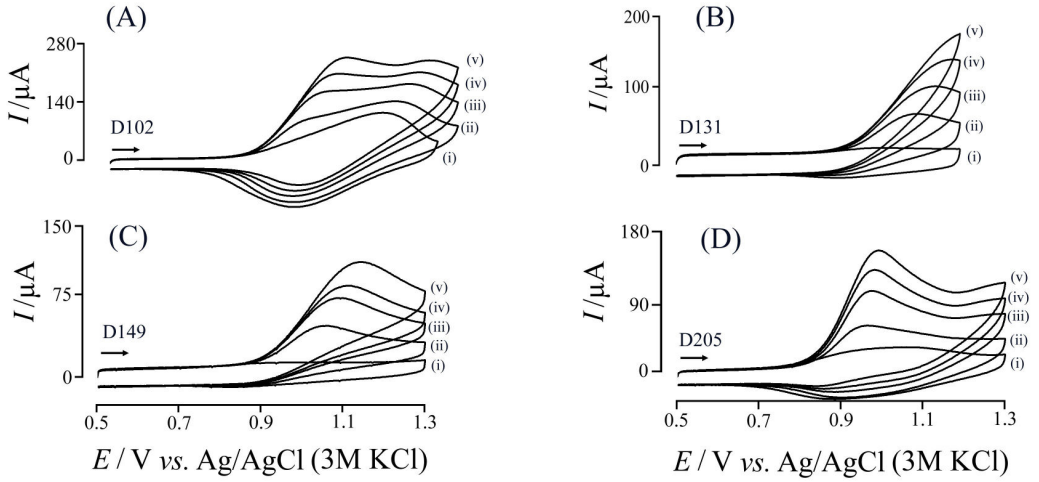

Figure 6.6 (A-D) Cyclic voltammograms (scan rate 16 Vs^{-1}) obtained with 9 mm^2 electrodes with (A) D102, (B) D131, (C) D149, (D) D205 adsorbed on FTO electrode and immersed in acetonitrile containing (i) 0, (ii) 100, (iii) 200, (iv) 300, and (v) 400 μM LiI.

Table 1. Data for cyclic voltammetry experiments for the adsorption and oxidation of indoline dyes on FTO and FTO-TiO_2 surfaces.

	FTO				**FTO-TiO_2**		
Dye	**E_{mid} / V vs. Ag/AgCl (3M KCl) P1 P2 [a]**	**Coverage /molecules cm^{-2} [b]**	**K_{FTO} / mol^{-1} dm^3 [c]**	**k_{FTO}/s^{-1} [d]**	**E_{mid}/V vs. Ag/AgCl (3M KCl) [e]**	**Coverage /molecules cm^{-2} [f]**	**k_{TiO2} / s^{-1} [d]**
D102	0.94 1.03	5.0×10^{13}	6×10^4	0.1	1.08	1.8×10^{16}	0.01
D131	0.91	7.8×10^{12}	2×10^3	>0.1	1.16	2.6×10^{16}	0.01
D149	0.88 0.99	5.7×10^{13}	5×10^4	0.06	0.92	1.2×10^{16}	0.008
D205	0.88 1.01	6.8×10^{13}	6×10^4	0.1	0.95	2.1×10^{16}	0.01

(a) midpoint potential for processes P1 and P2 obtained from ½ ($E_p^{ox} + E_p^{red}$)
(b) coverage per cm^2 (geometric area) calculated from the charge under the oxidation peak, dye bath 5×10^{-5} mol dm^{-3}. Compare to the full coverage 6.8×10^{13} molecules cm^{-2} from the corresponding Langmuir plots and the theoretical coverage 7.4×10^{13} molecules cm^{-2}
(c) Langmuirian binding constant obtained by assuming full coverage 6.8×10^{13} molecules cm^{-2}
(d) estimated from the decay of the voltammetric signal for dye oxidation during consecutive potential scans[28]
(e) midpoint potential for oxidation obtained from ½ ($E_p^{ox} + E_p^{red}$)
(f) coverage per cm^{-2} (geometric area) calculated from the charge under the peak, dye bath

6.4.2 Adsorption and oxidation of indoline dyes at FTO-TiO_2 electrode surfaces

The adsorption of indoline dyes onto a film of ca. 3 μm thick TiO_2 on FTO is readily achieved in the same type of acetonitrile:^{t}BuOH dye bath (see experimental). Figure 6.7 (A-D) shows typical cyclic voltammograms for the oxidation and back-reduction of D102, D131, D149, and D205 immobilised on FTO-TiO_2 and immersed in acetonitrile 0.1 M NBu_4PF_6. The magnitude of the peak currents is considerably higher compared to that observed at bare FTO and due to the higher currents a resistance effect is causing distortion of the voltammetric response. The observed resistance of ca. 300 Ω (see chapter 3.1.1) is likely to be due to the organic electrolyte solution phase. However, analysis of these peak responses is possible and informative.

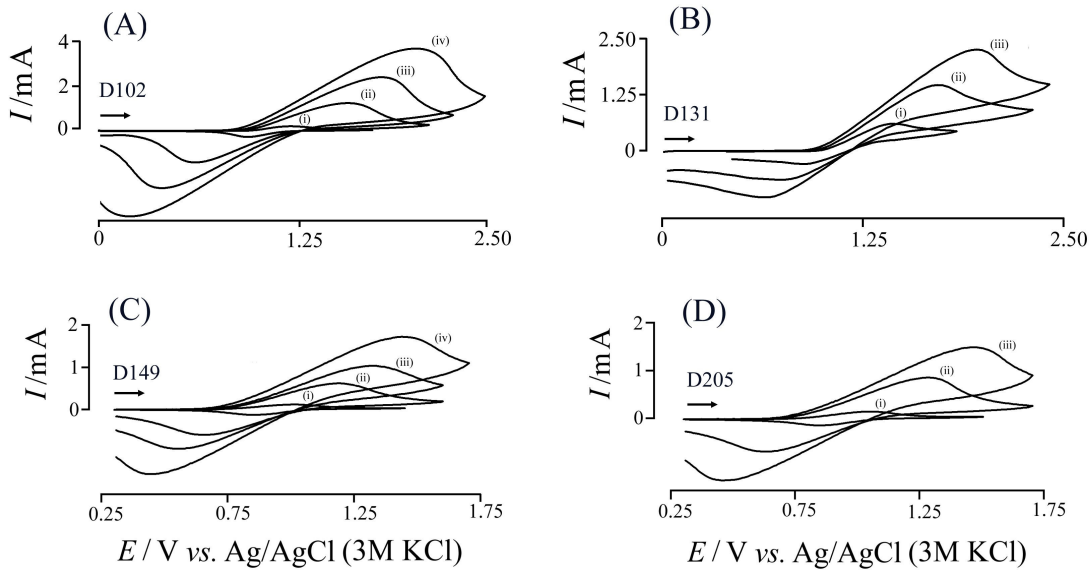

Figure 6.7 Cyclic voltammograms scan rate (i) 0.16, (ii) 1.6, (iii) 4, and (iv) 8 Vs^{-1} for the oxidation and back-reduction of (A) D102 and (C) D149; scan rate (i) 1.6, (ii) 4, and (iii) 8 Vs^{-1} for the oxidation and back-reduction of (B) D131 and (D) D205. The dyes were adsorbed onto 9 mm^2 FTO-TiO_2 (dye bath 5×10^{-4} M, 16 hours) and immersed in acetonitrile 0.1 M NBu_4PF_6. The charge underneath the oxidation peaks is constant for all the dyes (approximately 5.6-5.9 mC cm^{-2}) and independent of scan rate.

The midpoint potential for the reversible oxidation of D102 is E_{mid} = 1.08 V vs. Ag/AgCl which is slightly more positive compared to the process on FTO, which is

not surprising given the much more electro-positive nature of Ti(IV) compared to Sn(IV). For example a typical ionic radius for Ti^{4+} in octaedrical coordination is 61 pm compared to 69 pm for Sn^{4+} and Sn^{4+} in contrast to Ti^{4+} has filled d electrons shells. On TiO_2 there is no direct evidence for distinct redox systems (or aggregation) similar to that observed on FTO. This may be attributed to a substrate effect rather than lack of aggregation. Indoline dye aggregation has been observed and discussed for TiO_2 bound indoline dye molecules[30] and it is likely to also occur in this case. Data for D131, D149, and D205 show similar trends and D131 shows a slightly more positive midpoint potential (see Table 1).

The charge underneath the voltammetric oxidation responses in figure 6.7 (A-D) appears almost constant, independent of scan rate, and it varies between 5.6 mC cm^{-2} to 5.9 mC cm^{-2} (corresponding to ca. 3.3×10^{16} dye molecules cm^{-2}). Assuming spherical TiO_2 particles of ca. 9 nm diameter, a 3 μm TiO_2 film, and a molecular footprint of 2×10^{-18} m^2 per dye molecule, a full coverage of ca. 4.4×10^{16} dye molecules cm^{-2} is predicted in good agreement with the experimental value. For all four dyes the charge under the oxidation peak is constant and independent of scan rate from 1.6 Vs^{-1} to 16 Vs^{-1}. This confirms that all of the dye in the TiO_2 film is electrochemically active and transport of electrons via hopping/percolation is very fast. It is possible to obtain a lower limit for the apparent diffusion coefficient for electrons which move across the modified TiO_2 surface via a percolation mechanism starting from the FTO substrate (see equations 6.2-6.4).

6.2 $\quad D(FTO) \rightleftharpoons D^+(FTO) + e^-$

6.3 $\quad D(TiO_2) + D^+(FTO) \rightleftharpoons D^+(TiO_2) + D(FTO)$

6.4 $\quad D'(TiO_2) + D^+(TiO_2) \rightleftharpoons D'^+(TiO_2) + D(TiO_2)$

The extent of a diffusion layer $\delta_{\text{diffusion}}$ can be estimated with $\delta_{diffusion} = \sqrt{\frac{D_{app} RT}{\nu F}}$

where D_{app} is the apparent diffusion coefficient, R is the gas constant, T is the

absolute temperature, F is the Faraday constant, and v is the scan rate. Given that diffusion effects in voltammograms observed in figure 6.7 (A) are insignificant, a lower limit of the apparent diffusion coefficient is obtained with $D_{app} > \frac{\delta_{diffusion}{}^2 \, v \, F}{RT} = \frac{(3\times10^{-6})^2 \times 16 \times 96487}{8.31 \times 293} = 5\times10^{-9} m^2 s^{-1}$. This suggests that the rate of electron hopping (and therefore the rate of surface "hole" mobility in the dye layer) is surprisingly high and probably significantly higher when compared to the rate of diffusion in the solution phase. The hole-mobility μ can be calculated by using Einstein relation (equation 6.5)

6.5 $$D = \frac{\mu \times k_B \times T}{q}$$

Where D is the diffusion coefficient, μ is the hole-mobility, k_B is the Boltzman's constant, T is the temperature and q is the charge of one electron. Using D as 5×10^{-5} cm^2 s^{-1} a value of $\mu = 2 \times 10^{-3}$ cm^2 V^{-1} s^{-1} can be obtained. This value is showing a faster mobility of holes in the TiO_2 when is compared, for example, with values of μ using Spiro-MeOTAD as hole transport material $\mu = 1 \times 10^{-4}$ cm^2 V^{-1} s^{-1}.[31] A high surface "hole" mobility may cause faster recombination and energy losses (at the FTO surface), but may also cause faster reaction with iodide (at the interface with the electrolyte solution, vide supra) and therefore may improved performance. This high rate of apparent electron/hole surface diffusion is observed for all four indoline dyes adsorbed onto TiO_2. It is interesting to compare the value for this apparent diffusion coefficient with literature values for example for conducting polymers and redox active films. Electron hopping processes in redox polymers occur typically with D_{app} = 10^{-10} to 10^{-13} m^2s^{-1}.[32] Recent studies on electrochromic redox systems adsorbed onto nanocrystalline metal oxide films gave apparent diffusion coefficients ranging from 10^{-11} to 10^{-12} m^2s^{-1}.[33] The much faster rate of charge hopping observed here is likely to be due to delocalization effects similar to those observed in organic conductors based on π-stacked layers of TTF and TCNQ.[34] Conduction in these more conducting materials is often characterized by the Fermi velocity v_F and the scattering time τ_S which allow the apparent diffusion coefficient to be estimated as $D_{app} = \frac{v_F{}^2 \tau_S}{2}$ which in the case of the organic metal (TTF)(TCNQ) is approximately

10^{-5} m^2s^{-1} at room temperature.[35] A similar delocalization effect is proposed here for the indoline dye aggregates at the TiO_2 surface.

A further feature observed when cyclic voltammograms are recorded for the oxidation of indoline dyes adsorbed onto FTO-TiO_2 is demonstrated in figure 6.8 (A-D). Upon consecutive potential cycling at slower scan rate a gradual loss of the voltammetric response is observed. The apparent rate of dye loss can be expressed approximately in terms of a first order rate constant (see Table 1). For the indoline dye D102 k_{TiO2} is approximately 10^{-2} s^{-1}. The dye colour of the modified FTO-TiO_2 electrode is not affected by the observed deterioration of the voltammetric signal and therefore most of the D102 dye present at the TiO_2 surface appears to remain intact. It is interesting to compare this rate of the loss of the voltammetric response for D102 on TiO_2 with that for D102 on FTO. The degradation process on FTO appears approximately 10 times faster (see Table 1). Due to the percolation mechanism for electron transport from D(FTO) to D(TiO_2) (see equations 6.2-6.4) any degradation of dye on the FTO surface will cause a reduced charge mobility and eventually a significant loss of pathways for electron hopping. The fact that the apparent rate constant for the loss of the voltammetric signal for D102 on TiO_2 is slower compared to that for D102 on FTO is caused by the flexibility of the charge conduction process. Only when a substantial amount of D102 on FTO is degraded, the voltammetric response for D102 on TiO_2 is beginning to show deterioration. The mechanisms for both loss of the dye response for FTO and loss of the dye response for TiO_2 are likely to be the same. The behaviour for all four dyes on TiO_2 in terms of time dependence of the voltammetric responses is very similar (see Table 1). In order to obtain further insight into the charge hopping and degradation processes spectro-electrochemical experiments are reported next.

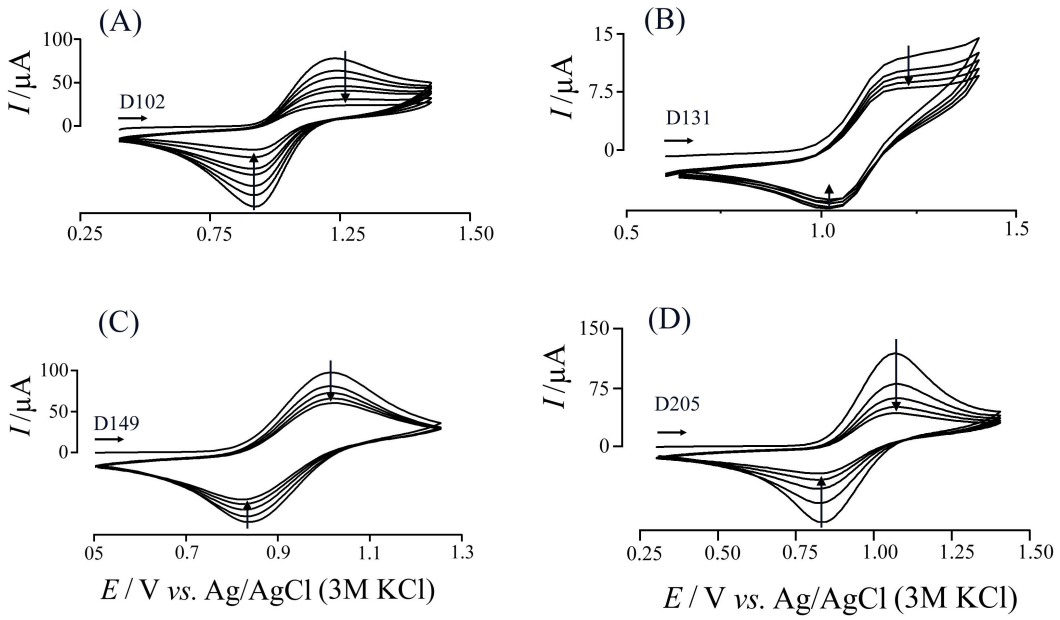

Figure 6.8 Multi-cycle voltammograms (20 cycles) for the oxidation and back-reduction of (A) D102 scan 1, 3, 5, 8, 10, 15, 20 shown, (B) D131 scan 1, 5, 10 15 20 shown, (C) D149 scan 1, 5, 10, 15, 20 shown, (D) D205 1, 5, 10, 15, 20 shown. Dyes were adsorbed onto 9 mm^2 FTO-TiO_2 electrodes (dye bath 5×10^{-4} M, 16 hours) and immersed into acetonitrile 0.1 M NBu_4PF_6. Scan rate 0.16 Vs^{-1}.

6.4.3 Spectroelectrochemical data for the oxidation of indoline dyes at FTO-TiO_2 electrode surfaces

In order to further investigate the reactivity of indoline dyes when adsorbed onto FTO-TiO_2 electrodes spectroelectrochemistry experiments were conducted. Figure 6.9 A-D shows for the four indoline dyes the comparison of the dye dissolved in acetonitrile ^{t}BuOH 50:50 and when adsorbed onto the FTO-TiO_2 substrate. Well-defined π-π* HOMO-LUMO absorption peaks are observed for D149 at 524 nm (in solution) and at 536 nm (on TiO_2) and for D205 at 523 nm (in solution) and at 533 nm (on TiO_2) approximately consistent with literature data (see Table 2).

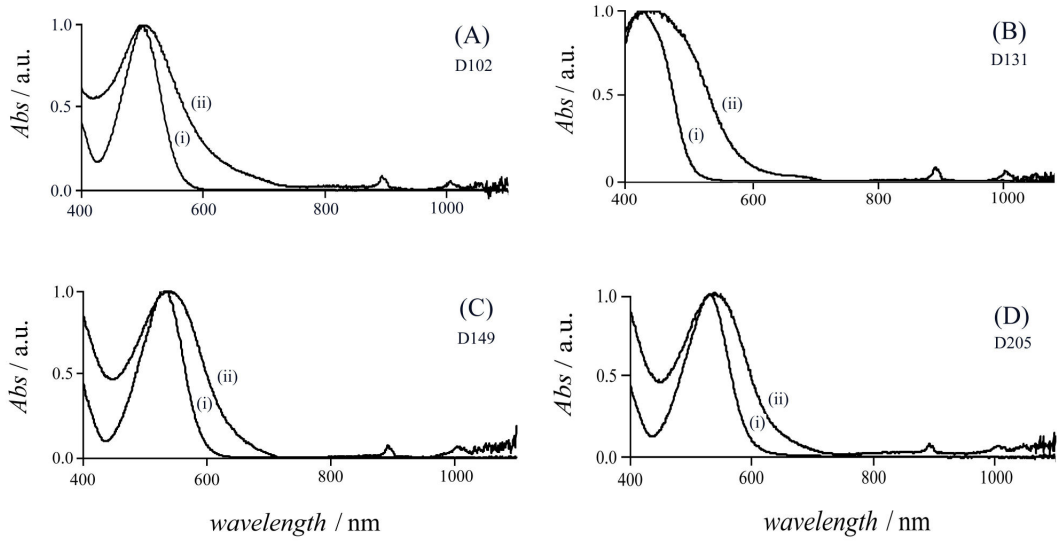

Figure 6.9 (A-D) Overlay of absorbance data for D102, D131, D149, and D205 (i) in solution acetonitrile ^{t}BuOH 50:50 and (ii) adsorbed onto FTO-TiO_2. The spectra have been normalised for comparison.

Figures 6.10 A-D show data obtained for the oxidation and back-reduction of D149 and D205 in acetonitrile 0.1 M NBu_4PF_6. The experiments were conducted separately for each dye and due to the very similar molecular structure (figure 6.1), the data are presented for comparison for both dyes in figure 6.10 A-D. The red shift has been explained based on J-aggregate formation (coupling of the transition dipole moments in the aggregated dye layer).[36] A further absorption peak exists at a shorter wavelength below 400 nm (not shown).

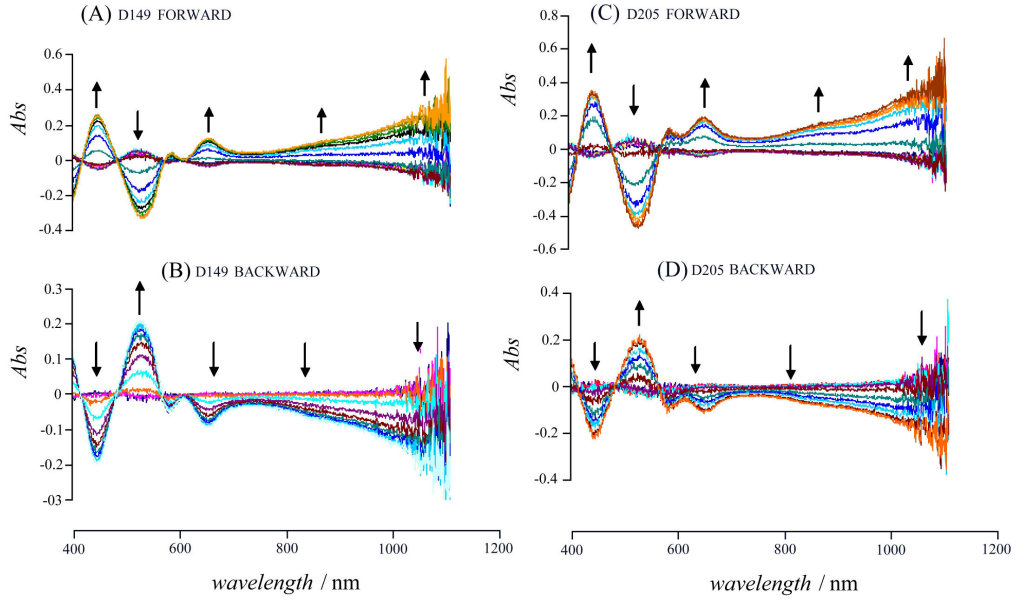

Figure 6.10 (A) and (C) Spectroelectrochemical data (changes in absorbance with increasing potential) for the oxidation of D149 (A) and D205 (C) adsorbed onto FTO-TiO_2 (films from a (5×10^{-4} M dye bath, 16 hours) and immersed in acetonitrile 0.1 M NBu_4PF_6. The potential is stepped from 0.2 V to 1.2 V vs. Ag/AgCl by 0.05 V every 5 s. (B) and (D) Spectroelectrochemical data (changes in absorbance with decreasing potential) from 1.2 V to 0.2 V vs. Ag/AgCl. Data acquired ten minutes after completion of experiments in (A) and (C).

When the potential of the FTO-TiO_2 electrode with D149 is gradually increased (see Figure 6.10A) an increase in absorbance at 445 nm/651 nm and a decrease at 583 nm are observed in difference spectra. This corresponds to a red-shift of the two main dye absorption bands to longer wavelengths upon oxidation. The absorption bands for the aggregated D149 have π-π* character[30] and the corresponding transitions for the indolinium cation (see D^+(π-π*) in Table 2) are probably electronically closely related. Well-defined isosbestic points indicate a relatively stable indolinium product adsorbed on the TiO_2 surface. However, incomplete chemical reversibility can be observed when comparing the magnitude of spectral changes for forward and backward processes (see figure 6.10), consistent with observations in cyclic voltammetry experiments (see figure 6.8).

Table 2. Spectroelectrochemical absorbance data for indoline dyes in solution and indoline/indolinium when adsorbed onto FTO-TiO_2 film electrodes immersed in acetonitrile 0.1 M NBu_4PF_6

Dye	λ_{max} for indoline in solution [(a)]	λ_{max} for indoline on TiO_2 [(b)]	λ_{max} for indolinium on TiO_2 [(c)]			
D102	494 nm	500 nm	ca. 460 nm	ca. 720 nm	ca. 800 nm	ca. 930 nm
D131	421 nm	440 nm	ca. 440 nm	721 nm	797 nm	1100 nm
D149	524 nm	536 nm	445 nm	651 nm	850 nm	1063 nm
D205	523 nm	533 nm	444 nm	650 nm	860 nm	1100 nm

(a) in acetonitrile:^{t}BuOH 50:50
(b) FTO-TiO_2 electrode with dye adsorbed form 5×10^{-4} mol dm^{-3} dye bath, immersed in acetonitrile 0.1 M NBu_4PF_6
(c) obtained form difference spectra during electrochemical oxidation of dye

Very interesting are the broad indolinium absorption bands at ca. 800 nm and a going beyond 1000 nm. These types of absorption bands are observed also for other organic radical cation materials[37] and have been assigned to mixed valence charge transfer.[38] The presence of near infrared charge transfer absorption bands is indicative for high charge mobility due to strong π orbital interaction.[39] This observation is in good agreement with the observation of exceptionally high apparent diffusion coefficients for electron hopping (vide supra). Spectroelectrochemical experiments were also carried out for the dyes D102 and D131 (see figure 6.11). Due the high resistance of the electrodes in those particular experiments the potential was scanned towards too positive values (0 V to 2.4 V) which probably caused the over oxidation of the dyes so that the extraction of data is more complicated. Nevertheless the spectroelectrochemical behaviour of D102 and D131 show similar trend to D149 and D205 presenting a broad absorption for the indolinium at ca. 800 nm and beyond 1000 nm. The fact that isosbestic points at ca. 500 nm for D102 and D131 are not clear is probably due to the over oxidation of the film.

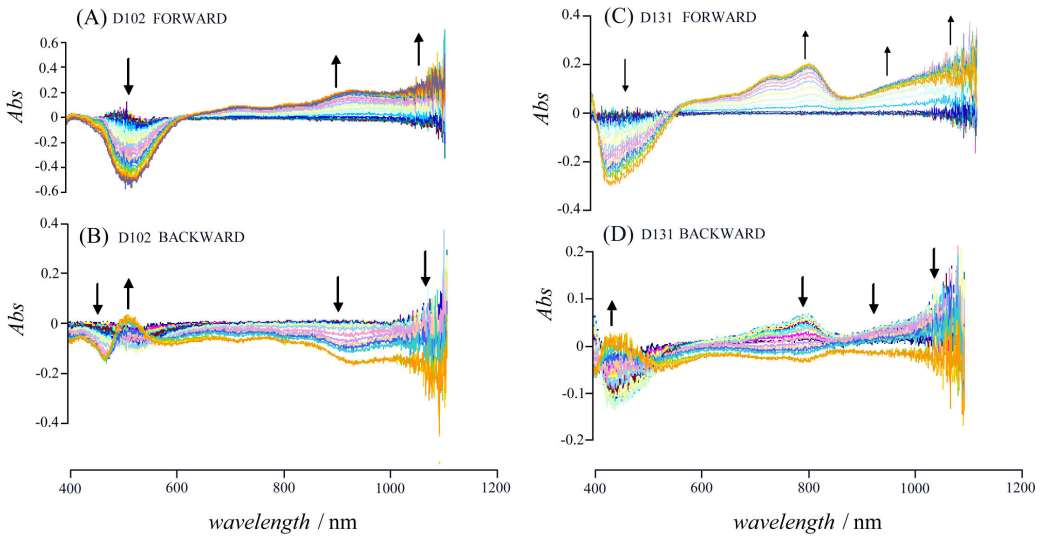

Figure 6.11 (A) and (C) Spectroelectrochemical data (changes in absorbance with increasing potential) for the oxidation of D102 (A) and D131 (C) adsorbed onto FTO-TiO_2 (films from a (5×10^{-4} M dye bath, 16 hours) and immersed in acetonitrile 0.1 M NBu_4PF_6. The potential is stepped from 0 V to 2.4 V vs. Ag/AgCl by 0.05 V every 5 s. (B) and (D) Spectroelectrochemical data (changes in absorbance with decreasing potential) from 2.4 V to 0 V vs. Ag/AgCl. Data acquired ten minutes after completion of experiments in (A) and (C).

Further experimental work for example investigating the spectro-electrochemistry as a function of surface coverage will be required to better understand and quantify aggregation phenomena for indoline dyes at the TiO_2 surface.

The implications of the dye aggregation effects on the solar cell performance are considerable. Attempts have been reported of suppressing dye aggregation with co-adsorbants such as chenodeoxycholic acid[40] and also the co-adsorption of two different dyes has been shown to improve efficiencies.[41] Higher hole mobility in the aggregated dye layer is likely to lead to additional recombination processes at the FTO contact. This could be avoided by a semiconductor "buffer layer"[42] or by chemical degradation of the dye at the FTO electrode surface as demonstrated in this study. Higher hole mobility may also be beneficial in solar cell applications by enhancing the hole transport in the nanocrystalline TiO_2 film towards the iodide/tri-iodide electrolyte solution side. This process is usually dominated by diffusion of the iodide anion in the solution phase which is lower (iodide diffusion coefficient D =

2.76×10^{-9} m^2s^{-1})[43] when compared to the lower limit to the apparent diffusion coefficients observed in this study ($D_{app} > 5 \times 10^{-9}$ m^2s^{-1}). Importantly, it has been suggested that dye layer hole conductivity is important for solid state devices where the redox electrolyte is replaced with a amorphous solid such as spiro-OMeTAD[44] and therefore the observation of high D_{app} could be of importance in this type of devices.

6.5 Conclusions

(1) Indoline dyes D102, D131, D149, and D205 have been adsorbed onto FTO electrodes and studied by voltammetry immersed in acetonitrile 0.1 M NBu_4PF_6. Chemically reversible responses were obtained at scan rates > 1 Vs^{-1} and aggregation phenomena are observed at high coverage.

(2) When adsorbed onto FTO-TiO_2 electrode surfaces, well-defined voltammetric responses suggest very fast hole/electron mobility in the aggregated indoline dye layer with an apparent diffusion coefficient of $D_{app} > 5 \times 10^{-9}$ m^2s^{-1}.

(3) A slow indolinium radical cation degradation process is observed for modified FTO and FTO-TiO_2 electrodes.

(4) In spectro-electrochemical measurements long wavelength charge transfer bands confirm the presence of aggregates and high charge carrier mobility.

Further experimental work will be required to more fully characterize and quantify the charge hopping process in indoline dye layers as a function of coverage. The fast rate of hole/electron conduction observed here could be of interest in a wider range of applications including fast electrochromic devices, flat display screens, and sensors.

References

1. Gratzel, M., *J. Photochem. Photobiol. C-Photochem. Rev.* **2003,** *4* (2), 145-153.
2. Gratzel, M., *Journal of Photochemistry and Photobiology a-Chemistry* **2004,** *164* (1-3), 3-14.
3. Gratzel, M., *Accounts Chem. Res.* **2009,** *42* (11), 1788-1798.
4. Kohle, O.; Gratzel, M.; Meyer, A. F.; Meyer, T. B., *Advanced Materials* **1997,** *9* (11), 904-&.
5. Wang, P.; Zakeeruddin, S. M.; Moser, J. E.; Nazeeruddin, M. K.; Sekiguchi, T.; Gratzel, M., *Nature Materials* **2003,** *2* (7), 498-498.
6. Jang, S. R.; Yum, J. H.; Klein, C.; Kim, K. J.; Wagner, P.; Officer, D.; Gratzel, M.; Nazeeruddin, M. K., *Journal of Physical Chemistry C* **2009,** *113* (5), 1998-2003.
7. Morandeira, A.; Lopez-Duarte, I.; O'Regan, B.; Martinez-Diaz, M. V.; Forneli, A.; Palomares, E.; Torres, T.; Durrant, J. R., *Journal of Materials Chemistry* **2009,** *19* (28), 5016-5026.
8. Li, Q. Q.; Lu, L. L.; Zhong, C.; Shi, J.; Huang, Q.; Jin, X. B.; Peng, T. Y.; Qin, J. G.; Li, Z., *Journal of Physical Chemistry B* **2009,** *113* (44), 14588-14595.
9. Wang, Z. S.; Li, F. Y.; Huang, C. H., *Journal of Physical Chemistry B* **2001,** *105* (38), 9210-9217.
10. Cherepy, N. J.; Smestad, G. P.; Gratzel, M.; Zhang, J. Z., *Journal of Physical Chemistry B* **1997,** *101* (45), 9342-9351.
11. Hara, K.; Kurashige, M.; Dan-oh, Y.; Kasada, C.; Shinpo, A.; Suga, S.; Sayama, K.; Arakawa, H., *New Journal of Chemistry* **2003,** *27* (5), 783-785.
12. Campbell, W. M.; Jolley, K. W.; Wagner, P.; Wagner, K.; Walsh, P. J.; Gordon, K. C.; Schmidt-Mende, L.; Nazeeruddin, M. K.; Wang, Q.; Gratzel, M.; Officer, D. L., *Journal of Physical Chemistry C* **2007,** *111* (32), 11760-11762.
13. Horiuchi, T.; Miura, H.; Uchida, S., *Journal of Photochemistry and Photobiology a-Chemistry* **2004,** *164* (1-3), 29-32.
14. Schmidt-Mende, L.; Bach, U.; Humphry-Baker, R.; Horiuchi, T.; Miura, H.; Ito, S.; Uchida, S.; Gratzel, M., *Advanced Materials* **2005,** *17* (7), 813-+.
15. Robertson, N., *Angewandte Chemie-International Edition* **2006,** *45* (15), 2338-2345.
16. Oyama, Y.; Harima, Y., *European Journal of Organic Chemistry* **2009,** (18), 2903-2934.
17. Polo, A. S.; Itokazu, M. K.; Iha, N. Y. M., *Coordination Chemistry Reviews* **2004,** *248* (13-14), 1343-1361.
18. Tian, H. N.; Yang, X. C.; Cong, J. Y.; Chen, R. K.; Teng, C.; Liu, J.; Hao, Y.; Wang, L.; Sun, L. C., *Dyes and Pigments* **2010,** *84* (1), 62-68.
19. Ito, S.; Miura, H.; Uchida, S.; Takata, M.; Sumioka, K.; Liska, P.; Comte, P.; Pechy, P.; Graetzel, M., *Chemical Communications* **2008,** (41), 5194-5196.
20. Kuang, D.; Uchida, S.; Humphry-Baker, R.; Zakeeruddin, S. M.; Gratzel, M., *Angewandte Chemie-International Edition* **2008,** *47* (10), 1923-1927.
21. Mishra, A.; Fischer, M. K. R.; Bauerle, P., *Angewandte Chemie-International Edition* **2009,** *48* (14), 2474-2499.
22. Li, X. D.; Zhang, D. W.; Sun, Z.; Chen, Y. W.; Huang, S. M., *Microelectronics Journal* **2009,** *40* (1), 108-114.

23. Howie, W. H.; Harris, J. E.; Jennings, J. R.; Peter, L. M., *Solar Energy Materials and Solar Cells* **2007,** *91* (5), 424-426.
24. Wang, Q.; Zakeeruddin, S. M.; Nazeeruddin, M. K.; Humphry-Baker, R.; Gratzel, M., *Journal of the American Chemical Society* **2006,** *128* (13), 4446-4452.
25. Fattori A, P. L., Belding SR, Compton RG, Marken F, *Journal of Electroanalytical Chemistry* **2010**, 640, 61-67
26. Konno, A.; Kumara, G. R. A.; Kaneko, S.; Onwona-Agyeman, B.; Tennakone, K., *Chemistry Letters* **2007,** *36* (6), 716-717.
27. Tanaka, H.; Takeichi, A.; Higuchi, K.; Motohiro, T.; Takata, M.; Hirota, N.; Nakajima, J.; Toyoda, T., *Solar Energy Materials and Solar Cells* **2009,** *93* (6-7), 1143-1148.
28. Fattori A, P. L., McCall KL, Robertson N, Marken F, *Journal of Solid State Electrochemistry* **2010**. Waiting for publication.
29. Peter, L. M., *Phys. Chem. Chem. Phys.* **2007,** *9* (21), 2630-2642.
30. Pastore, M.; De Angelis, F., *Acs Nano* **2010,** *4* (1), 556-562.
31. Snaith, H. J.; Gratzel, M., *Advanced Materials* **2007,** *19* (21), 3643-+.
32. Murray, R., *Molecular Design of Electrode Surfaces*. Wiley: New York, 1992.
33. Bonhote, P.; Gogniat, E.; Tingry, S.; Barbe, C.; Vlachopoulos, N.; Lenzmann, F.; Comte, P.; Gratzel, M., *Journal of Physical Chemistry B* **1998,** *102* (9), 1498-1507.
34. Bright, A. A.; Garito, A. F.; Heeger, A. J., *Physical Review B* **1974,** *10* (4), 1328-1342.
35. Galchenkov, L. A.; Ivanov, S. N.; Pyataikin, II, *Physics of the Solid State* **2004,** *46* (6), 1131-1140.
36. Horiuchi, T.; Miura, H.; Sumioka, K.; Uchida, S., *Journal of the American Chemical Society* **2004,** *126* (39), 12218-12219.
37. Chang, H. W.; Lin, K. H.; Chueh, C. C.; Liou, G. S.; Chen, W. C., *Journal of Polymer Science Part a-Polymer Chemistry* **2009,** *47* (16), 4037-4050.
38. Chiang, P. T.; Chen, N. C.; Lai, C. C.; Chiu, S. H., *Chemistry-a European Journal* **2008,** *14* (21), 6546-6552.
39. Richardson, D. E.; Taube, H., *Coordination Chemistry Reviews* **1984,** *60* (NOV), 107-129.
40. Lu, H. P.; Tsai, C. Y.; Yen, W. N.; Hsieh, C. P.; Lee, C. W.; Yeh, C. Y.; Diau, E. W. G., *Journal of Physical Chemistry C* **2009,** *113* (49), 20990-20997.
41. Ogura, R. Y.; Nakane, S.; Morooka, M.; Orihashi, M.; Suzuki, Y.; Noda, K., *Applied Physics Letters* **2009,** *94* (7).
42. Cameron, P. J.; Peter, L. M., *Journal of Physical Chemistry B* **2005,** *109* (15), 7392-7398.
43. Depauli, C.; Iwasita, T.; Giordano, M. C., *Journal of Electroanalytical Chemistry* **1973,** *45* (2), 233-245.
44. Boschloo, G.; Marinado, T.; Nonomura, K.; Edvinsson, T.; Agrios, A. G.; Hagberg, D. P.; Sun, L.; Quintana, M.; Karthikeyan, C. S.; Thelakkat, M.; Hagfeldt, A., *Thin Solid Films* **2008,** *516* (20), 7214-7217.

Chapter 7: Characterization of solar cells incorporating indoline dyes

Contents

7.1 Abstract

In order to complete the study on indoline dyes started in chapter 6, cells sensitized with D102, D131, D149, and D205 were fabricated and the IPCE (external quantum efficiency) and I-V characteristics of the DSCs were determined. All the indoline dyes show broad IPCE spectra between 400-600 nm and data consistent with the absorption of the dye onto TiO_2. D102 has a narrower absorption band compared to other dyes. I-V characteristics show high J_{sc} and V_{oc} which lead to good cell efficiencies.

7.2 Introduction

In the last few years organic dyes for dye sensitized solar cells have attracted particular attention for their high extinction coefficient and low production cost compared to Ru-based dyes.[1] As explained in the previous chapters the basic requirement for a working DSC should be an efficient injection upon the absorption of a photon of an electron from the HOMO of the dye into the conduction band of the porous semiconductor (usually TiO_2 colloid). The use as sensitizer of a class of compounds with similar molecular structure based on indoline core coded as D102, D131, D149, and D205 (see chapter 6), has been object of various studies due the fact that, by the use of these dyes, high cell efficiency have been reached. The maximum efficiency obtained so far with use of indoline dyes and in particular D205, has been reached by Ito et al. with an efficiency of $\eta = 9.5\%$.[2] The factors that determine the efficiency η are the open circuit voltage V_{OC}, the short circuit current J_{SC} and the fill factor FF.[3] J_{SC} is related to rate of electron injection to the photoelectrode, V_{OC} is related to the energy difference between the Fermi level of the photoelectrode and the Nernst potential of the redox couple in the electrolyte (see chapter 2.4). The fill factor instead is defined as the ratio (usually given as percent) of the actual maximum obtainable power, ($V_{mp} \times J_{mp}$) to the theoretical (not actually obtainable) power, ($J_{sc} \times V_{oc}$).

A major factor for low conversion efficiency for organic dyes is the formation of aggregates (mainly j-aggregates which gives a bathochromic or red shift) on the semiconductor surface (chapter 1.3.1.2).[4] This phenomenon would affect the light harvesting by filtering effect decreasing the performance of the cell. A way to

prevent aggregation is by the use of the co-adsorbent chenodeoxycholic acid (CDCA).[5]

In this chapter are presented the results obtained by the fabrications of DSCs sensitized with D102, D131, D149, D205 and plots of IPCE and I-V curve are shown.

7.3 Experimental

7.3.1 Instrumentation and chemicals

The description of instrumentation and chemicals used for carry out experiments reported in this chapter can be found in chapter 3.1.4, 3.1.5, and 3.2.1.

7.3.2 Procedures for cells preparation

The cells reported in this chapter were made and analyzed with help of Dr Hongxia Wang. FTO conductive glass substrates were coated with nanocrystalline TiO_2 (approximately 3μm) layers according to the procedure described in chapter 3.2.3. The electrodes were left for 16 hours in a 0.5 mM dye solution (1:1 acetonitrile ^{t}BuOH by volume). Photoelectrodes and counter electrodes were made following the procedure in chapter 3.2.3.1 and 3.2.3.2. Once made, the cells were filled with the electrolyte (see composition in chapter 3.2.3.3) and sealed. A schematic representation of a cell is depicted in figure 7.1.

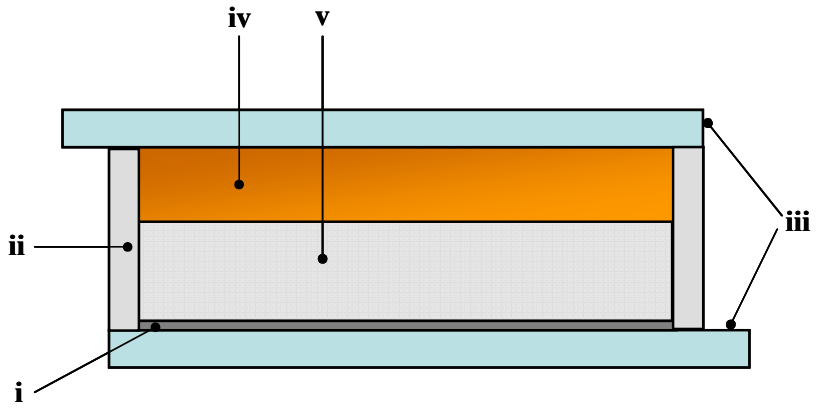

Figure 7.1 Diagram of a DSC. i) Pt; ii) hot melt spacer-sealant; iii) FTO electrodes; iv) electrolyte; v) TiO_2.

7.4 Results and discussion

7.4.1 IPCE spectra for indoline dyes

The IPCE is determined by the product of the light harvesting, electron injection, and electron collection efficiency (chapter 2.4 and chapter 3.1.4). Figure 7.2 A-D compares the IPCE spectra of cells made with the four indoline dyes plotted as a function of the excitation wavelength and are consistent with the absorption spectra of the dye adsorbed on TiO_2 films (see figure 6.9). An interesting characteristic of all organic dyes IPCE spectra is that they show a broad absorption in the range of ca. 400-600 nm. D102 (figure 7.2 A) shows a broad peak in the range 400-580 nm reaching an IPCE average maximum value of 78% D131 (figure 7.2 B) shows a peak between 400-560 nm with IPCE of 55%. D149 and D205 (figure 7.2 C-D) have very similar molecular structure (figure 6.1) and their IPCE is consistent with this similarity showing a broad spectra between 400-630 nm with an average IPCE of ca. 60%.

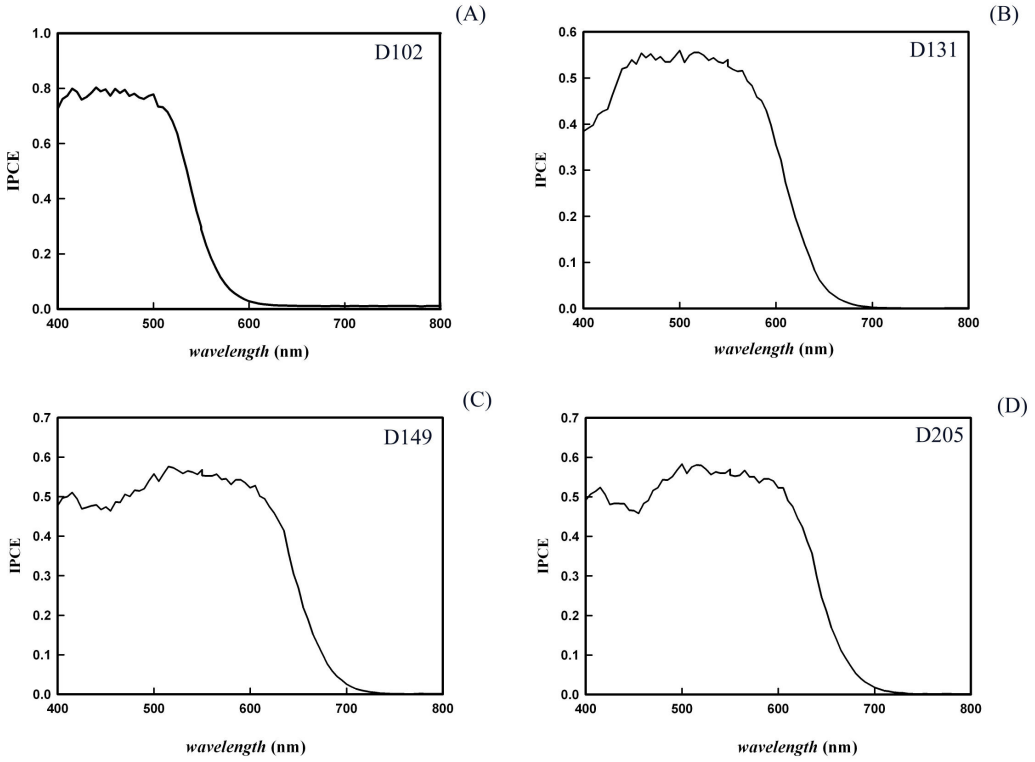

Figure 7.2 IPCE spectra of cells sensitized with (A) D102, (B) D131, (C) D149, (D) D205.

7.4.2 I-V characteristics for indoline dyes

The current-voltage characteristics of the DSC sensitized with D102, D131, D149 and D205 (measured under simulated AM 1.5, 1 Sun illumination) are shown in figure 7.3 A-D. For D102 (figure 7.3 A), high open-circuit voltage V_{oc} = 700 mV and a short-circuit current density j_{sc} = 7.8 mA/cm^2 are achieved. The overall photovoltaic performance of the cell gives an efficiency η = 3.5% with a ff = 0.63. D131 I-V curve in (figure 7.3 B) shows V_{oc} = 660 mV and a short-circuit current density j_{sc} = 9.61 mA/cm^2 with ff = 0.60 and overall efficiency η = 3.8%. The two dyes D149 and D205 show very similar behaviour with V_{oc} = 710 mV short-circuit current density j_{sc}= 11.63 mA/cm^2, ff = 0.55 and η = 4.5% efficiency for D149 in (figure 7.3 C). For D205 (figure 7.3 D) were calculated the values of V_{oc} = 740 mV short-circuit current density j_{sc} = 10.37 mA/cm^2 ff = 0.58 and η = 4.4% efficiency.

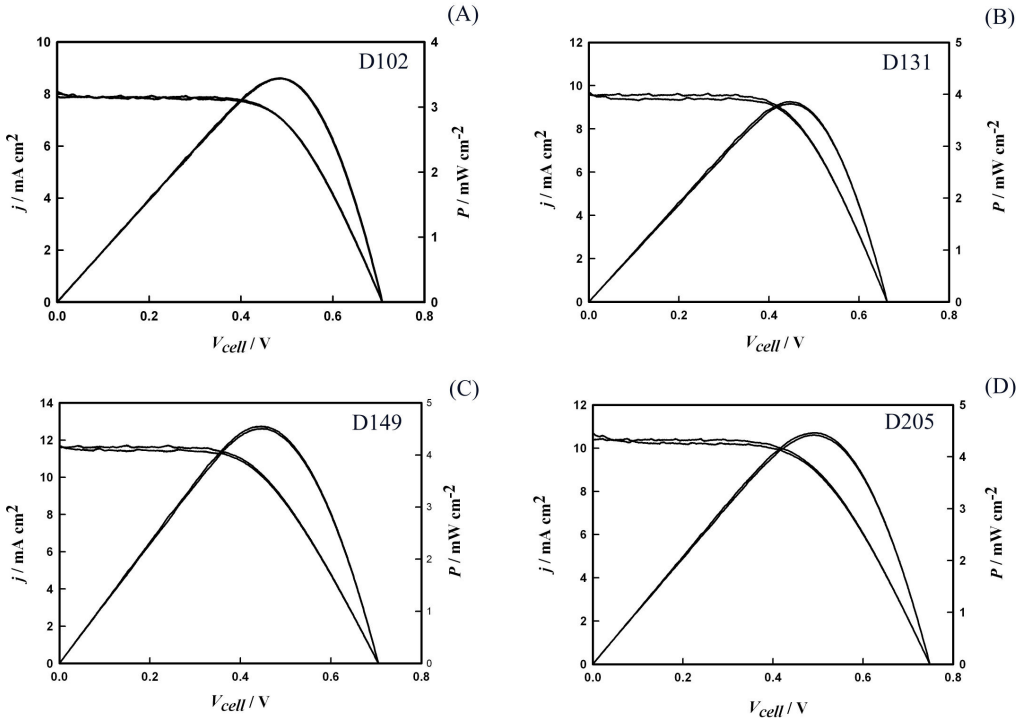

Figure 7.3 I-V curve characteristics for indoline dyes (A) D102, (B) D131, (C) D149, (D) D205.

The performance of the cells should be related to the molecular structure of the dyes[6] so the efficiency η should follow the trend η D205 > η D149 > η D102 > η D131

taking into account the increased π-conjugation so higher extinction coefficients and broader light harvesting spectra. In these experiments the highest performance was reached with the dyes D149 and D205 showing almost the same efficiency. Table 1 reassume the I-V characteristic of the cells which have a slightly different trend compared to other experiments found in the literature[7]. This is probably due to the manufacturing procedure.

Table 2. I-V characteristic of indoline dyes D012, D131, D149, and D205.

Table 2	***Cells performance***			
Dyes	V_{oc} ***(mV)*** [(a)]	J_{sc} ***(mA/cm²)*** [(b)]	***FF*** [(c)]	***η (%)*** [(d)]
D102	*0.79*	*7.94*	*0.63*	*3.5*
D131	*0.66*	*9.61*	*0.60*	*3.8*
D149	*0.71*	*11.63*	*0.55*	*4.5*
D205	*0.74*	*10.37*	*0.58*	*4.4*

(a) open circuit voltage
(b) short circuit current
(c) fill factor
(d) efficiency

7.5 Conclusions

Cells with indoline dyes were made showing good performances for a prototype cells. IPCE data for dyes show very broad absorbance in the range of 400-600 nm and consistent with absorbance spectra. I-V characteristics of the cells were obtained suggesting good efficiency.

References

1. Robertson, N., *Angewandte Chemie-International Edition* **2006,** *45* (15), 2338-2345.
2. Ito, S.; Miura, H.; Uchida, S.; Takata, M.; Sumioka, K.; Liska, P.; Comte, P.; Pechy, P.; Graetzel, M., *Chemical Communications* **2008,** (41), 5194-5196.
3. Jose, R.; Kumar, A.; Thavasi, V.; Fujihara, K.; Uchida, S.; Ramakrishna, S., *Applied Physics Letters* **2008,** *93* (2).
4. Pastore, M.; De Angelis, F., *Acs Nano* **2010,** *4* (1), 556-562.
5. Kay, A.; Gratzel, M., *Journal of Physical Chemistry* **1993,** *97* (23), 6272-6277.
6. Gratzel, M., *Accounts Chem. Res.* **2009,** *42* (11), 1788-1798.
7. Howie, W. H.; Harris, J. E.; Jennings, J. R.; Peter, L. M., *Solar Energy Materials and Solar Cells* **2007,** *91* (5), 424-426.

Conclusions

The main aim of this study was to investigate the reactivity and stability of Ru-based dyes (N719 and Z907) and indoline dyes (D102, D131, D149, and D205) for dye sensitized solar cell (DSC) applications. The dyes were adsorbed onto FTO or onto FTO/TiO_2 film electrodes. The comparison allows dye reactivity data and adsorption characteristics to be understood in more detail.

The dyes were adsorbed onto the electrodes via immersion into dye baths and studied as a function of concentration. Electrochemical experiments allowed dye amounts to be quantified and this allowed the determination of approximate Langmuirian binding constants. Organic dyes D102 and D205 exhibited binding constants in the same order of magnitude when compared to the ruthenium dyes presumably due to the carboxylate functional group binding to the surface in a similar manner in all cases.

The oxidation process for the dyes adsorbed at the surface of FTO electrodes was interpreted in terms of an EC_{irr} mechanism. At fast scan rates (16 Vs^{-1}) a reversible voltammetric response was obtained, however, at slower scan rates (lower than 0.2 Vs^{-1}) loss of dye activity occurred and degradation was observed. The comparison of the chemical rate constants for Ru-based dyes suggested N719 reacted faster compared to Z907 and for the organic dyes the chemical degradation rate constant for D149 was observed to be the highest.

When the dyes are adsorbed onto mesoporous TiO_2 (made from nanoparticles) the charge transfer occurred via interfacial electron hopping (electron percolation) between the immobilised redox centres. For all dyes investigated it has been shown that the hopping conduction of electrons is responsible for the voltammetric responses and for the redox behaviour of the dyes. In all cases the voltammetric responses were affected by the chemical degradation of the FTO-bound dyes in their oxidised form.

In the operating solar cell the dye, once oxidized, is reduced by electron transfer from the iodide/tri-iodide redox system. It has been shown that all dyes studied in this work catalyze the oxidation of iodide in acetonitrile and this even happened at low dye coverage.

Probably the most important result of this work is the fact that indoline dyes have shown an apparent diffusion coefficient which is substantially higher than those reported for the Ru-based dyes. This is consistent with very fast hole/electron mobility in the aggregated dyes probably due to delocalisation effects in j-aggregates. This behaviour when related to the dye in the operating DSC, could cause faster recombination and energy losses, but could also be beneficial by causing faster reaction with iodide in the electrolyte. Spectroelectrochemical experiments showed that near infrared charge transfer absorption bands due to π orbital interaction and indicative of high charge mobility. This would confirm the observation of the high apparent hole-diffusion coefficients for the electron hopping through the indoline film based redox centres.

Further spectroelectrochemical experiments as a function of surface coverage of indoline dyes on FTO/TiO_2 will be required to better understand the aggregation phenomena and to overall improve the physical and chemical properties of these dyes for the manufacture of higher quality dye sensitised solar cells.